

**NUMERICAL STUDY OF MAGNETOHYDRODYNAMIC MIXED  
CONVECTION IN A LID-DRIVEN WAVY TOP CAVITY  
CONTAINING TWO CIRCULAR CYLINDERS**

Thesis submitted for the award of the degree of  
**MASTER OF SCIENCE**

**IN  
MATHEMATICS**

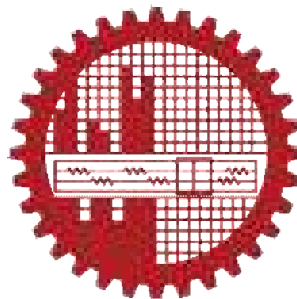
at the Bangladesh University of Engineering and Technology

By

**SHAMSUN NAHER SATHI**

**Student No.:1018092508F**

**Registration No.:1018092508F, Session: October-2018**



Department of Mathematics

Bangladesh University of Engineering and Technology (BUET)

Dhaka-1000, Bangladesh

March-2022

The thesis titled

**"NUMERICAL STUDY OF MAGNETOHYDRODYNAMIC MIXED CONVECTION IN A LID-DRIVEN WAVY TOP CAVITY CONTAINING TWO CIRCULAR CYLINDERS"**

Submitted by

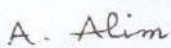




**SHAMSUN NAHER SATHI**

Student No. 1018092508F, Registration No. 1018092508, Session: October-2018, a full-time student of M. Sc. (Mathematics) has been accepted as satisfactory in partial fulfillment for the degree of

**Master of Science in Mathematics**

On 29 March, 2022

## **BOARD OF EXAMINERS**

1.   
\_\_\_\_\_  
**Dr. Md. Abdul Alim** Chairman  
Professor (Supervisor)  
Department of Mathematics, BUET, Dhaka-1000
2.   
\_\_\_\_\_  
**Head (Prof. Dr. Khandker Farid Uddin Ahmed)** Member  
Department of Mathematics, BUET, Dhaka-1000 (Ex-Officio)
3.   
\_\_\_\_\_  
**Dr. Khandker Farid Uddin Ahmed** Member  
Professor  
Department of Mathematics, BUET, Dhaka-1000
4.   
\_\_\_\_\_  
**Dr. Rehena Nasrin** Member  
Professor  
Department of Mathematics, BUET, Dhaka- 1000
5.   
\_\_\_\_\_  
**Dr. Goutam Kumar Saha** Member  
Professor (External)  
Department of NAME, BUET, Dhaka- 1000

## AUTHOR'S DECLARATION

I hereby announce that the work which is being presented in this thesis entitled

**“NUMERICAL STUDY OF MAGNETOHYDRODYNAMIC MIXED CONVECTION IN A LID-DRIVEN WAVY TOP CAVITY CONTAINING TWO CIRCULAR CYLINDERS”**

Submitted in partial fulfillment of the requirements for the decoration of the degree of **Master of Science**, department of Mathematics, BUET, Dhaka, is an actual plausible record of my personal work.

This work is original except where indicated by and attached with special reference in the context and no phase of it has been submitted for any attempt to get other degrees or diplomas.

All views expressed in the dissertation are those of the author and in no way or through no means symbolize those of Bangladesh University of Engineering and Technology, Dhaka. This dissertation has not been submitted to any other any university, educational institution for the publication either at a home or abroad.

*Shamsun Naher Sathi*

**Shamsun Naher Sathi**

M.Sc Student

Department of Mathematics

Date: 29 March, 2022

## PERMIT OF RESEARCH

This is to endorse that the work presented in this thesis is carried out by the author under the supervision of **Dr. Md. Abdul Alim**, Professor, Department of Mathematics, Bangladesh University of Engineering & Technology, Dhaka.

*A. Alim*

Dr. Md. Abdul Alim

*Shamsun Naher Sathi*  
Shamsun Naher Sathi

# DEDICATION

*All thanks to the Almighty Allah (swt), the most  
beneficent, the most merciful.*

*Every challenging work needs self-efforts as well as guidance of  
elders especially those who were very close to our heart. My humble  
effort*

*Dedicated to*

*My Beloved Parents & Siblings*

*Whose affection, love, encouragement and prayers of day and night  
make me able to get such success and honor.*

*& My Respectable Supervisor*

*Dr. Md. Abdul Alim*

*The pioneer of my life without whom I can't complete this  
thesis.*

# ACKNOWLEDGEMENT

Writing a significant scientific thesis is hard work and it would be impossible without support from various people. This Thesis becomes a reality with the kind support and help of many individuals. I would like to extend my sincere thanks to all of them.

In the first place, Thanks to Almighty ALLAH for giving me strength and ability to understand learn and complete this report successfully. Without the grace and blessing of Allah, no work would have been possible to achieve the goal line.

I have the privilege to express my deepest respect and sincerest gratitude first to my thesis supervisor **Dr. Md. Abdul Alim**, Professor, Department of Mathematics, Bangladesh University of Engineering and Technology (BUET), for his scholastic supervision, guidance, constant support, intuitive suggestions and mental support which have been found very benevolent for the outcome of the research. It would not have been possible to carry out this study successfully without continuous inspiration and relentless encouragement from supervisor. I am grateful to him for giving me such opportunity to work with him as a research student and for every attempt that he made to get me on the right track of the thesis.

I am also deeply indebted to **Dr. Khandker Farid Uddin Ahmed**, Professor and Head, Department of Mathematics, BUET, for his encouragement and counsel in the thesis of being successful to reach the objectives of this dissertation.

I am grateful from the core of my heart to Prof. **Dr. Rehena Nasrin**, Department of Mathematics, BUET, for her guidance and supports.

I am in debt of gratitude to the external member of the Board of Examiners, **Dr. Goutam Kumar Saha**, Professor, Department of Naval Architecture and Marine Engineering (NAME), BUET, Dhaka.

I would also like to express my thanks to all the respected teachers of this department for their support and valuable advices and staffs of the Department of Mathematics, BUET, Dhaka, for their kind help and cooperation.

Finally, words alone cannot express my thanks to my lovely parents and siblings for creating a delightful atmosphere as well as excusing me from family duties in order to complete the courses, research studies and final production of the thesis work.

# ABSTRACT

The problem of mixed convection and heat transfer in presence of magnetic field in a Lid-driven wavy top cavity containing two circular cylinders, two cases have been considered: (I) Variation of cylinders position vertically keeping size (radius,  $r$ ) of the cylinders as a constant and (II) Variation of cylinders size (radius,  $r$ ) keeping cylinders position at CP1 (0.1, 0.4) and CP2 (0.6, 0.4) as a constant. The bottom wall is kept at a constant hot temperature  $T_h$  and the wavy top wall is kept at a constant cold temperature  $T_c$  maintaining  $T_h > T_c$ , while the other walls are assumed to be adiabatic or insulated. The left wall and wavy top walls have a lid velocity where left wall moves from lower to upper and the wavy top wall moves from left to right with constant velocity. The gravitational force acts in the vertically downward direction and uniform magnetic field with a constant magnitude ( $B_0$ ) is applied parallel to the x-axis. The cavity is filled with fluid with  $Pr = 0.71$  that is considered Newtonian and incompressible where the fluid flow is assumed to be laminar. The physical problems have been represented mathematically by different sets of governing equations along with the corresponding boundary conditions. The nondimensional governing equations are discretized by using Galerkin weighted residual method of finite element formulation. The numerical results have been reported for the effect of Richardson numbers ( $0.1 \leq Ri \leq 10$ ) and magnetic field parameter, Hartmann numbers ( $0 \leq Ha \leq 50$ ). Three positions (0.6, 0.4), (0.6, 0.55) and (0.6, 0.25) of the semi heated cylinder CP2 have been considered in case (I) where the size (radius,  $r$ ) of the cylinders has maintained as a constant ( $r = 0.1$  m). Besides, in case (II), the size (radius,  $r$ ) of the semi heated cylinders has been altered from  $r = 0.10$  to  $0.20$  m keeping cylinders position at CP1 (0.1, 0.4) and CP2 (0.6, 0.4) as a constant. The strength of the velocity magnitude has been improved for both cases with the increase of Richardson number. But the strength of the velocity magnitude has been declined improved for both cases with the increase of Hartmann number. The maximum average velocity magnitude (2.66 m/s) is found for CP1 at (0.1, 0.4) and CP2 at (0.6, 0.4) is found for  $Ri = 10$ ,  $Pr = 0.71$ ,  $Ha = 50$  and cylinder size,  $r = 0.20$  m. Finally, the appreciable effects of heat transfer rate have been illustrated for the size variation of the semi heated cylinders compared to the position variation. The results indicate that the heat transfer rate increase with the increase of Richardson number and that, Hartmann number is a good control parameter for heat transfer in the flow. Comparisons with

previously published work are performed and the results are found to be in excellent agreement.



# CONTENTS

<b>BOARD OF EXAMINERS</b> .....	Error! Bookmark not defined.
<b>AUTHOR'S DECLARATION</b> .....	Error! Bookmark not defined.
<b>PERMIT OF RESEARCH</b> .....	<b>Error! Bookmark not defined.</b>
<b>DEDICATION</b> .....	<b>iv</b>
<b>ACKNOWLEDGEMENT</b> .....	<b>vi</b>
<b>ABSTRACT</b> .....	<b>vii</b>
<b>CONTENTS</b> .....	<b>ix</b>
<b>NOMENCLATURE</b> .....	<b>xii</b>
<b>LIST OF TABLES</b> .....	<b>xiv</b>
<b>LIST OF FIGURES</b> .....	<b>xiv</b>
<b>CHAPTER 1</b> .....	<b>1</b>
<b>Introduction and Literature Review</b> .....	<b>1</b>
1.1 Preface .....	1
1.2 Literature Review .....	1
1.3 Inspiration behind the Selection of Current Work.....	6
1.4 Main objectives of the present work.....	7
1.5 Outline of the Thesis.....	7
<b>CHAPTER 2</b> .....	<b>9</b>
<b>Preliminaries and Definitions</b> .....	<b>9</b>
2.1 Some definitions of fluids.....	10
2.1.1 Liquid and Gases.....	10
2.1.2 Incompressible fluid.....	10
2.1.3 Streamlines.....	11
2.1.4 Laminar Flow.....	12
2.1.5 Mixed Convection.....	12
2.1.6 Mixed Convection Heat Transfer in Cavities .....	13
2.1.7 Magnetohydrodynamics.....	13
2.1.8 Boussinesq Approximation.....	14
2.2 Finite Element Method .....	15
2.3 Algorithm.....	16
2.4 Dimensionless Parameters Relating to Fluid Flows .....	16
2.4.1 Reynolds Number (Re) .....	16
2.4.2 Prandlt Number (Pr).....	17
2.4.3 Grashof Number ( <i>Gr</i> ) .....	17
2.4.4 Richardson Number (Ri).....	18
2.4.5 Hartmann Number (Ha).....	18

2.4.6 Nusselt Number (Nu).....	19
<b>CHAPTER 3.....</b>	<b>20</b>
<b>Physical Model and Mathematical Formulation .....</b>	<b>20</b>
3.1 Mathematical Modelling.....	20
3.2 Physical Configuration .....	20
3.3 Mathematical Formulation.....	21
3.3.1 Governing equation.....	21
3.3.2 Dimensional Boundary Conditions.....	22
3.3.3 Non-dimensional Variables .....	23
3.3.4 Non-dimensional Governing Equations.....	23
3.3.5 Non-Dimensional Boundary Conditions.....	24
3.4 Numerical Analysis .....	24
3.4.1 Finite Element Formulation and Computational procedure.....	24
3.4.2 Grid Size Sensitivity Test .....	28
3.4.3 Mesh Generation.....	29
3.4.4 Program validation and comparison with Previous work .....	30
<b>CHAPTER 4.....</b>	<b>32</b>
<b>Result and Discussion .....</b>	<b>32</b>
4.1 Introduction.....	32
4.2 Case – I (Variation of cylinders position).....	32
4.2.1 Effect of cylinders position at CP1 (0.10, 0.40) & CP2 (0.60, 0.40).....	32
4.2.1.1 Effect of Richardson number .....	32
4.2.1.2 Effects of Hartmann number .....	35
4.2.1.3 Heat Transfer Rates.....	37
4.2.2 Effect of cylinders position at CP1 (0.10, 0.40) & CP2 (0.60, 0.55).....	38
4.2.2.1 Effect of Richardson number .....	38
4.2.2.2 Effects of Hartmann number .....	41
4.2.2.3 Heat Transfer Rates.....	43
4.2.3 Effect of cylinders position at CP1 (0.10, 0.40) & CP2 (0.60, 0.25).....	44
4.2.3.1 Effects of Richardson number.....	44
4.2.3.2 Effects of Hartmann number .....	46
4.2.3.3 Heat Transfer Rates.....	49
4.3 Case – II (Variation of cylinders size).....	50
4.3.1 Effect of cylinders size when $r = 0.10$ m .....	50
4.3.2 Effect of cylinders size when $r = 0.15$ m .....	50
4.3.2.1 Effect of Richardson Number .....	50
4.3.2.2 Effect of Hartmann Number.....	52
4.3.2.3 Heat Transfer Rates.....	55
4.3.3 Effect of cylinders size when $r = 0.20$ m .....	55
4.3.3.1 Effect of Richardson Number .....	56
4.3.3.2 Effect of Hartmann Number.....	58
4.3.3.3 Heat Transfer Rates.....	60

4.4 Comparative Study .....	61
4.4.1 Comparison of Nuav between with one cylinder and with two cylinders ....	61
4.4.2 Comparison between present result and previous study .....	61
<b>CHAPTER 5.....</b>	<b>63</b>
<b>Conclusions and Future Research.....</b>	<b>63</b>
5.1 Summary of the Major Outcomes.....	63
5.1.1 Case – I: Variation of Cylinders position .....	63
5.1.2 Case – I: Variation of Cylinders size .....	64
5.2 Conclusions.....	64
5.3 Future Research .....	65
<b>REFERENCES .....</b>	<b>66</b>

# NOMENCLATURE

$B_0$	Magnetic induction ( $\text{Wb/m}^2$ )
CP	Cylinder position
$c_p$	Specific heat at constant pressure ( $\text{J/kg.K}$ )
$g$	Gravitational acceleration ( $\text{ms}^{-2}$ )
Gr	Grashof number
$h$	Convective heat transfer coefficient ( $\text{W/m}^2\text{K}$ )
H	Height of the cavity (m)
Ha	Hartmann number
$k$	Thermal conductivity of fluid ( $\text{Wm}^{-1}\text{K}^{-1}$ )
L	Length of the cavity (m)
$n$	Dimensional distance either along x or y direction (m)
N	Non-dimensional distance either along X or Y direction
$\text{Nu}_{\text{local}}$	Local Nusselt Number
$\text{Nu}_{\text{av}}$	Average Nusselt number
$p$	Pressure
P	Non-dimensional pressure
Pr	Prandtl number
Ri	Richardson number
Re	Reynolds number
$r$	Radius of the semi heated cylinders
T	Dimensional fluid temperature (K)
$u$	Velocity in x-direction (m/s)
$u_{\text{lid}}$	Magnitude of velocity of lid
U	Dimensionless horizontal velocity
$v$	Velocity in y-direction (m/s)
V	Dimensionless vertical velocity

$x, y$	Cartesian coordinates (m)
$X, Y$	Dimensionless Cartesian coordinates

### **Greek symbols**

$\alpha$	Thermal diffusivity ( $m^2s^{-1}$ )
$\beta$	Coefficient of thermal expansion ( $K^{-1}$ )
$\theta$	Dimensionless fluid temperature
$\mu$	Dynamic viscosity of the fluid ( $m^2s^{-1}$ )
$\nu$	Kinematic viscosity of the fluid ( $m^2s^{-1}$ )
$\rho$	Density of the fluid ( $kgm^{-3}$ )
$\sigma$	Fluid electrical conductivity ( $\Omega^{-1}.m^{-1}$ )

### **Subscripts**

$h$	Hot
$c$	Cold
$av$	Average

## LIST OF TABLES

Table No.	Caption	Page No.
3.1	Grid sensitivity check at $Pr = 0.71$ , $Ri = 1.0$ and $Ha = 50$	28
3.2	Comparison of average Nusselt number ( $Nu_{av}$ ) for various Hartmann number	30
4.1	Comparison of average Nusselt Number ( $Nu_{av}$ ) along the heated bottom wall between with one cylinder and with two cylinders of the cavity where $r = 0.1$ m, $Pr = 0.71$ , CP1 at (0.1, 0.4) and CP2 at (0.6, 0.4)	61
4.2	Comparison of Average Nusselt Number ( $Nu_{av}$ ) with Chamkha [16] and Rahman et al. [39] for different Hartmann Number ( $Ha$ )	62

## LIST OF FIGURES

Figure No.	Caption	Page No.
2.1	Incompressible fluid	11
2.2	Minimalist Abstract Flow Curvy and wavyStreamlines	11
2.3	2D non uniform steady laminar channel flow around a cylinder	12
2.2	Flow chart of the computational procedure	16
3.1	Schematic diagram of the wavy top cavity with boundary condition	21
3.2	Grid independency study for different elements while $Pr = 0.71$ , $Ri = 1$ , $Ha = 50$	29
3.3	Mesh generation of mixed convection in lid-driven cavity	30
3.4	Comparison of the streamlines and isotherms for numerical solution between the (a) Ali et al. (2016) and (b) Present work	31
4.1	Effect of Richardson number on (a)streamlines and (b)isotherms for $Pr = 0.71$ , $Ha = 10$ where $r = 0.10$ m.	33
4.2	Variation of velocity profiles along the line $y = 0.1$ of cavity	34

Figure No.	Caption	Page No.
	for $Ha = 10$ , $Pr = 0.71$ and $r = 0.10$ m varying $Ri$	
4.3	Variation of local Nusselt number along the line $y = 0.1$ of cavity with Richardson number for $Pr = 0.71$ , $Ha = 10$	35
4.4	Effect of Hartmann number on (a)streamlines and (b)isotherms for $Pr = 0.71$ , $Ri = 1.0$ and $r = 0.10$ m	36
4.5	Variation of velocity profiles along the line $y = 0.1$ of cavity for $Ri = 1.0$ , $Pr = 0.71$ and $r = 0.10$ m varying $Ha$	37
4.6	Variation of local Nusselt Number along the line $y = 0.1$ of cavity for $Ri = 1.0$ , $Pr = 0.71$ and $r = 0.10$ m varying $Ha$	38
4.7	Variation of the average Nusselt number against $Ha$ for selected value $Ri$ , $Pr = 0.71$ , and $r = 0.10$ m	38
4.8	Effect of Richardson number on (a)streamlines and (b)isotherms for $Pr = 0.71$ , $Ha = 10$ and $r = 0.1$ m.	39
4.9	Variation of velocity profiles along the line $y = 0.1$ of cavity for $Ha = 10$ , $Pr = 0.71$ and $r = 0.10$ m varying $Ri$	40
4.10	Variation of local Nusselt number along the line $y = 0.1$ of cavity with Richardson number for $Pr = 0.71$ , $Ha = 10$	40
4.11	Effect of Hartmann number on (a)streamlines and (b)isotherms for $Pr = 0.71$ , $Ri = 1.0$ and $r = 0.10$ m	41
4.12	Variation of velocity profiles along the line $y = 0.1$ of cavity for $Ri = 1.0$ , $Pr = 0.71$ and $r = 0.10$ m varying $Ha$	42
4.13	Variation of local Nusselt number along line $y = 0.1$ of cavity for $Ri = 1$ and $Pr = 0.71$ varying $Ha$	43
4.14	Variation of the average Nusselt number against $Ha$ for selected value $Ri$ , $Pr = 0.71$ , and $r = 0.10$ m	44
4.15	Effect of Richardson number on (a) streamlines and (b)isotherms for $Pr = 0.71$ , $Ha = 10$ where $r = 0.10$ m.	45
4.16	Variation of velocity profiles along line $y = 0.1$ of cavity for $Ri = 1$ and $Pr = 0.71$ varying $Ha$	46
4.17	Variation of local Nusselt number along the line $y = 0.1$ of cavity with $Ri$ for $Pr = 0.71$ , $Ha = 10$	46
4.18	Effect of Hartmann number on (a) streamlines and (b)isotherms for $Pr = 0.71$ , $Ri = 1.0$ and $r = 0.10$ m	47
4.19	Variation of velocity profiles along the line $y = 0.1$ of cavity	48

Figure No.	Caption	Page No.
	for $Ri= 1.0$ , $Pr= 0.71$ and $r = 0.10$ m varying $Ha$	
4.20	Variation of local Nusselt number along the $y = 0.1$ of cavity for $Ri = 1$ and $Pr= 0.71$ varying $Ha$	49
4.21	Variation of the average Nusselt number against $Ha$ for selected value $Ri$ , $Pr = 0.71$ , and $r = 0.10$ m	49
4.22	Effect of Richardson number on (a) streamlines and (b) isotherms for $Pr = 0.71$ , $Ri = 1.0$ and $r = 0.15$ m	51
4.23	Variation of velocity profiles along the line $y = 0.1$ of cavity with Richardson number for $Pr = 0.71$ , $Ha = 10$	52
4.24	Variation of local Nusselt number along the line $y = 0.1$ of cavity with $Ri$ for $Pr = 0.71$ , $Ha = 10$	52
4.25	Effect of Hartmann number on (a) streamlines and (b) isotherms for $Pr = 0.71$ , $Ri = 1.0$ and $r = 0.15$ m	53
4.26	Variation of velocity profiles along the line $y = 0.1$ of cavity for $Ri= 1.0$ , $Pr= 0.71$ and $r = 0.10$ m varying $Ha$	54
4.27	Variation of local Nusselt number along line $y = 0.1$ of cavity for $Ri = 1$ and $Pr= 0.71$ varying $Ha$	54
4.28	Variation of the average Nusselt number against $Ha$ for selected value $Ri$ , $Pr = 0.71$ when $r = 0.15$ m	55
4.29	Effect of Richardson number on (a) streamlines and (b) isotherms for $Pr= 0.71$ , $Ha = 10$ where $r = 0.20$ m.	56
4.30	Variation of velocity profiles along the line $y = 0.1$ of cavity for $Ha = 10$ , $Pr= 0.71$ and $r = 0.10$ m varying $Ri$	57
4.31	Variation of local Nusselt number along the line $y = 0.1$ of cavity with $Ri$ for $Pr = 0.71$ , $Ha = 10$	57
4.32	Effect of Hartmann number on (a) streamlines and (b) isotherms for $Pr = 0.71$ , $Ri = 1.0$ and $r = 0.10$ m	58
4.33	Variation of velocity profiles along the line $y = 0.1$ of cavity for $Ri= 1.0$ , $Pr= 0.71$ and $r = 0.10$ m varying $Ha$	59
4.34	Variation of local Nusselt number along the line $y = 0.1$ of cavity for $Ri = 1$ and $Pr= 0.71$ varying $Ha$	60
4.35	Variation of the average Nusselt number against $Ha$ for selected value $Ri$ , $Pr = 0.71$ when $r = 0.20$ m	60
4.36	Comparison of average Nusselt Number with Chamkha	62



<b>Figure No.</b>	<b>Caption</b>	<b>Page No.</b>
	[16], Rahman et al. [39] and Present research	

# CHAPTER 1

## Introduction and Literature Review

### 1.1 Preface

Fluid mechanics is the study of fluid behavior at rest and in motion. Fluid dynamics is one of the most important branches of fluid mechanics. It is used to model a huge range of physical phenomena and plays an important role in science and technology. The branches of fluid dynamics include hydrodynamics and aerodynamics and the solutions of fluid dynamics problems are usually associated with the behavior of fluid properties and also used in calculating forces and moments on aircraft, determining the mass flow rate, predicting weather patterns etc.

Mixed convection or combined forced convection and free convection, occurs when free convection and forced convection mechanisms act together to transfer heat. This is also defined as situations where both pressure forces and buoyant forces interact. The mixed convection in enclosures continues to be a very active area of research during the past few decades. Mixed convection heat transfer is an important phenomenon in engineering systems due to its wide applications in electronic cooling, heat exchangers and thermal systems. Combined forced and free convection flow as well as heat transfer in cavities has been investigated widely due to its potential applications in engineering fields. The phenomenon of heat transfer was known to a human being even in the primitive age when they used solar energy as a source of heat. Heat transfer in its initial stage was conceived with the invention of fire in the early age of human civilization. Since then its knowledge and use have been progressively increasing each day as it is directly related to the growth of human civilization. With the invention of the steam engine by James Watt in 1765 A. D., the phenomenon of heat transfer got its first industrial recognition and after that its use extended to a great extent and spread out in different spheres of engineering fields.

### 1.2 Literature Review

Analysis of mixed convection usually induced in enclosed cavities or channels containing heating elements on it are important from both theoretical and practical points of view. Most of the common enclosure used in industries are wavy cavity, cylinder,

rectangular, trapezoidal and triangular. Because of applicability of wavy cavity in various fields it has received a considerable attention and numerous studies related to mixed convection in enclosure cavity have been reported in order to investigate the heat transfer and fluid flow in such geometry. Mixed convection in a cavity is relevant to many industrial and environmental applications such as heat exchangers, nuclear and chemical reactors, cooling of electronic equipment etc. Considering several researches, it has been found that mixed convection flow and heat transfer in different geometrical enclosures have been the topic of many mathematical studies. They used different types of boundary conditions in lid driven cavity here. MHD plays very significant roles in those because of the effect of it. Combined forced and free convection flow as well as heat transfer in cavities has been investigated widely due to its potential applications in engineering fields, such as, ventilation of rooms, lubrication technologies, drying technologies, food processing, float glass production, solar collectors and solar pads etc. A large number of research works have been done on different shapes of cavities. Some of them are reflected in the present literature review.

Raizah et al. [1] investigated MHD mixed convection of hybrid nanofluid in a wavy porous cavity employing local thermal non-equilibrium condition. They observed that the magnetic field impacted on the mixed convection flow within an undulating cavity filled by hybrid nanofluids and porous media. Alsabery et al. [2,3] reported the effect of solid cylinder on entropy generation and convective heat transfer in a wavy cavity heated from below. The outcomes were investigated for nanofluids to address the effect of using composite nanoparticles toward the flow and temperature patterns and entropy generation. Moreover, they seen that, an augmenting in the porosity of the medium causes an increase in heat transfer from the wall to the fluid and therefore an increase in the convective flow and consequently a decrease in the Bejan number. Öztop et al. [4] Analyzed mixed convection of MHD flow in nanofluid filled and partially heated wavy walled lid driven enclosure. They showed that the rate of heat transfer decreases with increasing the Hartmann number. Cheong et al. [5] considered the natural convection in a wavy porous cavity with sinusoidal heating and internal heat generation. Sheremet et al. [6,7] studied free convection in a partially heated wavy porous cavity filled with a nanofluid under the effects of Brownian diffusion and thermophoresis. Abu-Nada and Chamkha [8] numerically simulated the mixed convection flow of a nanofluid in a lid-driven cavity with a wavy wall. They found that the heat transfer rate increases with the volume fraction of nanoparticles for all values of Richardson numbers and bottom wall geometry ratios. Mansour et al. [9] considered numerically the problem of natural convection in wavy

porous cavities under the influence of thermal radiation using a thermal non-equilibrium model. Nasrin and Parvin [10] carried out a numerical study on mixed convection flow in a lid-driven cavity with sinusoidal wavy surface in Presence of magnetic effect to present the flow and heat transfer patterns in two-dimensional fluid regions. Moreover, in this analysis they reported that the average Nusselt number is optimum for the greater Reynolds number and lower magnetic field effect. Rostami [11] numerically simulated the unsteady natural convection in an enclosure with vertical wavy walls. Al-Amiri et al. [12] investigated the effect of sinusoidal wavy bottom surface on mixed convection heat transfer in a lid-driven cavity. They investigated the effect of Richardson number, undulation number and amplitude of the wavy surface on flow structure and heat transfer characteristics. Misirlioglu et al. [13] studied numerically natural convection inside an inclined wavy enclosure filled with a porous medium. Das and Mahmud [14] have studied natural convection inside a wavy enclosure. Their results illustrated that the amplitude and the number of undulations of the wavy wall affect heat transfer characteristics inside the cavity. Mahmud et al. [15] Analyzed free convection in an enclosure with vertical wavy walls. They observed that the higher heat transfer at lower aspect ratios for a certain value of the Grashof number. The problem of unsteady laminar combined convection flow and heat transfer of an electrically conducting and heat generating or absorbing fluid in a vertical lid-driven cavity in the presence of magnetic field was formulated by Chamkha [16].

Many scientists, versed engineers and researchers studied the problems of MHD mixed convection for different types of cavities. Amongst them, Selimefendigi [17] investigated the effect of magnetic field on mixed convection due to double rotating cone in a 3D enclosure and recommended that magnetic field reduces the convection effect, and average Nusselt number significantly improved with the size and speed of rotating cones. In addition, abstractions of various shaped within closed or open enclosure are used to control the flow circulation and temperature distribution within enclosure. Several studies have been accomplished related to the natural/mixed/forced convection flow in presence of different abstractions. Hydrodynamic mixed convection in a lid-driven cavity with corner heater is numerically simulated by Munshi et al. [18, 19]. They found that heat transfer rate increased with increasing Richardson number and Hartmann number which was a good control parameter for heat transfer in fluid flow in the cavity. A numerical study is carried out to analyze magneto-hydrodynamic mixed convection flow and heat transfer in a hexagonal cavity by Ali et al. [20]. They observed that the heat transfer rate is dominant for greater Richardson number with lower Hartman number and also found that

average temperature enhanced slowly due to the larger Richardson number as well as Hartman number. Udhayakumar et al. [21] did investigation of magnetohydrodynamic mixed convection over an isothermal circular cylinder in presence of an aligned magnetic field. Rashidi et al. [22] investigated magnetic field effect on mixed convection heat transfer of nanofluid in a channel with sinusoidal walls. Aghaei et al. [23] reported a numerical study of magnetic field on mixed convection and entropy generation of nanofluid in a trapezoidal enclosure. In addition, heat generation predicated to decrease the average Nusselt number whereas heat absorption increases it. Later on, A Numerical investigation on mixed convection in a lid-driven square cavity has been performed in the presence of uniform magnetic field by Malleswaran and Sivasankaran [24]. The magnetic field affects the average heat transfer rate more on vertical heaters than on the horizontal heaters. Saha et al. [25] have performed the numerical effect of internal heat generation or absorption on MHD mixed convection flow in a lid driven cavity. Significant reduction in the average Nusselt number was produced as the strength of the applied magnetic field was increased. Khudheyer [26] numerically simulated the MHD mixed convection in double lid- driven differentially heated trapezoidal cavity. The results show that at mixed convection regime ( $Ri = 1$ ) and in the absences of the magnetic field ( $Ha = 0$ ), the maximum heat transfer occurs for trapezoidal cavity at inclined wall angle (300). Selimefendigil and Oztop [27] studied magnetic field effect on mixed convection in a lid driven cavity and revealed that the magnetic field effect decreases the average heat transfer rate. Malleswaran et al. [28] studied the effect of heating location and size on MHD mixed convection in a lid-driven cavity. They concluded that on increasing the Richardson number, the overall heat transfer is increased whether the length and the location of the heater is considered or not. Magneto-hydrodynamic mixed convection in a lid driven cavity along with a heated circular hollow cylinder positioned at the center of the cavity is studied numerically by Farid et al. [29]. The results showed that the aforesaid parameters have noticeable effect on the flow pattern and heat transfer characteristics inside the cavity. The conjugate effect of joule heating and magneto-hydrodynamics mixed convection in an obstructed lid-driven square cavity was investigated by Rahman et al. [30].

The investigation of mixed convection heat and mass transfer in vertical ducts with film evaporation has been numerically examined in detail. Rabani [31] conducted a numerical study of mixed convection in a lid driven triangular cavity and observed highest heat transfer occurs for assisting mixed convection flow. A lattice Boltzmann solution was performed by Ekici [32] using Newtonian fluid to improve the heat transfer process.

Omeri [33] conducted a numerical investigation of a mixed convection flow in a lid-driven cavity. Heat and mass transfer due to double diffusive mixed convection in a parallel plate reactor in presence of chemical reaction and heat generation was analyzed by Parvin and Alim [34]. Sivasankaran et al. [35] reported a numerical study on mixed convection flow in a lid driven square enclosure. In this analysis, they observed that the flow patterns remain unchanged for increasing heater length at any fixed value of mixed convection parameter. Mixed convection heat transfer in a lid-driven cavity along with a heated circular hollow cylinder positioned at the center of the cavity has been analyzed numerically by Billah et al. [36]. They found that the flow field and temperature distribution strongly depend on the cylinder diameter and also the solid–fluid thermal conductivity ratio at the three convective regimes. Dariz et al. [37] investigated the fin effect on mixed convection heat transfer in a lid-driven cavity. Heat transfer was observed for the cavity with fewer fins and high Richardson number. Numerical simulations are carried out for mixed convection flow in a vented cavity with a heat conducting horizontal square cylinder by Rahman et al. [38]. The results indicated that the flow field and temperature distributions inside the cavity are strongly dependent on the Richardson numbers and the position of the inner cylinder. Manca et al. [39] have found that the effect of a stronger buoyancy determines a penetration of thermal plume front for  $Re = 100$ . Their experimental investigation has further extended for mixed convection in an open cavity with a heated wall bounded by a horizontal unheated plate where the heated wall is on the opposite side of the forced inflow. They [40] have carried out experimental investigations on mixed convection in an open cavity with a heated wall on the inflow side, bounded by a horizontally unheated plate. The flow visualization illustrates two nearly distinct fluid motions for  $Re = 1000$ : a parallel forced flow in the channel and a recirculation flow inside the cavity. Oztop et al. [41] have studied steady state two-dimensional mixed convection Problem in a vertical two-sided lid driven differentially heated square cavity. The left and right moving walls were maintained at different constant temperatures while upper and bottom walls were thermally insulated. Last of all, Hossain et al. [42] studied about a finite element analysis on MHD free convection flow in open square cavity containing heated circular cylinder. They calculated about the effects of Hartmann number  $Ha$ , Rayleigh number  $Ra$ , heat flux  $q$  for steady state, incompressible, laminar and MHD free convection flow in a square open cavity containing a heated circular cylinder. The flow with all  $Ra$  in this work has been affected by the buoyancy force. Temperature fields are illustrated in the flow region.

In the light of the above literatures, little attention is given to the problem of MHD mixed convection heat transfer in a lid driven wavy top cavity containing two circular cylinders which will be investigated numerically in this proposed study.

### **1.3 Inspiration behind the Selection of Current Work**

Over decades, micropolar fluid has been the focus of research of many researchers working in the fluid mechanics owing to its practical. From the historical review it is clear that during the past two decades, several experiments and numerical calculations have been presented for describing the phenomenon of mixed convection in open cavities. Most of the cavities commonly used in industries are wavy, cylindrical, rectangular, square and triangular and so on. Magneto-hydrodynamic (MHD) mixed convection in square cavities has received more considerable attention for its application in several thermal engineering problems, for example in the design of electronic devices, solar thermal receivers, geothermal reservoirs, etc. The MHD principles are used in the case of electromagnetic pumps, heat exchangers, in space vehicles propulsion. The important application of MHD is the MHD generator using ionized gas as an armature, electronic pumping of liquid metal coolants in a nuclear reactor, stirring and levitation in the metallurgical industries. Because of these and many other applications, it is felt necessary to carry out research intensively in the field of MHD mixed convection flow. From the historical review, it is clear that during the past two decades several experiments and numerical calculation have been presented for describing the phenomenon of MHD mixed convection in cavities. Those studies have been focused to study the effect on flow and heat transfer for different Richardson numbers and Hartmann numbers. Numerical studies are therefore essential to observe the variation in fluid flow and heat transfer due to the above physical changes with different boundary conditions, which form the basis of the inspiration behind the selection of current work.

In this research works it can observe that the study of mixed convection flow is become the center point of my research. In the literature review section, the type of boundary conditions and many types of enclosure to build research will be described. However, after studying these articles I feel a great interest in Magnetohydrodynamic mixed convection in a lid-driven with using a wavy top wall containing two circular cylinders. There uses wavy top wall which create extra effect of the cavity. This can change the outlook and this type of cavity may apply in many industrial sectors. Why it is so effective it can be defined in the result and discussion section.

## 1.4 Main objectives of the present work

A review of earlier studies indicates that the mixed convection heat transfer in presence of magnetic field in a lid-driven wavy cavity having circular cylinders has not been analyzed yet. The aim of the proposed study is to investigate the effect of magnetic field on heat transfer and fluid flow for mixed convection in lid driven wavy top cavity containing two circular cylinders. Results will be presented for different non-dimensional governing and physical parameters in terms of streamlines, isotherms, heat transfer rate as well as average temperature of the fluid in the cavity.

The specific objectives of the present research work are to:

- (i) To develop the mathematical models regarding the effects on heat transfer for MHD mixed convection in a cavity containing two circular cylinders.
- (ii) To solve the model equations using the finite element method.
- (iii) To investigate the effects of governing parameters namely Richardson number  $Ri$  and Hartmann number  $Ha$  on the flow and thermal field inside the cavity for various boundary conditions.
- (iv) To investigate the effects of different positions and sizes of cylinders on the flow field and temperature distribution.
- (v) To compare results with other relevant published works.

## 1.5 Outline of the Thesis

This dissertation contains seven chapters. This thesis is concerned with the analysis effects on heat flow for MHD mixed convection within wavy top cavity based on heat line concept. There are many cavity configurations for the study of conjugate effect of conduction and mixed convection flow. In this study we have considered a wavy top cavity.

In Chapter 1, a general framework for the description of convective heat transfers has been presented and discussed their properties, also relevant discussion on dimensionless parameter. In this chapter a brief introduction is presented with aim and objective and also inspiration behind the selection of current Work. This chapter also consists of a literature review of the past studies on fluid flow and heat transfer in cavities. In this state-of-the-art review, different aspects of the previous studies have been mentioned categorically.



In Chapter 2, we have discussed the computational technique of the problem for viscous incompressible flow.

In Chapter 3, Mathematical modeling and Finite Element Formulation are employed in this study and explained elaborately.

In Chapter 4, a detailed parametric study on mixed convection heat transfer in presence of magnetic field in a lid-driven wavy top cavity containing two circular cylinders is conducted. Effects of the major parameters such as Richardson number, Hartmann number and the physical parameter such as cylinders position within the cavity have been presented.

Finally, in Chapter 5, the dissertation is rounded off with the conclusions. Lastly, the main achievements and some ideas of further work have been summarized.

# CHAPTER 2

## Preliminaries and Definitions

Computational fluid dynamics (CFD) is the process of mathematically modeling a physical phenomenon involving fluid flow and solving it numerically using the computational prowess. Computational fluid dynamics (CFD) computation involves the formation of a set numbers that constitutes a practical approximation of real-life system. The outcome of computation process improves the understanding of the performance of a system. Computational fluid dynamics (CFD) has been rapidly gaining popularity over the past several years for technological as well as scientific interests. It is a science that, with the help of digital computers, produces quantitative predictions of fluid-flow phenomena based on the conservation laws (conservation of mass, momentum and energy) governing fluid motion. It uses data structure to solve issues of fluid flow like velocity, density and chemical compositions. This technology is used in areas like cavitation prevention, aerospace engineering, HVAC engineering electronics manufacturing and way more. It is used by many industries in their development work to analyze, optimize and verify the performance of designs before costly prototypes and physical tests. For many problems of industrial interest, experimental techniques are extremely expensive or even impossible due to the complex nature of the flow configuration. Analytical methods are often useful in studying the basic physics involved in a certain flow problem, however, in many interesting problems; these methods have limited direct applicability. The dramatic increase in computational power over the past several years has led to a heightened interest in numerical simulations as a cost-effective method of providing additional flow information, not readily available from experiments, for industrial applications, as well as a complementary tool in the investigation of the fundamental physics of turbulent flows, where analytical solutions have so far been unattainable. It is not expected (or advocated), however, that numerical simulations replace theory or experiment, but that they are used in conjunction with these other methods to provide a more complete understanding of the physical problem at hand.

Mathematical model of physical phenomena may be ordinary or partial differential equations, which have been the subject of analytical and numerical investigations. The partial differential equations of fluid mechanics and heat transfer are solvable for only a limited number of flows. To obtain an approximate solution numerically, we have to use a

discretization method, which approximated the differential equations by a system of algebraic equations, which can then be solved on a computer. The approximations are applied to small domains in space and/or time so the numerical solution provides results at discrete locations in space and time. Much as the accuracy of experimental data depends on the quality of the tools used, the accuracy of numerical solutions depends on the quality of discretization used. Computational fluid dynamics (CFD) computation involves the formation of a set number that constitutes a practical approximation of a real-life system. The outcome of the computation process improves the understanding of the performance of a system. Thereby, engineers need CFD codes that can make physically realistic results with good quality accuracy in simulations with finite grids. Contained within the broad field of computational fluid dynamics are activities that cover the range from the automation of well-established engineering design methods to the use of detailed solutions of the Navier-Stokes equations as substitutes for experimental research into the nature of complex flows. CFD has been used for solving a wide range of fluid dynamics problem. It is more frequently used in fields of engineering where the geometry is complicated or some important feature that cannot be dealt with standard methods.

## **2.1 Some definitions of fluids**

We present here some basic definitions which are related to the current study

### **2.1.1 Liquid and Gases**

Fluids include both liquid and gases. The feature that distinguishes a fluid from a solid is the inability of fluid, while remaining in a state of equilibrium, resist shearing forces. The distinction between a liquid and gas is readily appreciated but is difficult to define in a concise manner. A definite mass of a particular liquid will have a definite volume which will vary only slightly with temperature and Pressure. The volume of a definite mass of gas, on the other hand, is almost infinitely variable and its dependence on Pressure and temperature will be given by the equation of state. A liquid will exhibit a free surface if a large space is available than the required to contain its volume. A gas, on the other hand, will fill any space available to it, the pressure adjusting itself accordingly.

### **2.1.2 Incompressible fluid**

An incompressible fluid is one whose elements undergo no changes in volume or density. In other words, a fluid problem is called incompressible if the density changes have negligible effects on the solution. Liquids are relatively incompressible. Liquid is incompressible because of the quality of its particles. The volume of liquid doesn't change

with the pressure. That's why it is not easy to compress it. Example of incompressible fluid flow: The stream of water flowing at high speed from a garden hose pipe.

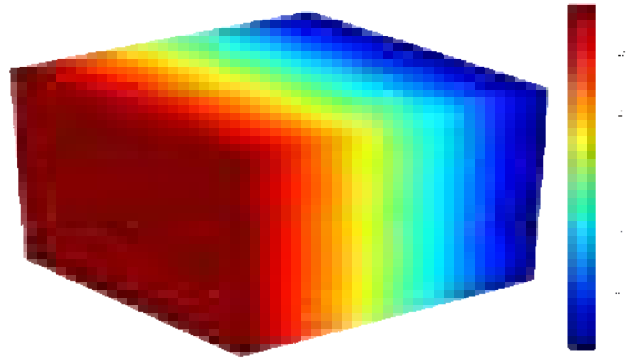


Figure-2.2: Incompressible fluid

### 2.1.3 Streamlines

The definition of a streamline is such that at one instant in time streamlines cannot cross; if one streamline forms a closed curve, this represents a boundary across which fluid particles cannot pass. Although a streamline has no associated cross-sectional area, adjacent streamlines may be used to define a so-called stream tube. This concept is widely used in fluid mechanics since the flow within a given stream tube may be treated as if it is isolated from the surrounding flow. As a result, the conservation equations may be applied to the flow within a given stream tube and consequently the streamline pattern Provides considerable insight into the velocity and Pressure changes. For example, if the streamlines describing an incompressible fluid flow converge, this implies that the velocity increases and the associated Pressure reduces. This can be understood by this figure-1.4

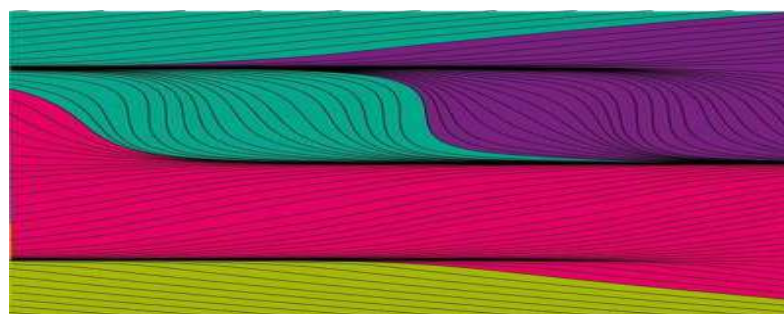
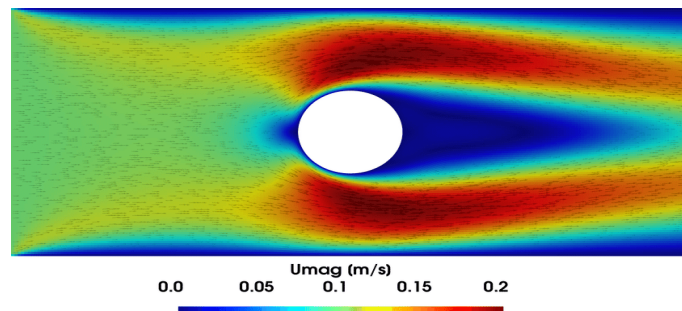


Figure-2.3: Minimalist Abstract Flow Curvy and wavy Streamlines

### 2.1.4 Laminar Flow

The flow of a viscous fluid in which particles moves in parallel layers, each of which has a constant velocity but is in motion relative to its neighboring layers is known as laminar flow. That's mean, there are no cross-currents perpendicular to the direction of the flow, nor eddies or swirls of fluids. In laminar flow, the motion is characterized by high momentum diffusion and low momentum convection.

For example, when a fluid is moving through a closed channel such as tube or between two flat plates is laminar flow.



**Figure 2.3:** 2D non uniform steady laminar channel flow around a cylinder

### 2.1.5 Mixed Convection

Mixed convection is a combination of forced and free convections which is the general case of convection when a flow is determined by both an outer force system and an inner volumetric force, by the nonuniform density distribution of a fluid medium in a gravity field. In other words, the convection heat transfer which is neither dominated by pure forced not pure free convection, but is rather a combination of the two is referred as combined or mixed convection. The most vivid manifestation of mixed convection is the motion of the temperature stratified mass of air and water areas of the Earth that the traditionally studied in geophysics. However, mixed convection is found in the systems of much smaller scales, i.e., in many engineering devices. On heating or cooling of channel walls, and at the small velocities of a fluid flow that are characteristic of a laminar flow, mixed convection is almost always realized. Pure forced laminar convection may be obtained only in capillaries. Studies of turbulent channel flows with substantial gravity field effects have actively developed since the 1960s after their becoming important in engineering Practice by virtue of the growth of heat loads and channel dimensions in modern technological applications (thermal and nuclear power engineering, pipeline transport). Mixed convection involves features from both forced and natural flow conditions. The buoyancy effects become comparable to the forced flow effects at small

and moderate Reynolds numbers. Since the flow is partly forced, a reference velocity value is normally known.

### **2.1.6 Mixed Convection Heat Transfer in Cavities**

Mixed convection in cavities is a topic of contemporary importance, because cavities filled with fluid are central components in a long list of engineering and geophysical systems. The flow and heat transfer induced in a cavity differs fundamentally from the external mixed convection boundary layer. Mixed convection in a cavity unlike the external mixed convection boundary layer that is caused by the heat transfer interaction between a single wall and a very large fluid reservoir is the result of the complex interaction between finite size fluid systems in thermal communication with all the walls that confine it. The complexity of this internal interaction is responsible for the diversity of flows that can exist inside cavity. The phenomenon of mixed convection in cavities is varied by the geometry and the orientation of the cavity. Judging by the potential engineering applications, the cavity phenomena can loosely be organized into two classes.

#### 1. Vented cavity and 2. Lid-driven cavity

In a vented cavity, where the interaction between the external forced stream provided by the inlet and the buoyancy driven flows induced by the heat source leads to the possibility of complex flows. Therefore, it is important to understand the fluid flow and heat transfer characteristics of mixed convection in a vented cavity. On the other hand, the fluid flow and heat transfer in a lid driven cavity where the flow is induced by a shear force resulting from the motion of a lid combined with the buoyancy force due to non-homogeneous temperature of the cavity wall, provides another problem, studied extensively by researchers to understand the interaction between buoyancy and shearing forces in such flow situation. The interaction between buoyancy driven and shear driven flows inside a closed cavity in a mixed convection regime is quite complex. Therefore, it is also important to understand the fluid flow and heat transfer characteristics of mixed convection in a lid-driven cavity.

### **2.1.7 Magnetohydrodynamics**

Magneto-hydrodynamics (MHD) is the academic discipline which studies the dynamics of electrically conducting fields. Examples of such fluids include plasmas, liquid metals and salt water. The word Magneto-hydrodynamics (MHD) is derived from “magneto” meaning “magnetic field”, “hydro” meaning “liquid” and “dynamics” meaning “movement”. The field of MHD was initiated by Hannes Alfvén, for which he received the Nobel Prize in

Physics in 1970. The idea of MHD is that magnetic fields can induce current in a moving conducting fluid, which create forces on the fluid and also change the magnetic field itself. The set of equations which describe MHD are a combination of the Navier-Stokes equations of fluid dynamics and Maxwell's equations of electromagnetism. These differential equations have to be solved simultaneously, either analytically or numerically. MHD is a continuum theory and as such it cannot treat kinetic phenomena, i.e. those in which the existence of discrete particles or of a non-thermal velocities distribution are important. The simple form of MHD, ideal MHD, assumes that fluid has so little resistivity that it can be treated as a perfect conductor. This is the limit of infinite magnetic Reynolds number in ideal MHD, Lenz's law dictates that the fluid is in a sense tied to the magnetic field lines. Now, here are some MHD effects on particular sectors:

- (i) MHD has the ability to create a force between two different mediums, without contact.
- (ii) MHD is that branch of science, which deals with the flow of electrically conducting fluids in electric & magnetic fields.
- (iii) This electromagnetic force generated the same order of magnitude as the hydrodynamical & inertia force. The eqn. of motion takes this force.
- (iv) MHD applied to astrophysical & geophysical problems. Such as the motion of the sea induce magnetic field that perturb the earth's magnetic field. The electromagnetic force due to the interaction of currents & earth's magnetic field propels ocean movement.
- (v) Engineers make use of MHD in their design of the heat exchanger, pumps & flow metals etc.

### **2.1.8 Boussinesq Approximation**

The Boussinesq approximation is a way to solve nonisothermal flow such as natural convection problems, without having to solve for the full compressible formulation of the Navier-Stokes equations. The Boussinesq approximation was a popular method for solving nonisothermal flow, particularly in previous years, as computational costs were lower when solving this method and convergence was more likely to be achieved. The approximation is accurate when density variations are small as this reduces the nonlinearity of the problem. It assumes that variations in density have no effect on the flow field, except that they give rise to buoyancy forces. In more practical terms, this approximation is typically used to model liquids around room temperature, natural ventilation in buildings, or dense gas dispersion in industrial set-ups.

While the Boussinesq approximation has been used to simplify the implementation of some CFD solvers, its use these days is becoming less prevalent. This is because it only slightly reduces the nonlinearity of the system and, with today's solvers and computational hardware, consequently leads to marginal reduction in computational costs.

## 2.2 Finite Element Method

The finite element method (FEM) is a powerful computational technique for solving problems which are described by partial differential equations or can be formulated as functional minimization. The basic idea of the finite element method is to view a given domain as an assemblage of simple geometric shapes, called finite elements, for which it is possible to systematically generate the approximation functions needed in the solution of partial differential equations by the variational or weighted residual method. The computational domains with irregular geometries by a collection of finite elements make the method a valuable practical tool for the solution of the boundary layer, initial and eigenvalue problems arising in various fields of engineering.

The approximation functions, which satisfy the governing equations and boundary conditions, are often constructed using ideas from interpolation theory. Approximating functions in finite elements are determined in terms of nodal values of a physical field which is sought. A continuous physical problem is transformed into a discretized finite element problem with unknown nodal values. For a linear problem, a system of linear algebraic equations should be solved. Values inside finite elements can be recovered using nodal values.

The major steps involved in finite element analysis of a typical problem are:

1. Discretization of the domain into a set of finite elements (mesh generation).
2. Weighted-integral or weak formulation of the differential equation to be analyzed.
3. Development of the finite element model of the problem using its weighted integral or weak form.
4. Assembly of finite elements to obtain the global system of algebraic equations.
5. Imposition of boundary conditions.
6. Solution of equations.
7. Post computation of solution and quantities of interest.



## 2.3 Algorithm

The algorithm was originally put forward by the iterative Newton-Raphson algorithm; the discrete forms of the continuity, momentum and energy equations are solved to find out the value of the velocity and the temperature. It is essential to guess the initial values of the variables. Then the numerical solutions of the variables are obtained while the convergent criterion is fulfilled.

The simple algorithm is shown by the flow chart below

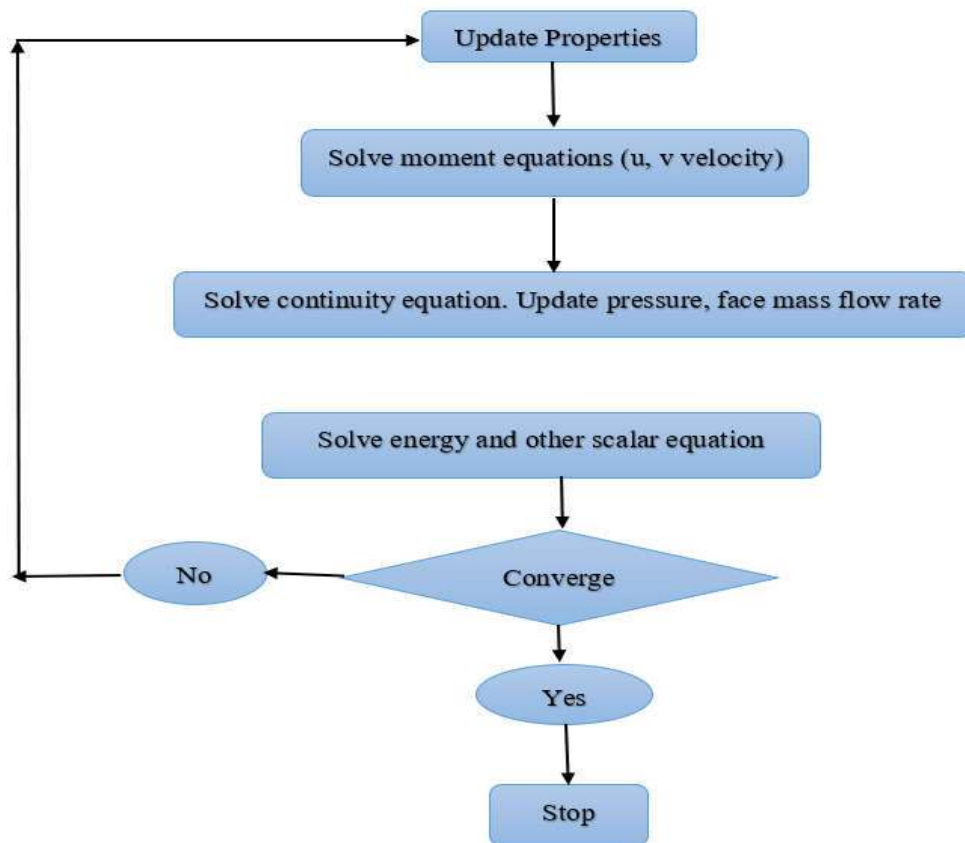


Figure 2.5: Flow chart of the computational procedure

## 2.4 Dimensionless Parameters Relating to Fluid Flows

The dimensionless parameters can be regarded as measures of the relative importance of certain aspects of the flow. Some dimensionless parameters related to our study are discussed below:

### 2.4.1 Reynolds Number (Re)

Reynolds number is an important dimensionless quantity in fluid mechanics used to help predict flow patterns in different fluid flow situations. The concept was introduced by

George Gabriel Stokes in 1851, but the Reynolds number is named after Osborne Reynolds (1842-1912), who popularized its use in 1883. The Reynolds number is defined as the ratio of momentum forces to viscous forces and consequently quantifies the relative importance of these two parts of forces for given flow conditions. This ratio is called the Reynolds number, which is a dimensionless quantity, and is defined as

$$Re = \frac{\text{Inertial Forces}}{\text{Friction Force}} = \frac{\rho u L}{\mu} = \frac{u L}{\nu}$$

Here,  $u$ ,  $L$ ,  $\rho$  and  $\mu$  are characteristic values of reference velocity, characteristic length; density and coefficient of viscosity of the fluid flow respectively and  $\nu = \frac{\mu}{\rho}$  is the kinematic viscosity.

### 2.4.2 Prandtl Number (Pr)

The Prandtl number (Pr) is a dimensionless number, defined as the ratio of momentum diffusivity (kinematic viscosity) to thermal diffusivity. It is named after the German physicist Ludwig Prandtl. It is defined as

$$Pr = \frac{\text{Viscous diffusion rate}}{\text{Thermal diffusion rate}} = \frac{\nu}{\alpha} = \frac{C_p \mu}{\kappa}$$

Where  $\nu$  is the kinematic viscosity,  $\nu = \frac{\mu}{\rho}$ ,  $\alpha$  is the thermal diffusivity and  $\alpha = \frac{\kappa}{C_p \rho}$ ,  $\mu$  is the dynamic viscosity,  $\kappa$  is the thermal conductivity,  $C_p$  is the specific heat and  $\rho$  is the density.

Small values of the Prandtl number,  $Pr \ll 1$ , means the thermal diffusivity dominates. Where with large values,  $Pr \gg 1$ , the momentum diffusivity dominates the behavior.

### 2.4.3 Grashof Number (Gr)

Grashof number (Gr) is a dimensionless number in fluid which approximates the ratio of the buoyancy to viscous force acting on a fluid. On the other hand, Grashof number is a measure of the relative magnitudes of the buoyancy force and the opposing viscous force acting on the fluid. It is named after the German mathematician Franz Grashof. The Grashof number is a way to quantify the opposing forces. Mathematically Grashof number is the ratio of buoyancy force to viscous force. It is defined as

$$Gr = \frac{\text{Buoyancy force}}{\text{Viscous force}} = \frac{g \beta (T_s - T_\infty)}{\nu^2}$$

where  $g$  is the acceleration due to gravity,  $\beta$  is the volumetric thermal expansion coefficient,  $T_s$  is the wall temperature,  $T_\infty$  is the ambient temperature,  $L$  is the characteristic length and  $\nu$  is the kinematics viscosity.

The Grashof number  $Gr$  plays same role in free convection as the Reynolds number  $Re$  plays in forced convection. As such, the Grashof number provides the main criterion in determining whether the fluid flow is laminar or turbulent in free convection. The transition to turbulent flow occurs in the range  $10^8 < Gr_L < 10^9$  for natural convection from vertical flat plates. At higher Grashof numbers, the boundary layer is turbulent; at lower Grashof numbers, the boundary layer is laminar that is in the range  $10^3 < Gr_L < 10^6$ .

#### 2.4.4 Richardson Number (Ri)

Richardson number represents the importance of natural convection relative to the forced convection. It is the dimensionless number that expresses the ratio of the buoyancy term to the flow shear term.

The Richardson number in this context is defined as

$$Ri = \frac{\text{Buoyancy term}}{\text{Flow shear term}} = \frac{g \beta (T_{hot} - T_{ref}) L}{V^2}$$

Where  $g$  is the gravitation acceleration,  $\beta$  is the thermal expansion coefficient,  $T_{hot}$  is the hot wall temperature,  $T_{ref}$  is the reference temperature,  $L$  is the characteristic length, and  $V$  is the characteristic velocity. The Richardson number can also be expressed by using a combination of the Grashof number and Reynolds number,

$$Ri = \frac{Gr}{Re^2}$$

Typically, the natural convection is negligible when  $Ri < 0.1$ , forced convection is negligible when  $Ri > 10$ , and neither is negligible when  $0.1 < Ri < 10$ . It may be noted that usually, the forced convection is large relative to natural convection except in the case of extremely low forced flow velocities. However, buoyancy often plays a significant role in defining the laminar-turbulent transition of a mixed convection flow.

#### 2.4.5 Hartmann Number (Ha)

Hartmann number ( $Ha$ ) is the ratio of electromagnetic force to the viscous force first introduced by Hartmann. It is frequently encountered in fluid flows through magnetic fields. It is defined by

$$Ha = B_0 L \sqrt{\frac{\sigma}{\mu}}$$

Where,  $B_0$  is the magnetic field,  $L$  is the characteristic length scale,  $\sigma$  is the electrical conductivity,  $\mu$  is the viscosity. In addition, it is a dimensionless quantity characterizing flow of conducting fluid in a transverse magnetic field, being the product of the magnetic

flux density, a representative length, and the square root of the ratio of electrical conductivity to viscosity.

### 2.4.6 Nusselt Number (Nu)

The Nusselt number represents the enhancement of heat transfer through a fluid layer as a result of convection relative to conduction across the same fluid layer. Nusselt number is a measure of the ratio between heat transfer by convection ( $\alpha$ ) and heat transfer by conduction alone ( $\lambda/L$ ). Nusselt number, named after German engineer Wilhelm Nusselt, Nu, is the dimensionless parameter characterizing convective heat transfer. It is defined as,

$$Nu = \frac{\text{Convective Heat Transfer}}{\text{Conductive Heat Transfer}} = \frac{hL}{\kappa}$$

where  $k$  is the thermal conductivity of the fluid,  $h$  is the heat transfer coefficient and  $L$  is the characteristic length.

In contrast to the definition given above, known as average Nusselt number, local Nusselt number is defined by taking the length to be the distance from the surface boundary to the local point of interest. If  $Nu = 1$  then for fluid layer represent heat transfer by pure conduction across layer.  $Nu \gg 1$  then Convection is more effective.

# CHAPTER 3

## Physical Model and Mathematical Formulation

### 3.1 Mathematical Modelling

Mathematical modelling is the process of using mathematics to make predictions about the world to understand situations and to assist in making decisions. The convection heat transfer which is neither dominated by pure forced nor pure free convection, rather a combination of the two, is referred to as combined or mixed convection. The generalized governing equations are used based on the conservation laws of mass, momentum and energy. As the heat transfer depends upon a number of factors, a dimensional analysis is presented to show the important non-dimensional parameters which will influence the dimensionless heat transfer parameter, i. e. Nusselt number.

In this chapter, the study of mixed convection flow around this cavity will describe part by part. First of all, I have to build the governing equation with continuity equation, Navier-Stock equation and energy equation according to Present model formulation. Then I changed the governing equations with dimensionless scale. Moreover, using Finite element method to complete the formulation of model and code validation is also workout for accuracy of the method.

### 3.2 Physical Configuration

The geometry of the wavy top cavity containing two circular cylinders with boundary conditions are considered in the present problem in figure-3.1 along with the important geometric parameters. In this figure, two semi heated cylindrical blocks are made two holes inside the wavy top cavity. The height and length of the cavity are denoted  $H$  and  $L$  gradually. The length of the cavity perpendicular to its plane is assumed to be long enough; hence the problem is considered two dimensional. The bottom wall is kept at a constant heat temperature ( $T_h$ ) whereas the wavy top wall is kept at a constant cold temperature ( $T_c$ ) maintaining  $T_h > T_c$ . The semi heated circular cylinders are kept at CP1 (0.1, 0.4) and CP2 (0.6, 0.4) of the cavity and altered the sizes (radius) of cylinders for  $r = 0.10$  m. The left and right walls of the cavity are kept adiabatic. The left wall and wavy top walls have a lid velocity where left wall moves from lower to upper and the wavy top wall moves from left to right with constant velocity. The gravitational force acts in the vertically downward direction and uniform magnetic field with a constant

magnitude( $B_0$ ) is applied parallel to the x-axis. The cavity is filled with fluid with  $Pr = 0.71$  that is considered Newtonian and incompressible where the fluid flow is assumed to be laminar. The boundary conditions for velocity have been considered as no-slip on solid boundaries. The density which varies according to the Boussinesq approximation.

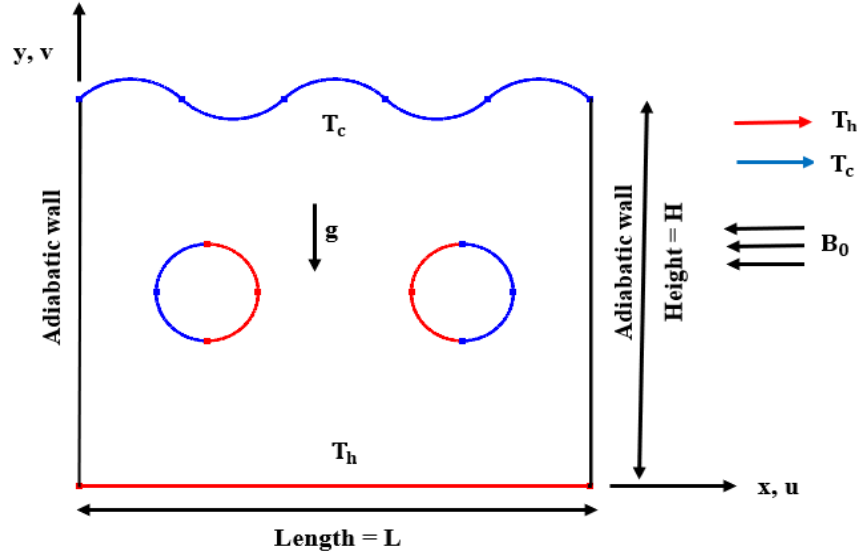


Figure 3.1: Schematic diagram of the wavy top cavity with boundary condition

### 3.3 Mathematical Formulation

The several steps of the mathematical formulation for the above physical configurations are shown as follows

#### 3.3.1 Governing equation

The fundamental laws used to solve the fluid flow and heat transfer problems are the conservation of mass (continuity equations), conservation of momentum (momentum equations), and conservation of energy (energy equations), which constitute a set of coupled, nonlinear, partial differential equations. The viscous dissipation term in the energy equation is neglected. The electrically conducting fluids are assumed to be Newtonian fluids with constant fluid properties, except for the density in the buoyancy force term. It is assumed that, Boussinesq approximation is valid and radiation made of heat transfer, joule heating and Hall effects are neglected according to other modes of heat transfer. Also, for laminar incompressible thermal flow, the buoyancy force is included here as a body force in the y-momentum equation. In general, the enclosure fluid is assumed to be Newtonian and incompressible, steady and laminar flow. The electrically conducting fluids interact with an external horizontal uniform magnetic field of constant magnetic flux density  $B_0$ . Assuming that the flow-induced magnetic field is very small

compared to  $B_0$  and considering electrically insulated cavity walls. The electromagnetic force can be reduced to the damping factor  $-\sigma B_0^2 v$ , where  $v$  is the vertical velocity component. Thus, the Lorentz force depends only on the velocity component perpendicular to the magnetic field.

Following the previous assumptions, the system of equations governing the two – dimensional form as follows:

Continuity Equation

$$\frac{\partial u}{\partial x} + \frac{\partial v}{\partial y} = 0 \quad (3.1)$$

Momentum Equations

$$u \frac{\partial u}{\partial x} + v \frac{\partial u}{\partial y} = -\frac{1}{\rho} \frac{\partial p}{\partial x} + \nu \left( \frac{\partial^2 u}{\partial x^2} + \frac{\partial^2 u}{\partial y^2} \right) \quad (3.2)$$

$$u \frac{\partial v}{\partial x} + v \frac{\partial v}{\partial y} = -\frac{1}{\rho} \frac{\partial p}{\partial y} + \nu \left( \frac{\partial^2 v}{\partial x^2} + \frac{\partial^2 v}{\partial y^2} \right) + g\beta(T - T_c) - \frac{\sigma B_0^2 v}{\rho} \quad (3.3)$$

Energy Equations

$$u \frac{\partial T}{\partial x} + v \frac{\partial T}{\partial y} = \alpha \left( \frac{\partial^2 T}{\partial x^2} + \frac{\partial^2 T}{\partial y^2} \right) \quad (3.4)$$

Where  $x$  and  $y$  are the distances measured along the horizontal and vertical directions respectively;  $u$  and  $v$  are the velocity components in the  $x$  and  $y$  directions;  $T$  denotes the fluid temperature,  $T_c$  denotes the reference temperature for which buoyant force vanishes,  $p$  is pressure,  $\rho$  is the density,  $\nu$  is the kinematic viscosity,  $\beta$  is the thermal expansion coefficient,  $g$  is the gravitational force,  $\sigma$  is the electric conductivity,  $B_0$  is the magnitude of magnetic field and  $\alpha = \frac{\kappa}{\rho C_p}$  is the thermal diffusivity of the fluid.

### 3.3.2 Dimensional Boundary Conditions

No-slip boundary conditions are used and problems are specified as follows:

On the wavy top wall:  $u = U$ ,  $v = 0$ ,  $T = T_c$

On the bottom wall:  $u = v = 0$ ,  $T = T_h$

On the right adiabatic wall:  $u = 0$ ,  $v = 0$ ,  $\frac{\partial T}{\partial x} = 0$

On the left adiabatic wall:  $u = 0$ ,  $v = V$ ,  $\frac{\partial T}{\partial x} = 0$

For circular cylinders: Cylinder CP1 left side and CP2 right side:  $u = 0, v = 0, T = T_c$

CP1 right side and CP2 left side:  $u = 0, v = 0, T = T_h$

### 3.3.3 Non-dimensional Variables

The non-dimensional parameters that are used for making the governing equations (3.1–3.4) into dimensionless form are stated as follows:

$$X = \frac{x}{L}, Y = \frac{y}{L}, U = \frac{u}{u_{lid}}, V = \frac{v}{u_{lid}}, P = \frac{p}{\rho u_{lid}}, \theta = \frac{T - T_c}{T_h - T_c}$$

The non-dimensional numbers that appear

$$Pr = \frac{\nu}{\alpha}, Gr = \frac{g\beta(T_h - T_c)L^3}{\nu^2}, Re = \frac{u_{lid}L}{\nu}, Ha = B_0L\sqrt{\frac{\sigma}{\mu}}, Ri = \frac{Gr}{Re^2}$$

Where, X and Y are the coordinates varying along horizontal and vertical directions, U and V are the velocity components in the X and Y directions respectively,  $\theta$  is the temperature, P is the dimensionless Pressure and  $\alpha$  is thermal diffusivity of the fluid respectively. The dimensionless parameters are the Prandtl number Pr, Grashof number Gr, Reynolds number Re, Hartmann number and Richardson Number.

### 3.3.4 Non-dimensional Governing Equations

The non-dimensional governing equations for steady two-dimensional mixed convection flow in the cavity after substitution the non-dimensional variables or numbers into equations (3.1 – 3.4), we get,

Continuity Equation

$$\frac{\partial U}{\partial X} + \frac{\partial V}{\partial Y} = 0 \quad (3.5)$$

Momentum Equations

$$U \frac{\partial U}{\partial X} + V \frac{\partial U}{\partial Y} = -\frac{\partial P}{\partial X} + \frac{1}{Re} \left( \frac{\partial^2 U}{\partial X^2} + \frac{\partial^2 U}{\partial Y^2} \right) \quad (3.6)$$

$$U \frac{\partial V}{\partial X} + V \frac{\partial V}{\partial Y} = -\frac{\partial P}{\partial Y} + \frac{1}{Re} \left( \frac{\partial^2 V}{\partial X^2} + \frac{\partial^2 V}{\partial Y^2} \right) + Ri\theta - \frac{Ha^2}{Re} V \quad (3.7)$$

Energy Equations

$$U \frac{\partial \theta}{\partial X} + V \frac{\partial \theta}{\partial Y} = \frac{1}{Re Pr} \left( \frac{\partial^2 \theta}{\partial X^2} + \frac{\partial^2 \theta}{\partial Y^2} \right) \quad (3.8)$$

Here Pr is Prandtl number, Gr is the Grashof number, Re is the Reynolds number, Ri is the Richardson Number and Ha is the Magnetic parameter or Hartmann number.



### 3.3.5 Non-Dimensional Boundary Conditions

On the wavy top wall:  $U = 0.5, V = 0, \theta = 0$

On the bottom wall:  $U = V = 0, \theta = 1$

On the right adiabatic wall:  $U = 0, V = 0, \frac{\partial \theta}{\partial X} = 0$

On the left adiabatic wall:  $U = 0, V = 0.5, \frac{\partial \theta}{\partial X} = 0$

For circular cylinders: Cylinder CP1 left side and CP2 right side:  $U = V = 0, \theta = 0$

CP1 right side and CP2 left side:  $U = V = 0, \theta = 1$

First, the heat transfer by conduction was equated to the heat transfer by convection

$$h * \Delta T = -\kappa \frac{\partial T}{\partial n}$$

where  $n$  is the non-dimensional distances either along  $x$  or  $y$ -direction acting normal to the surface. By introducing the dimensionless variables into equation (3.9) the local Nusselt number is defined as:

$$Nu_L = -\frac{\partial \theta}{\partial N} \Big|_{surface}$$

The average Nusselt number on the cold wall is obtained as follows:

$$Nu_{av} = -\frac{\partial \theta}{\partial N} \Big|_{surface} dS$$

## 3.4 Numerical Analysis

The governing equations along with the boundary conditions are solved numerically, employing Galerkin weighted residual finite element techniques discussed below.

### 3.4.1 Finite Element Formulation and Computational procedure

To derive the finite element equations, the method of weighted residuals Zienkiewicz and Taylor (1991) is applied to the equations (3.5) – (3.8) as

$$\int_A N_\alpha \left( \frac{\partial U}{\partial X} + \frac{\partial V}{\partial Y} \right) dA = 0 \quad (3.9)$$

$$\int_A N_\alpha \left( U \frac{\partial U}{\partial X} + V \frac{\partial U}{\partial Y} \right) dA = -\int_A H_\lambda \left( \frac{\partial P}{\partial X} \right) dA + \frac{1}{Re} \int_A N_\alpha \left( \frac{\partial^2 U}{\partial X^2} + \frac{\partial^2 U}{\partial Y^2} \right) dA \quad (3.10)$$

$$\int_A N_\alpha \left( U \frac{\partial V}{\partial X} + V \frac{\partial V}{\partial Y} \right) dA = - \int_A H_\lambda \left( \frac{\partial P}{\partial Y} \right) dA + \frac{1}{Re} \int_A N_\alpha \left( \frac{\partial^2 V}{\partial X^2} + \frac{\partial^2 V}{\partial Y^2} \right) dA \quad (3.11)$$

$$+ Ri \int_A N_\alpha \theta dA - \frac{Ha}{Re} \int_A N_\alpha V dA$$

$$\int_A N_\alpha \left( U \frac{\partial \theta}{\partial X} + V \frac{\partial \theta}{\partial Y} \right) dA = \frac{1}{Re Pr} \int_A N_\alpha \left( \frac{\partial^2 \theta}{\partial X^2} + \frac{\partial^2 \theta}{\partial Y^2} \right) dA \quad (3.12)$$

where  $A$  is the element area,  $N_\alpha$  ( $\alpha = 1, 2, \dots, 6$ ) are the element interpolation functions for the velocity components and the temperature, and  $H_\lambda$  ( $\lambda = 1, 2, 3$ ) are the element interpolation functions for the pressure.

Gauss's theorem is then applied to equations (3.10) - (3.12) to generate the boundary integral terms associated with the surface tractions and heat flux. Then equations (3.10) - (3.12) become,

$$\int_A N_\alpha \left( U \frac{\partial U}{\partial X} + V \frac{\partial U}{\partial Y} \right) dA + \int_A H_\lambda \left( \frac{\partial P}{\partial X} \right) dA \quad (3.13)$$

$$- \frac{1}{Re} \int_A \left( \frac{\partial N_\alpha}{\partial X} \frac{\partial U}{\partial X} + \frac{\partial N_\alpha}{\partial Y} \frac{\partial U}{\partial Y} \right) dA = \int_{S_0} N_\alpha S_x dS_0$$

$$\int_A N_\alpha \left( U \frac{\partial V}{\partial X} + V \frac{\partial V}{\partial Y} \right) dA + \int_A H_\lambda \left( \frac{\partial P}{\partial Y} \right) dA - \frac{1}{Re} \int_A \left( \frac{\partial N_\alpha}{\partial X} \frac{\partial V}{\partial X} + \frac{\partial N_\alpha}{\partial Y} \frac{\partial V}{\partial Y} \right) dA \quad (3.14)$$

$$- Ri \int_A N_\alpha \theta dA + \frac{Ha^2}{Re} \int_A N_\alpha V dA = \int_{S_0} N_\alpha S_y dS_0$$

$$\int_A N_\alpha \left( U \frac{\partial \theta}{\partial X} + V \frac{\partial \theta}{\partial Y} \right) dA + \frac{1}{Re Pr} \int_A \left( \frac{\partial N_\alpha}{\partial X} \frac{\partial \theta}{\partial X} + \frac{\partial N_\alpha}{\partial Y} \frac{\partial \theta}{\partial Y} \right) dA = \int_{S_w} N_\alpha q_w dS_w \quad (3.15)$$

Here (3.13) - (3.14) specifying surface tractions ( $S_x$ ,  $S_y$ ) along outflow boundary  $S_0$  and (3.15) specifying velocity components and fluid temperature or heat flux ( $q_w$ ) that flows into or out from domain along wall boundary  $S_w$ .

The basic unknowns for the above differential equations are the velocity components  $U$ ,  $V$  the temperature,  $\theta$  and the pressure,  $P$ . The six nodes triangular element is used in this work for the development of the finite element equations. All six nodes are associated with velocities as well as temperature; only the corner nodes are associated with pressure. This means that a lower order polynomial is chosen for pressure and which is satisfied through continuity equation. The velocity component and the temperature distributions and linear interpolation for the pressure distribution according to their highest derivative orders in the differential equations (3.5) - (3.8) as

$$U(X, Y) = N_{\beta} U_{\beta} \quad (3.16)$$

$$V(X, Y) = N_{\beta} V_{\beta} \quad (3.17)$$

$$\theta(X, Y) = N_{\beta} \theta_{\beta} \quad (3.18)$$

$$P(X, Y) = H_{\lambda} P_{\lambda} \quad (3.19)$$

where  $\beta = 1, 2, \dots, 6$ ;  $\lambda = 1, 2, 3$ .

Substituting the element velocity component distributions, the temperature distribution, and the pressure distribution from equations (3.16) - (3.19), the finite element equations can be written in the form,

$$K_{\alpha\beta^x} U_{\beta} + K_{\alpha\beta^y} V_{\beta} = 0 \quad (3.20)$$

$$K_{\alpha\beta^x} U_{\beta} U_{\gamma} + K_{\alpha\beta^y} V_{\beta} V_{\gamma} + M_{\alpha\mu^x} P_{\mu} + \frac{1}{Re} (S_{\alpha\beta^{xx}} + S_{\alpha\beta^{yy}}) U_{\beta} = Q_{\alpha^u} \quad (3.21)$$

$$K_{\alpha\beta^x} U_{\beta} V_{\gamma} + K_{\alpha\beta^y} V_{\beta} V_{\gamma} + M_{\alpha\mu^y} P_{\mu} + \frac{1}{Re} (S_{\alpha\beta^{xx}} + S_{\alpha\beta^{yy}}) V_{\beta} - \frac{Ra}{Re^2 Pr} K_{\alpha\beta} \theta_{\beta} + \frac{Ha^2}{Re} K_{\alpha\beta} V_{\beta} = Q_{\alpha^v} \quad (3.22)$$

$$K_{\alpha\beta^x} U_{\beta} \theta_{\gamma} + K_{\alpha\beta^y} V_{\beta} \theta_{\gamma} + \frac{1}{Re.Pr} (S_{\alpha\beta^{xx}} + S_{\alpha\beta^{yy}}) \theta_{\beta} = Q_{\alpha^{\theta}} \quad (3.23)$$

where the coefficients in element matrices are in the form of the integrals over the element area and along the element edges  $S_0$  and  $S_w$  as

$$K_{\alpha\beta^x} = \int_A N_{\alpha} N_{\beta,x} dA \quad (3.24a)$$

$$K_{\alpha\beta^y} = \int_A N_{\alpha} N_{\beta,y} dA \quad (3.24b)$$

$$K_{\alpha\beta^x} = \int_A N_{\alpha} N_{\beta} N_{\gamma,x} dA \quad (3.24c)$$

$$K_{\alpha\beta^y} = \int_A N_{\alpha} N_{\beta} N_{\gamma,y} dA \quad (3.24d)$$

$$K_{\alpha\beta} = \int_A N_{\alpha} N_{\beta} dA \quad (3.24e)$$

$$S_{\alpha\beta^{xx}} = \int_A N_{\alpha,x} N_{\beta,x} dA \quad (3.24f)$$

$$S_{\alpha\beta^{yy}} = \int_A N_{\alpha,y} N_{\beta,y} dA \quad (3.24g)$$

$$M_{\alpha\mu^x} = \int_A H_{\alpha} H_{\mu,x} dA \quad (3.24h)$$

$$M_{\alpha\mu^y} = \int_A H_\alpha H_{\mu,y} dA \quad (3.24i)$$

$$Q_{\alpha^u} = \int_{S_0} N_\alpha S_x dS_0 \quad (3.24j)$$

$$Q_{\alpha^v} = \int_{S_0} N_\alpha S_y dS_0 \quad (3.24k)$$

$$Q_{\alpha^\theta} = \int_{S_w} N_\alpha q_w dS_w \quad (3.24l)$$

These element matrices are evaluated in closed form ready for numerical simulation. Details of the derivation for these element matrices are omitted herein.

The derived finite element equations (3.20) - (3.23) are nonlinear. These nonlinear algebraic equations are solved by applying the Newton-Raphson iteration technique by first writing the unbalanced values from the set of the finite element equations (3.20) - (3.23) as,

$$F_{\alpha^p} = K_{\alpha\beta^x} U_\beta + K_{\alpha\beta^y} V_\beta \quad (3.25a)$$

$$F_{\alpha^u} = K_{\alpha\beta\gamma^x} U_\beta U_\gamma + K_{\alpha\beta\gamma^y} V_\gamma U_\gamma + M_{\alpha\mu^x} P_\mu - \frac{1}{Re} (S_{\alpha\beta^{xx}} + S_{\alpha\beta^{yy}}) U_\beta - Q_{\alpha^u} \quad (3.25b)$$

$$F_{\alpha^v} = K_{\alpha\beta\gamma^x} U_\beta V_\gamma + K_{\alpha\beta\gamma^y} V_\gamma V_\gamma + M_{\alpha\mu^y} P_\mu - \frac{1}{Re} (S_{\alpha\beta^{xx}} + S_{\alpha\beta^{yy}}) V_\beta - Ri K_{\alpha\beta} \theta_\beta - Q_{\alpha^v} \quad (3.25c)$$

$$F_{\alpha^\theta} = K_{\alpha\beta\gamma^x} U_\beta \theta_\gamma + K_{\alpha\beta\gamma^y} V_\beta \theta_\gamma - \frac{1}{Re.Pr} (S_{\alpha\beta^{xx}} + S_{\alpha\beta^{yy}}) \theta_\beta - Q_{\alpha^\theta} \quad (3.25d)$$

This leads to a set of algebraic equations with the incremental unknowns of the element nodal velocity components, temperatures, and pressures in the form,

$$\begin{bmatrix} K_{pu} & K_{pv} & 0 & 0 \\ K_{uu} & K_{uv} & 0 & K_{up} \\ K_{\theta u} & K_{\theta v} & K_{\theta\theta} & 0 \\ K_{vu} & K_{vv} & K_{v\theta} & K_{vp} \end{bmatrix} \begin{Bmatrix} \Delta p \\ \Delta u \\ \Delta \theta \\ \Delta v \end{Bmatrix} = - \begin{Bmatrix} F_{\alpha^p} \\ F_{\alpha^u} \\ F_{\alpha^\theta} \\ F_{\alpha^v} \end{Bmatrix} \quad (3.26)$$

$$\text{where } K_{uu} = K_{\alpha\beta\gamma^x} U_\beta + K_{\alpha\gamma\beta^x} U_\gamma + K_{\alpha\beta\gamma^y} V_\beta + \frac{1}{Re} (S_{\alpha\beta^{xx}} + S_{\alpha\beta^{yy}})$$

$$K_{uv} = K_{\alpha\beta\gamma^y} U_\gamma$$

$$K_{u\theta} = 0, \quad K_{up} = M_{\alpha\mu^x}$$

$$K_{vu} = K_{\alpha\beta\gamma^x} V_\gamma$$

$$K_{vv} = K_{\alpha\beta\gamma^x} U_\beta + K_{\alpha\beta\gamma^y} V_\gamma + K_{\alpha\beta\gamma^y} V_\gamma + \frac{1}{Re} (S_{\alpha\beta^{xx}} + S_{\alpha\beta^{yy}})$$

$$K_{v\theta} = -Ri K_{\alpha\beta}, K_{vp} = M_{\alpha\mu^y}$$

$$K_{\theta u} = K_{\alpha\beta\gamma^x} \theta_\gamma, K_{\theta v} = K_{\alpha\beta\gamma^y} \theta_\gamma$$

$$K_{\theta\theta} = K_{\alpha\beta\gamma^x} U_\beta + K_{\alpha\beta\gamma^y} V_\beta + \frac{1}{Re.Pr} (S_{\alpha\beta^{xx}} + S_{\alpha\beta^{yy}}),$$

$$K_{pu} = K_{\alpha\beta^x}, K_{pv} = K_{\alpha\beta^y} \text{ and } K_{\theta p} = K_{p\theta} = K_{pp} = 0$$

The iteration process is terminated if the percentage of the overall change compared to the previous iteration is less than the specified value.

To solve the sets of the global nonlinear algebraic equations in the form of matrix, the Newton-Raphson iteration technique has been adapted through PDE solver with MATLAB interface. The convergence of solutions is assumed when the relative error for each variable between consecutive iterations is recorded below the convergence criterion  $\varepsilon$  such that

$$|\Psi^{n+1} - \Psi^n| < \varepsilon, \text{ where } n \text{ is number of iteration and } \Psi = U, V, \theta.$$

The convergence criterion was set to  $\varepsilon = 10^{-5}$ .

### 3.4.2 Grid Size Sensitivity Test

Preliminary results are obtained to inspect the field variables grid independence solutions. In order to obtain a grid independent solution, a grid refinement study is performed for a wavy top wall containing two circular cylinders with  $Pr = 0.71$ ,  $Ri=1.0$  and  $Ha= 50$ .

Number of Degrees	Elements	$Nu_{av}$
4404	1763	1.79412
5560	2248	1.80056
7840	3271	1.80579
20344	8879	1.81482
54392	24540	1.81635
67388	31038	1.81648

**Table 3.1:** Grid sensitivity check at  $Pr = 0.71$ ,  $Ri = 1.0$  and  $Ha = 50$ 

Six different non-uniform grids with the following number of nodes and elements were considered for the grid refinement tests. Six different non-uniform grids the elements 1763, 2248, 3271, 8779, 24540 and 31038 are considered for the grid refinement test with their nodes. It is observed that grid independence is achieved with 24540 elements where there is a significant change in  $Nu$  with a further increase of mesh elements. Therefore, all calculations are done using this grid resolution. This is described in Table 3.1 and as seen in Figure 3.2. Test for the accuracy of grid fineness has been carried out to find out the optimum grid number.

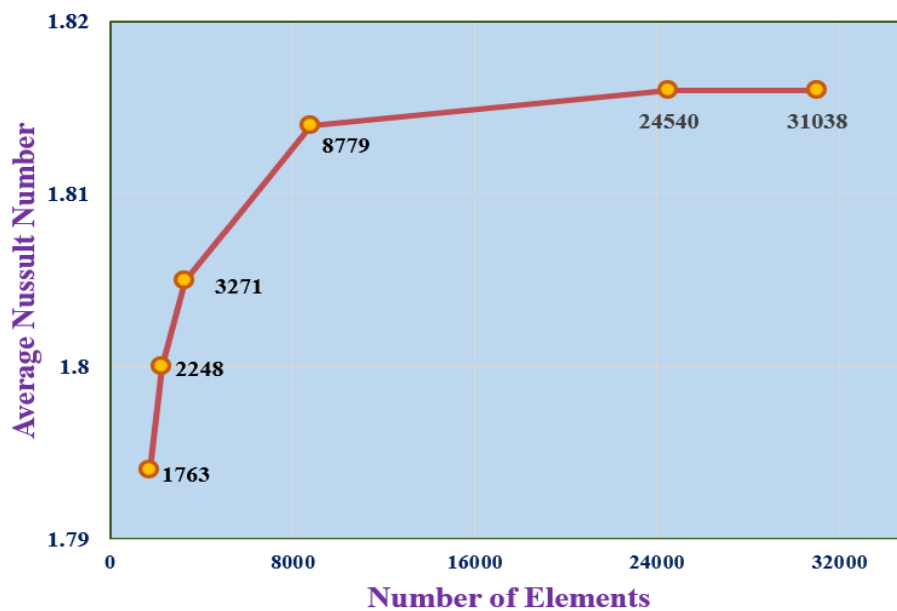


**Figure 3.2:** Grid independency study for different elements while  $Pr = 0.71$ ,  $Ri = 1$ ,  $Ha = 50$

### 3.4.3 Mesh Generation

Mesh generation is the practice of creating a mesh, a subdivision of a continuous geometric space into discrete geometric and topological cells. Usually, the cells partition the geometric input domain. Mesh cells are used as discrete local approximations of the larger domain. A mesh that covers the geometric domain which the problem is to be solved specifies the discrete positions at which the variables are to be computed. It divides the solution domain into finite elements, which are sub – domains with a finite number of domains. The method's use of a set of finite elements to create computational domains with irregular geometries makes it a useful tool for solving boundary value problems in a wide range of engineering areas. The present numerical technique will discretize the computational domain into unstructured triangles by Delaunay Triangular method. The

Delaunay triangulation is a geometric structure that has enjoyed great popularity in mesh generation since the mesh generation was in its infancy. In two dimensions, the Delaunay triangulations of a vertex set. Figure – 3.3 shows the mesh mode for the present numerical computation. Mesh generation has been done meticulously.

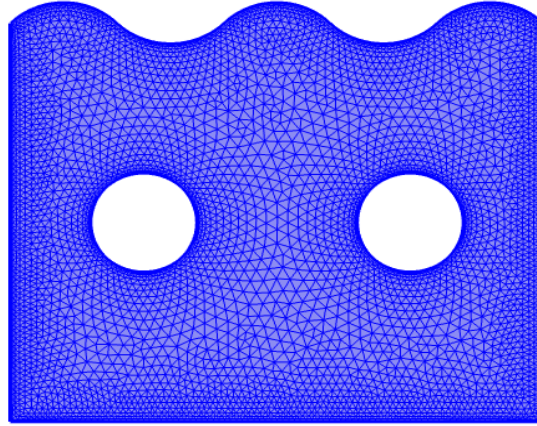


**Figure – 3.3:** Mesh generation of mixed convection in lid-driven wavy top cavity.

#### 3.4.4 Program validation and comparison with Previous work

For the validation of the code, a hexagonal cavity with MHD is considered by finite element weighted residual method whose inclined left wall and right walls (i.e. side walls) are subjected to cold  $T_c$  temperature, top and bottom walls are subjected to uniformly hot  $T_h$  temperature. In order to check the accuracy of the numerical results obtained in this problem, the average Nusselt number was compared with the results presented by Ali et al. [20] at  $Pr = 1.42$ ,  $Ri = 1.0$  and  $Re = 100$ . To validate the numerical model and the solution procedure of the present study, the present results obtained for magnetic field effects are compared with the results of Ai et al. [20] considering similar enclosure with similar boundary conditions that is shown in Table 3.2. Table 3.2, a comparison between the average Nusselt numbers is presented. The results from the present experiment are almost same as Ali et al. [20].

<b>Ha</b>	<b>Ali et al. [20] (<math>Nu_{av}</math>)</b>	<b>Present work (<math>Nu_{av}</math>)</b>
<b>0</b>	4.33	4.30
<b>10</b>	4.05	4.01
<b>20</b>	3.97	3.72
<b>50</b>	3.93	3.54

**Table 3.2:** Comparison of average Nusselt number ( $Nu_{av}$ ) for various Hartmann number

The Present numerical code is validated against the problem magnetohydrodynamic mixed convection flow in a hexagonal enclosure studied by Ali et al. [20]. Validation of the code has done by comparing streamlines and isotherms results are shown in Figure-3.4. As seen from this figure the obtained results which showed a good agreement. This validation boosts the confidence in the numerical outcome of the Present work.

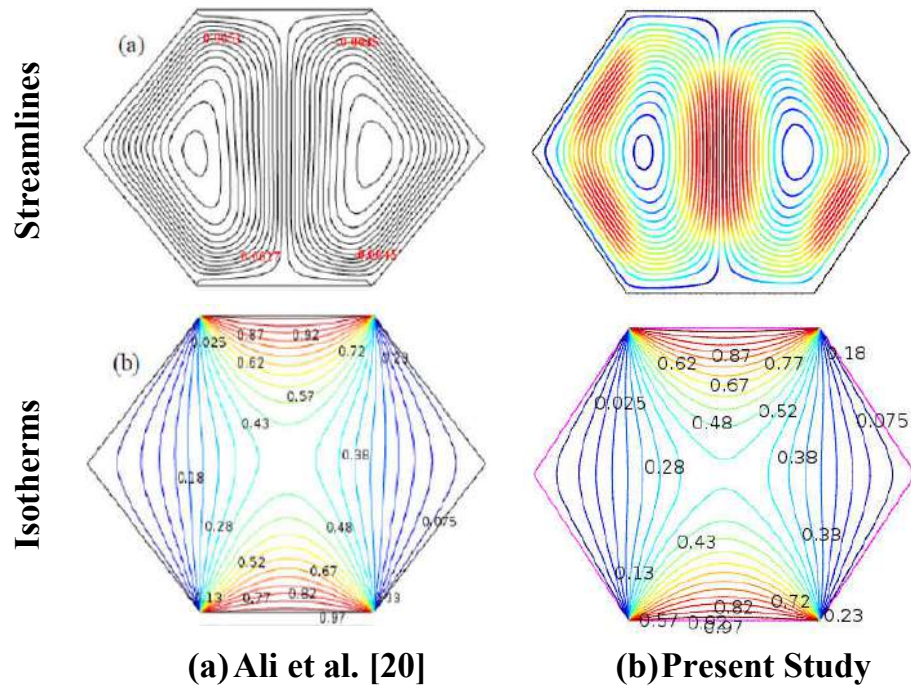


**Figure 3.4:** Code validation of the streamlines and isotherms for numerical solution between the (a) Ali et al. [20] and (b) Present work



# CHAPTER 4

## Result and Discussion

### 4.1 Introduction

As portrayed earlier, the overall objective of the current chapter is to explore the outcome and discussion of this thesis. The effects of cylinders location and size on MHD mixed convection flow and temperature fields as well as heat transfer rates of the fluid inside a lid-driven wavy top cavity has been numerically investigated with the help Galerkin finite element method. Numerical results have been delimited in order to determine the effects of the considered parameters. The result of this thesis has been shown part by part with some individual appraisal. Finally, the results have been displayed in terms of streamlines, isotherms, average velocity magnitude, Local Nusselt Number, average Nusselt number and related graphs and charts.

### 4.2 Case – I (Variation of cylinders position)

The influences of the different positions of the semi heated cylinders inside the wavy top square cavity have been performed in terms of different non-dimensional numbers. In this case, the semi heated cylinder's position (CP2) is considered at various places in the wavy top square cavity while CP1 remaining at (0.10, 0.40) & CP2 (0.60, 0.40). It has supposed to take only three locations of cylinder CP2 out of multiple positions. The positions have been considered at (0.60, 0.40), (0.60, 0.25) and (0.60, 0.55) of the wavy top square cavity. Effects of Richardson number (Ri), Hartmann number (Ha) and Heat transfer rates have discussed in this case.

#### 4.2.1 Effect of cylinders position at CP1(0.10, 0.40) & CP2(0.60, 0.40)

In this section, results of the numerical investigation of mixed convection heat transfer in presence of magnetic field in a lid-driven wavy top cavity having circular cylinders are numerically presented. The results have been obtained cylinders position CP1 (0.10, 0.40) and CP2 (0.60, 0.40) for the Richardson number, Hartmann number and the rate of heat transfer. The results of this parametric study are shown in Figure 4.1- 4.7 respectively.

##### 4.2.1.1 Effect of Richardson number

The effects of Richardson number (Ri) on streamlines and isotherms for the present configuration at  $Ha = 10$ ,  $Pr = 0.71$  has been demonstrated in Figure 4.1(a)–(b). In this

section, the cylinder's positions are CP1 at (0.10, 0.40) and CP2 is at (0.60, 0.40) of the cavity and the size (radius)  $r = 0.10$  m.

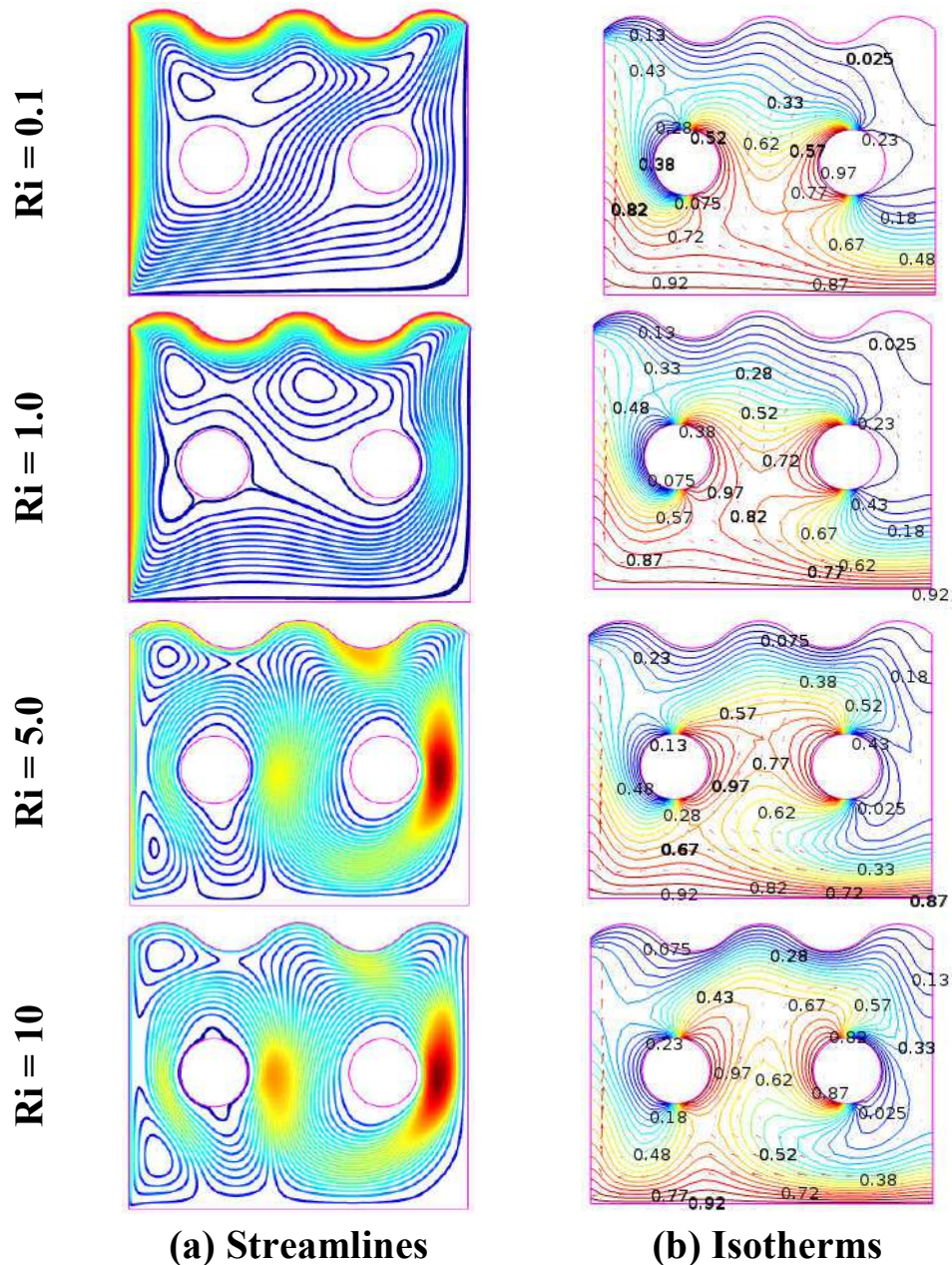


**Figure 4.1:** Effect of Richardson number on (a) streamlines and (b) isotherms for  $Pr = 0.71$ ,  $Ha = 10$  while CP1 are at (0.10, 0.40) and CP2 is at (0.60, 0.40) and  $r = 0.10$  m.

Richardson number represents the relative importance of mixed convection or combined forced convection and free convection. From Figure 4.1 (a), it is seen that when  $Ri = 0.1$  the strength of buoyancy force inside the cavity is significant and one vortex appear inside the cavity generated by the movement of the lid wall. Knowing the flow rate of velocity there has a great impact on streamlines. This is because the flow rate is changing with

streamlines. In which side the velocity has been changing, the streamlines are changed that particular way with a different value of the dimensionless number. It is observed that the velocity magnitude is increasing quickly with the increase of Richardson number from  $Ri = 0.1$  to 10 for cylinders positions CP1(0.10,0.40) and CP2 (0.60,0.40) inside the cavity. Again, when  $Ri = 1$  the flow structure is similar to  $Ri = 0.1$  but two vortices appear inside the cavity which one is major vortex and another one is a minor vortex. Further again when Richardson number increases ( $Ri = 5$  and 10), the strength of the buoyancy force is more significant. The physical fact behind it's that the greater effect of the Richardson number increases the buoyancy force to influence the flow field.

Conduction dominant heat transfer from the isotherms is exhibited in Figure 4.1 (b) at Radius,  $r = 0.10$  m,  $Pr = 0.71$  and  $Ha = 10$ . The heated isothermal lines have been changed their directions gradually for different  $Ri$ . The curvature of the isotherms increases with increasing  $Ri$  and the heat lines are condensed between the semi heated cylinders, which means increasing heat transfer through convection.

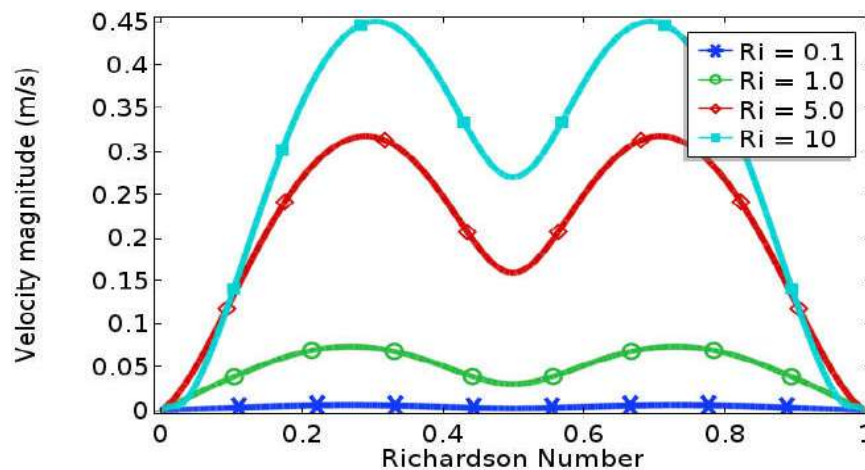


**Figure 4.2:** Variation of velocity profiles along the line  $y = 0.1$  of cavity for  $Ha = 10$ ,  $Pr = 0.71$  and  $r = 0.10$  m varying  $Ri$

The effect of Richardson number ( $Ri$ ) on the vertical component of the velocity profiles along the line  $y = 0.1$  of the cavity at  $r = 0.10$  m and  $Ha = 10$  is displayed in Figure 4.2. It can be seen from the figure that for lower values of Richardson number, velocity profiles bring smaller change but the higher value of Richardson number, velocity profiles cause larger change. The velocity profile increases with the increasing of Richardson Number. For  $Ri = 0.1$  the velocity is like straight line but for Richardson number  $Ri = 5.0$  and 10 one concave down and two concave up.

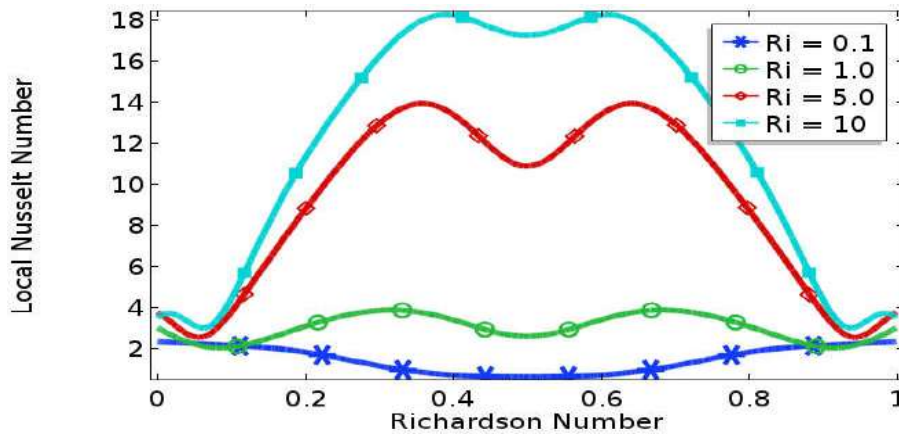


**Figure 4.3:** Variation of local Nusselt number along the line  $y = 0.1$  of cavity with Richardson number for  $Pr = 0.71$ ,  $Ha = 10$

The variation of the local Nusselt number distribution alongside the bottom heated wall of the enclosure for  $Pr = 0.71$  and  $Ha = 10$  varying Richardson number ( $Ri$ ) is shown in Figure 4.3. It can be seen from the figure that the local Nusselt number increases with increasing Richardson number in a major portion of the bottom heated wall.

#### 4.2.1.2 Effects of Hartmann number

The influence of Hartman number on the streamlines and isotherms for different values of  $Ha$  with  $Ri = 1.0$ ,  $Pr = 0.71$  has been demonstrated in Figure 4.4 (a)–(b) respectively.

From Figure 4.4 (a) it can be seen that when  $Ha = 0$  the strength of buoyancy force inside the cavity is more significant and two vortices appear inside the cavity which one is major vortex is produced by the movement of the lid wall and another one is minor vortex produced by the right half of the cavity. Again, when  $Ha = 10$  and  $30$  the strength of buoyancy force inside the cavity is significant and two vortices appear inside the cavity. Further again when  $Ha = 50$ , produced one vortex appear inside the cavity generated by the movement of the lid wall. The physical fact behind it's that the flow circulation decreases with increasing Hartmann number (increasing the strength of the magnetic field). This is because; applied magnetic field tends to slow down the fluid motions within the cavity. This means that the flow field strongly depends on the effect magnetic field.

On the other hand, conduction dominant heat transfer is observed from the isotherms are almost similar and uniformly distributed due to the greater values of Hartmann number ( $Ha$ ) is shown in Figure 4.4 (b); which is consistent to the effect of the magnetic field.

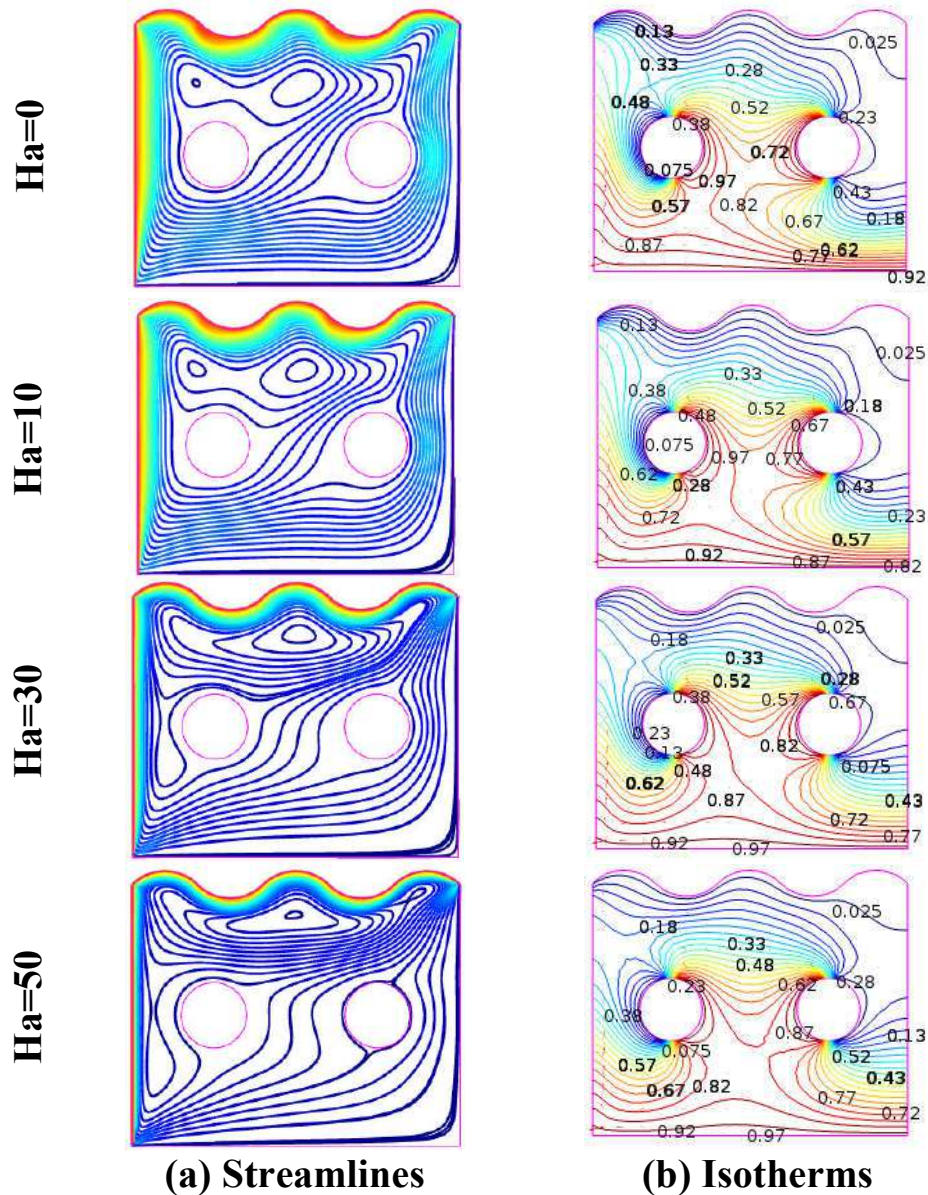


**Figure 4.4:** Effect of Hartmann number on (a) streamlines and (b) isotherms for  $Pr = 0.71$ ,  $Ri = 1.0$  while CP1 are at  $(0.10, 0.40)$  and CP2 is at  $(0.60, 0.40)$  and  $r = 0.10$  m.

The effect of Hartmann number ( $Ha$ ) on the vertical component of the velocity profiles along the line  $y = 0.1$  of the cavity at  $r = 0.10$  m,  $Pr = 0.71$  and  $Ri = 1.0$  is displayed in Figure 4.5. It can be observed that the changing rate of velocity is decreasing for every Hartmann number. It can be seen from the figure that for higher values of Hartmann number, velocity profiles bring smaller change but the lower value of Hartmann number, velocity profiles cause larger change.

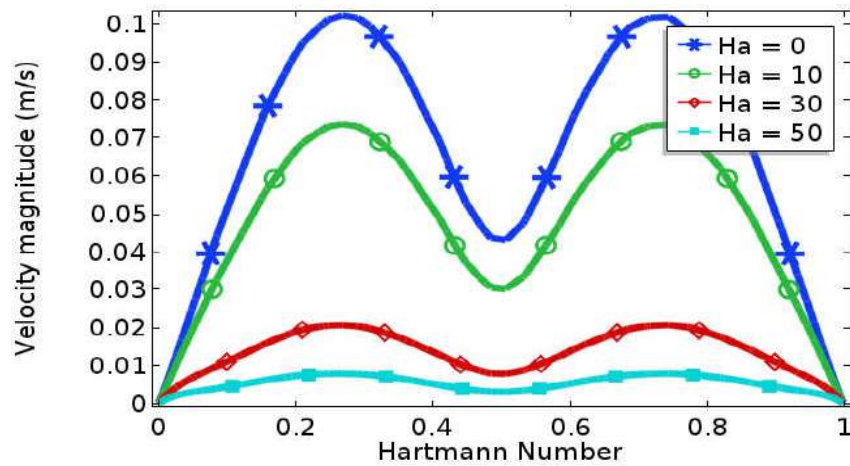


**Figure 4.5:** Variation of velocity profiles along the line  $y = 0.10$  of cavity for  $Ri = 1.0$ ,  $Pr = 0.71$  and  $r = 0.10$  m varying  $Ha$

The variation of the local Nusselt number distribution along the line  $y = 0.10$  of the enclosure for  $Pr = 0.71$  and  $Ri = 1$  varying Hartmann number ( $Ha$ ) is shown in Figure 4.6. It can be seen from the figure that the changing rate of local Nusselt number is increasing for increasing Hartmann number  $Ha = 0, 10$ . Again the change rate of local Nusselt number is decreasing for increasing Hartmann number  $Ha = 30$  and  $50$ . Moreover, the local Nusselt number has one concave up and two concaves down for  $Ha = 0$  and  $10$ .

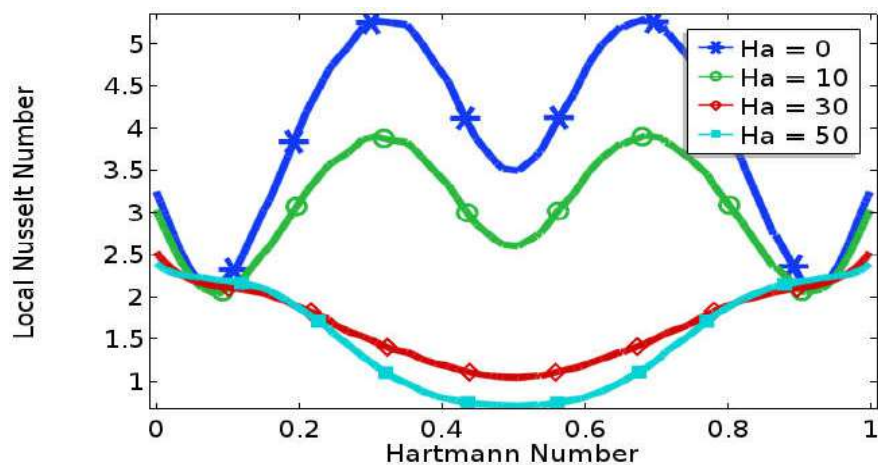


**Figure 4.6:** Variation of local Nusselt number along the line  $y = 0.10$  of cavity for  $Ri = 1.0$ ,  $Pr = 0.71$  and  $r = 0.10$  m varying  $Ha$

### 4.2.1.3 Heat Transfer Rates

In this section, results of the numerical investigation of mixed convection heat transfer in presence of magnetic field in a lid-driven wavy cavity having vertical fin are numerically

presented. The average Nusselt number versus Hartmann numbers and Richardson numbers heat transfer rates are shown in Figure 4.7 given below.

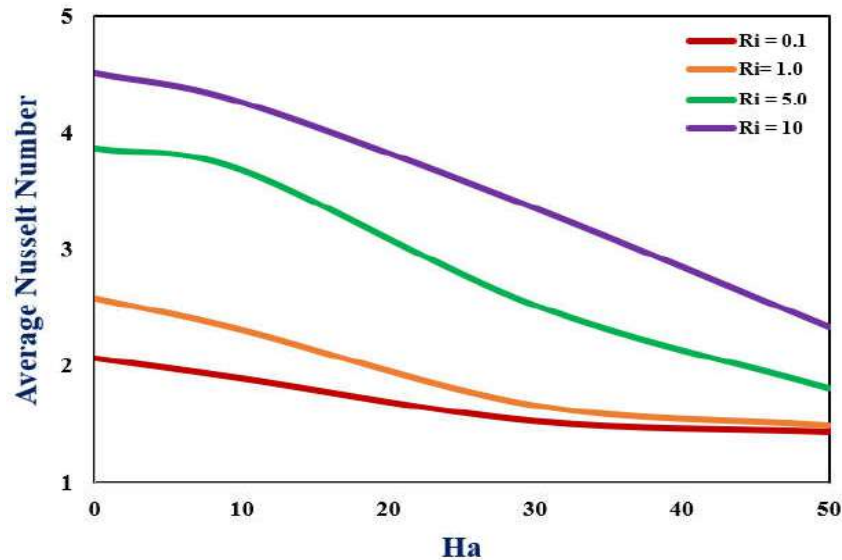


**Figure 4.7:** Variation of the average Nusselt number against  $Ha$  for selected value  $Ri$  while  $Pr = 0.71$ ,  $r = 0.10$  m at CP1(0.1, 0.4) & CP2 (0.1, 0.6)

Figure 4.7 illustrate that the average Nusselt number ( $Nu_{av}$ ) versus Hartmann number along the heated bottom wall for various Richardson number ( $Ri$ ) with  $r = 0.10$  m and  $Pr = 0.71$  while the value of the remaining parameters is kept fixed. It can be seen from this Figure, the average Nusselt number increases when the value of the Richardson number increases.

#### 4.2.2 Effect of cylinders position at CP1(0.10, 0.40) & CP2(0.60, 0.55)

In this section, results of the numerical investigation of mixed convection heattransfer in presence of magnetic field in a lid-driven wavy top cavity having circular cylinders are numerically presented. The results have been obtained cylinders position at CP1 (0.10, 0.40) and CP2 (0.60, 0.55) for the Richardson number, Hartmann number and the rate of heat transfer.

##### 4.2.2.1 Effect of Richardson number

The effects of Richardson number  $Ri$  ( $= 0.1, 1, 5, 10$ ) on streamlines and isotherms for the present configuration at  $Ha = 10$ ,  $Pr = 0.71$ ,  $r = 0.1$  m has been demonstrated in figure 4.8 (a)–(b) respectively. In this section, the cylinder's positions CP1 are at (0.10, 0.40) and CP2 is at (0.60, 0.55) of the cavity and the size (radius)  $r = 0.10$  m.

From Figure 4.8 (a), it is seen that when  $Ri = 0.1$  the strength of buoyancy force inside the cavity is significant and one vortex appear inside the cavity generated by the movement of

the lid wall. It is observed that the velocity magnitude is increasing quickly with the increase of Richardson number from  $Ri = 0.1$  to 10 for cylinders positions  $CP1(0.10,0.40)$  and  $CP2(0.60, 0.55)$  inside the cavity. Again, when  $Ri = 1$  the flow structure is similar to  $Ri = 0.1$  but two vortices appear inside the cavity which one is major vortex and another one is a minor vortex. But at  $Ha = 30$  and 50 the vortex of the size is changed and core of vortex shifted to the circular shape.

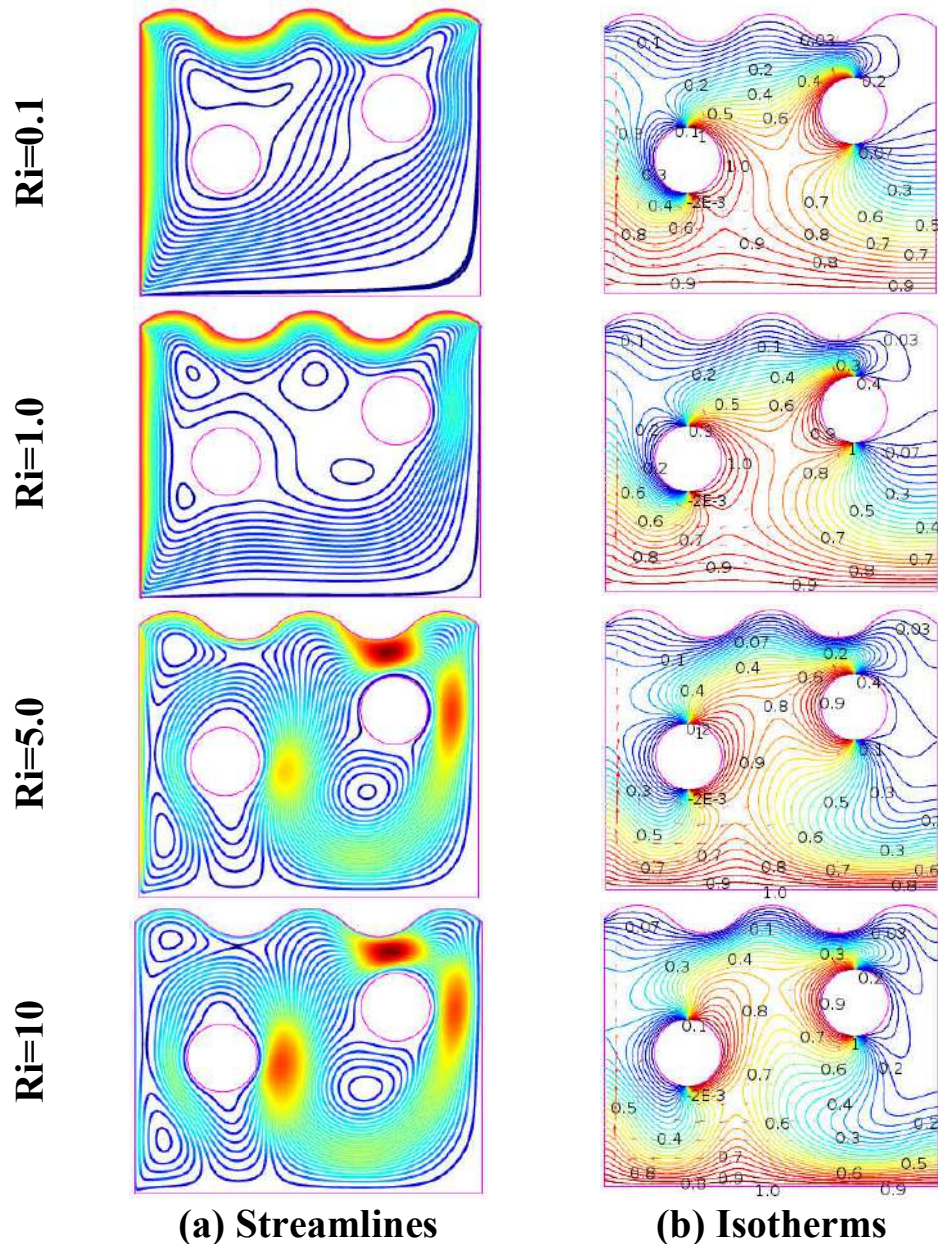


**Figure 4.8:** Effect of Richardson number on (a) streamlines and (b) isotherms for  $Pr = 0.71, Ha = 10$  while  $CP1$  are at  $(0.10, 0.40)$  and  $CP2$  is at  $(0.60, 0.55)$  and  $r = 0.10$  m.

Conduction dominant heat transfer from the isotherms is exhibited in Figure – 4.8 (b) when  $Pr = 0.71$  and  $Ha = 10$ . The heated isothermal lines have been changed their



directions gradually for different  $Ri$ . The curvature of the isotherms increases with increasing  $Ri$  and the heat lines are condensed to the semi heated circular cylinders and the bottom wall, which means increasing heat transfer through convection.

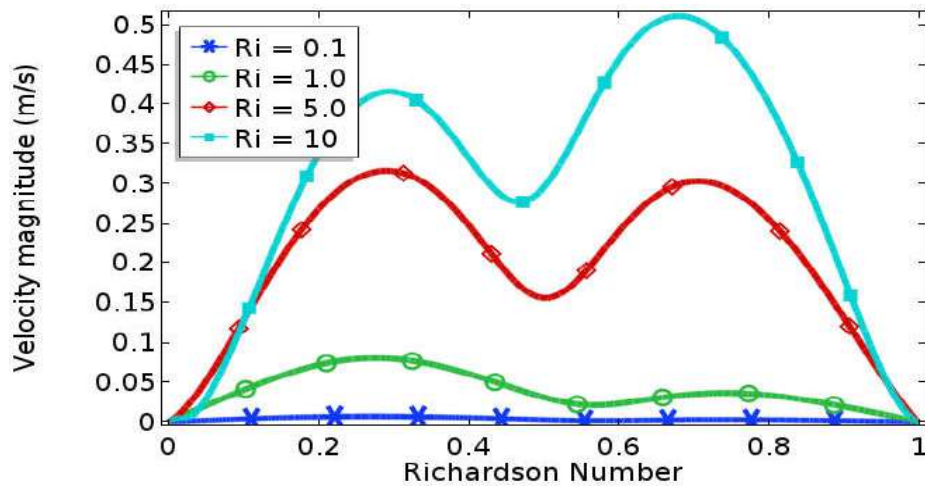


**Figure 4.9:** Variation of velocity profiles along the line  $y = 0.10$  of cavity for  $Ha = 10$ ,  $Pr = 0.71$  and  $r = 0.10$  m varying  $Ri$

The effect of Richardson number ( $Ri$ ) on the vertical component of the velocity profiles along the horizontal line of the cavity at  $r = 0.10$  m and  $Ha = 10$  is displayed in Figure 4.9. It can be seen from the figure that for lower values of Richardson number, velocity profiles bring smaller change but the higher value of Richardson number, velocity profiles cause larger change. Moreover, the absolute value of the maximum and minimum value of the velocity increases with increasing Richardson number (increasing the buoyancy force).

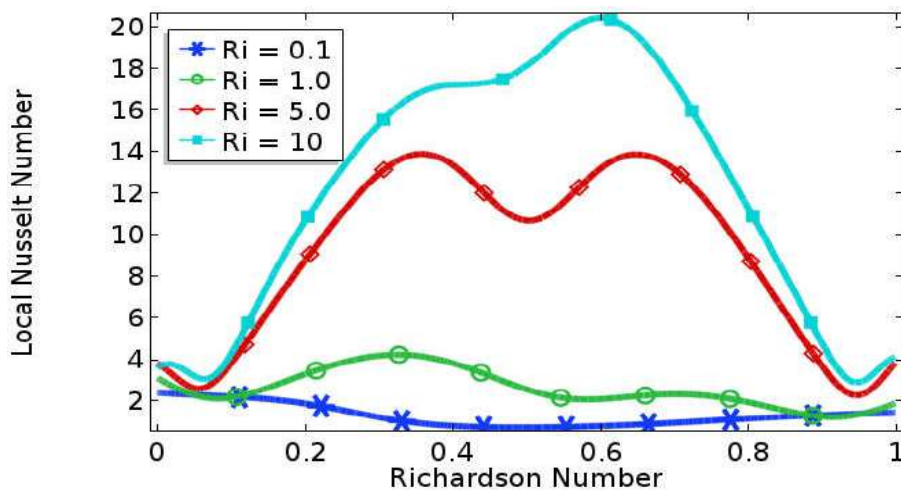


**Figure 4.10:** Variation of local Nusselt number along the line  $y = 0.10$  of cavity with Richardson number for  $Pr = 0.71$ ,  $Ha = 10$

The variation of the local Nusselt number distribution along the bottom heated wall of the enclosure for  $Pr= 0.71$  and  $Ha= 10$  varying Richardson number ( $Ri$ ) is shown in Figure 4.10. It can be seen from the figure that the local Nusselt number increases with increasing Richardson number in a major portion of the bottom heated wall.

#### 4.2.2.2 Effects of Hartmann number

A numerical analysis has been performed in this research to investigate the effects of Hartmann number ( $Ha$ ) of the semi heated cylinders in the cavity while  $Ri$  and  $Pr$  are fixed at 1.0 and 0.71 respectively.

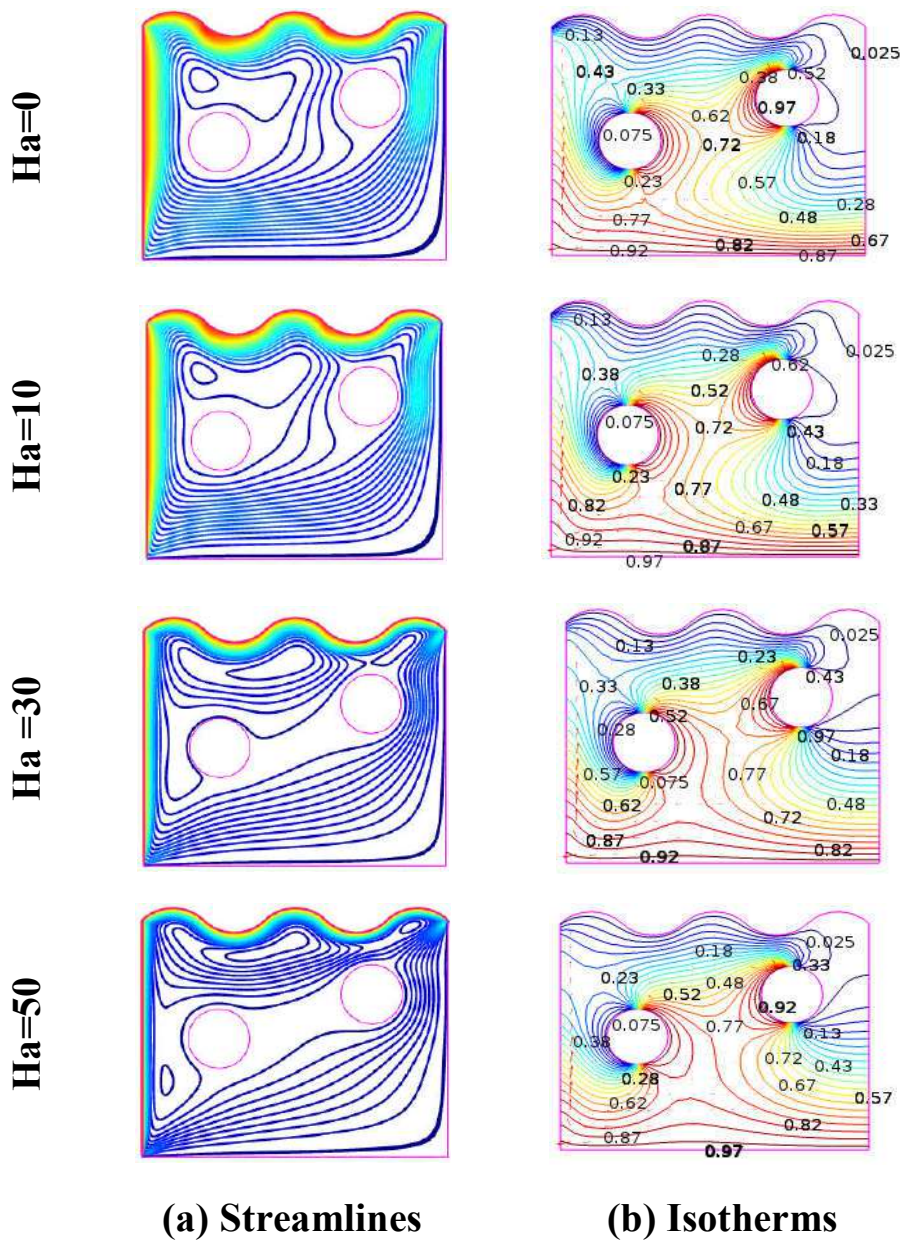


**Figure 4.11:** Effect of Hartmann number on (a) streamlines and (b) isotherms for  $Pr = 0.71$ ,  $Ri = 1.0$  and  $r = 0.10$  m

The influence of Hartman number on the streamlines and isotherms for different values of  $Ha (= 0, 10, 30, 50)$  with  $Ri = 1.0$ ,  $Pr = 0.71$ ,  $r = 0.1$  m has been demonstrated in figure 4.11 (a)–(b) in terms of dimensionless velocity profiles and local Nusselt number along the line  $y = 0.10$  of the cavity are shown in Figure 4.12 and Figure 4.13 respectively. From Figure 4.11 (a) it can be seen that when  $Ha = 0$  and  $10$  the strength of buoyancy force inside the cavity is more significant and two vortices appear inside the cavity which one major vortex is produced by the movement of the lid wall and another one is minor vortex is produced by the right half of the cavity. For Hartmann number  $Ha = 0$  and  $10$  the flow circulations are almost same and made an elliptic shape near the wavy wall. Again, when  $Ha = 30$  the strength of buoyancy force inside the cavity is significant and two vortices appear inside the cavity. Further again when  $Ha = 50$ , produced are also two vortices appear inside the cavity. The physical fact behind it's that the flow circulation decreases with increasing Hartmann number (increasing the strength of the magnetic field). This is because; applied magnetic field tends to slow down the fluid motions within the cavity. This means that the flow field strongly depends on the effect magnetic field.

On the other hand, conduction dominant heat transfer is observed from the isotherms are almost similar and uniformly distributed due to the greater values of Hartmann number ( $Ha$ ) is shown in Figure 4.11 (b); which is consistent to the effect of the magnetic field. Moreover, those lines are quite similar to the variation of  $Ha$  without changing the point place.

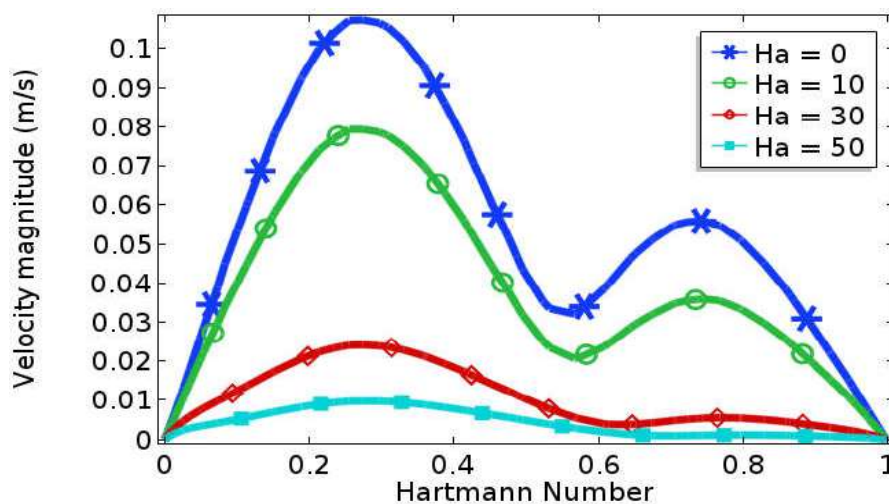


**Figure 4.12:** Variation of velocity profiles along the line  $y = 0.1$  of cavity for  $Ri = 1.0$ ,  $Pr = 0.71$  and  $r = 0.10$  m varying  $Ha$

The effect of Hartmann number (Ha) on the vertical component of the velocity profiles along the horizontal line of the cavity at  $r = 0.1$  m,  $Pr = 0.71$  and  $Ri = 1.0$  is displayed in Figure 4.12. It can be observed that the changing rate of velocity is decreasing for every Hartmann number. It can be seen from the figure that for higher values of Hartmann number, velocity profiles bring smaller change but the lower value of Hartmann number, velocity profiles cause larger change.

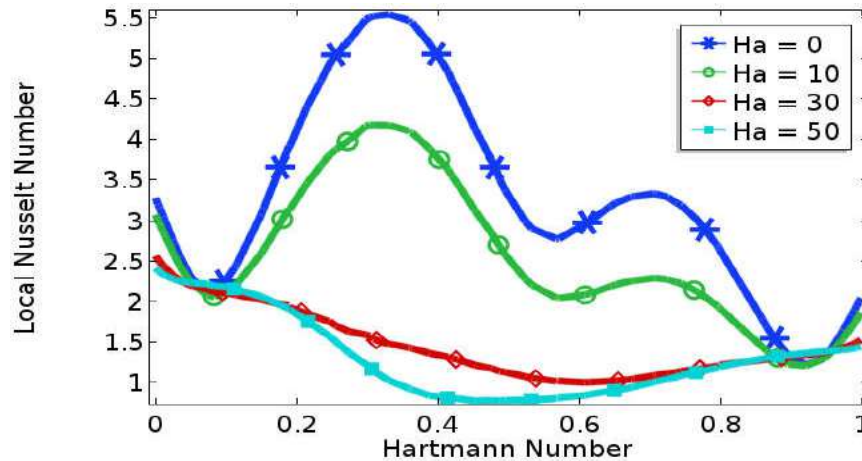


**Figure 4.13:** Variation of local Nusselt number along the line  $y = 0.1$  of cavity for  $Ri = 1$  and  $Pr = 0.71$  varying  $Ha$

The variation of the local Nusselt number distribution along the line  $y = 0.1$  of the enclosure for  $Pr = 0.71$  and  $Ri = 1$  varying Hartmann number ( $Ha$ ) is shown in Figure 4.13. It can be seen from the figure that the changing rate of local Nusselt number is increasing for Hartmann number  $Ha = 0$  and  $Ha = 10$  but decreasing for  $Ha = 30$  and  $Ha = 50$ . Moreover, the local Nusselt number has one concave up and two concave down the effect of Hartmann number for  $Ha = 0$  and  $Ha = 10$ .

#### 4.2.2.3 Heat Transfer Rates

In this section, the effects of Richardson number on average Nusselt number at the heat source is displayed as a function of Hartmann number at some particular Richardson number in Figure 4.14 in below. Figure 4.14 illustrate that the average Nusselt number ( $Nu_{av}$ ) versus Hartmann number along the heated bottom wall for various Richardson number ( $Ri$ ) with Radius  $r = 0.1$  m and  $Pr = 0.71$  while the value of the remaining parameters is kept fixed. It can be seen from this Figure, the average Nusselt number increases when the value of the Richardson number increases. At a constant Richardson number, with a decrease in Hartmann number the buoyancy force increases and the heat transfer is enhanced.

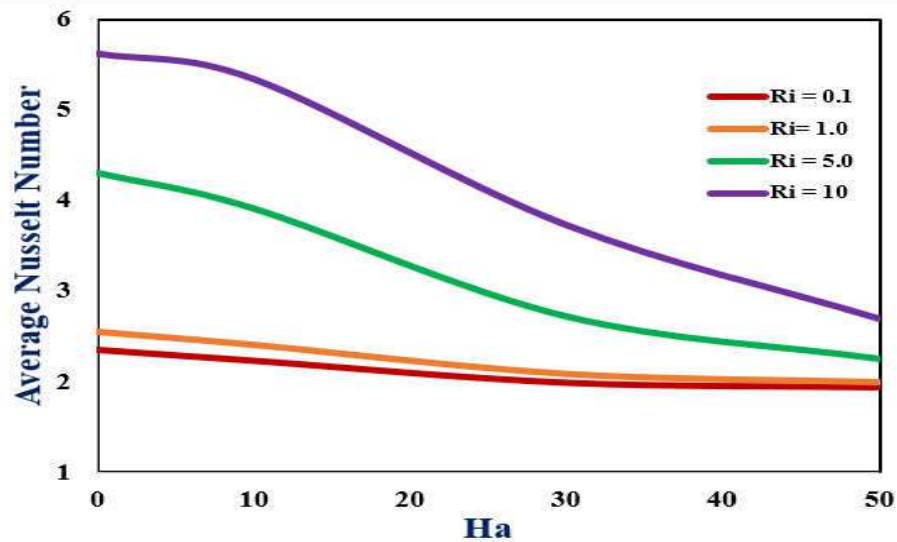


**Figure 4.14:** Variation of the average Nusselt number against  $Ha$  for selected value  $Ri$  while  $Pr = 0.71$ , CP1(0.1, 0.4) CP2 (0.1, 0.55) and  $r = 0.10$  m

### 4.2.3 Effect of cylinders position at CP1(0.10, 0.40) & CP2(0.60, 0.25)

In this section, the results have been obtained cylinders position CP1 (0.10, 0.40) and CP2 (0.60, 0.25) for the Richardson number, Hartmann number and the rate of heat transfer. The results of this parametric study are shown in Figure 4.19- 4.27 respectively.

#### 4.2.3.1 Effects of Richardson number

The effects of Richardson number  $Ri$  ( $= 0.1, 1, 5, 10$ ) on streamlines and isotherms for the present configuration at  $Ha = 10$ ,  $Pr = 0.71$ ,  $r = 0.1$  m has been demonstrated in figure 4.15 (a)–(b) respectively where the cylinder's positions (CP1) are at (0.10, 0.40) and CP2 is at (0.60, 0.25) of the cavity and the size (radius)  $r = 0.10$  m.

From Figure 4.15 (a), it is observed that the velocity magnitude is increasing quickly with the increase of Richardson number from  $Ri = 0.1$  to 10. Again, when  $Ri = 1$  the flow structure is similar to  $Ri = 0.1$  but two vortices appear inside the cavity which one is major vortex and another one is a minor vortex. Further again when Richardson number increases ( $Ri = 5$  and 10), the strength of the buoyancy force is more significant. Since the cylinder position CP2 is considered near the heated bottom wall, so with increasing the  $Ri$  values from 5 to 10 some heated lines are also noticed inside the cavity.

Conduction dominant heat transfer from the isotherms is exhibited in Figure 4.15 (b) when  $Pr = 0.71$  and  $Ha = 10$ . The heated isothermal lines have been changed their directions gradually for different  $Ri$ . The curvature of the isotherms increases with increasing  $Ri$  and

the heat lines are condensed between two semi heated cylinders and the heated bottom, which means increasing heat transfer through convection.

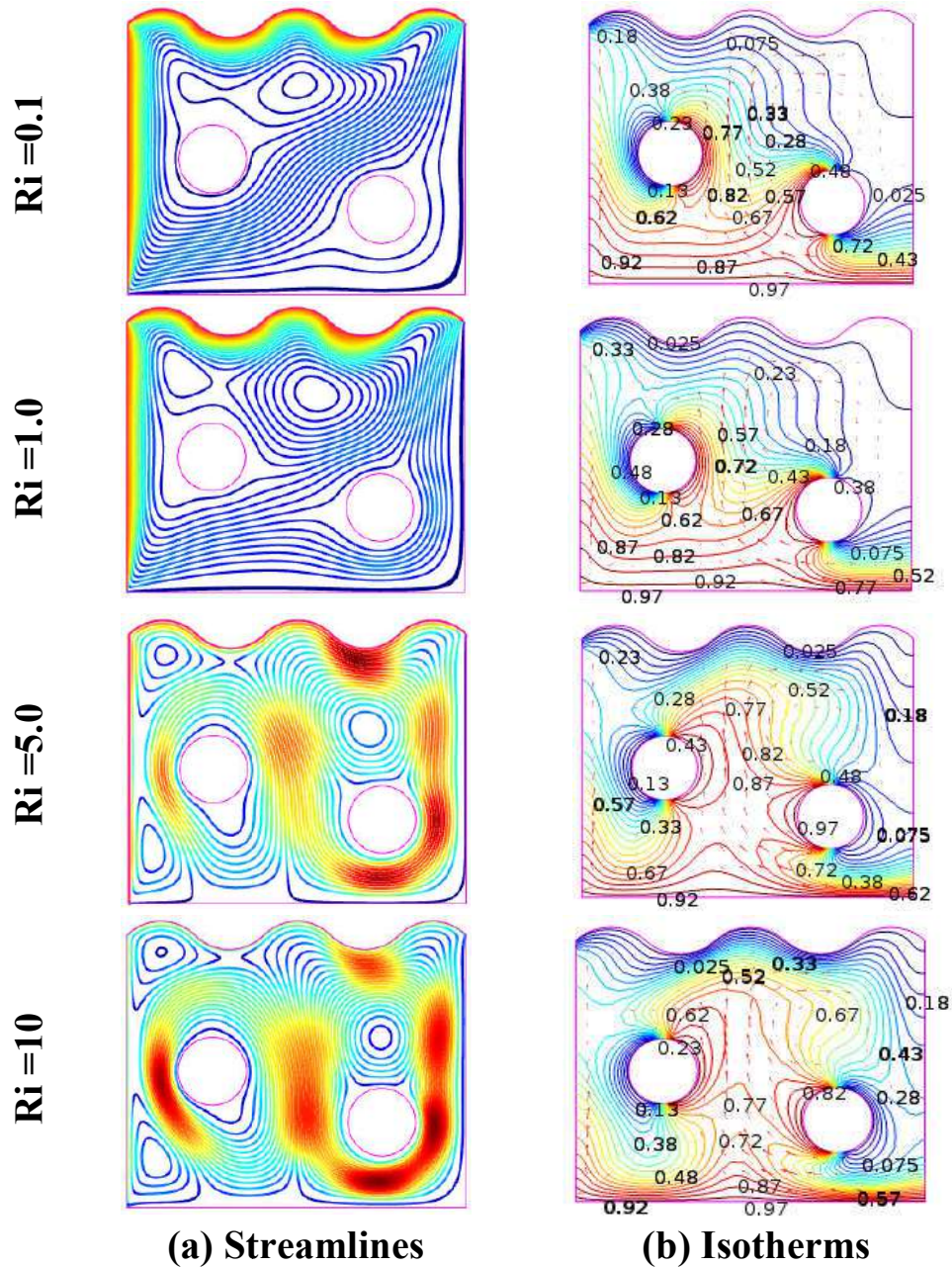


**Figure 4.15:**Effect of Richardson number on (a) streamlines and (b)isotherms for  $Pr=0.71$ ,  $Ha = 10$  where  $r = 0.10$  m.

The effect of Richardson number ( $Ri$ ) on the vertical component of the velocity profiles along the horizontal line of the cavity at  $r = 0.10$  m and  $Ha = 10$  is displayed in Figure 4.16. It can be seen from the figure that for lower values of Richardson number, velocity profiles bring smaller change but the higher value of Richardson number, velocity profiles cause larger change.

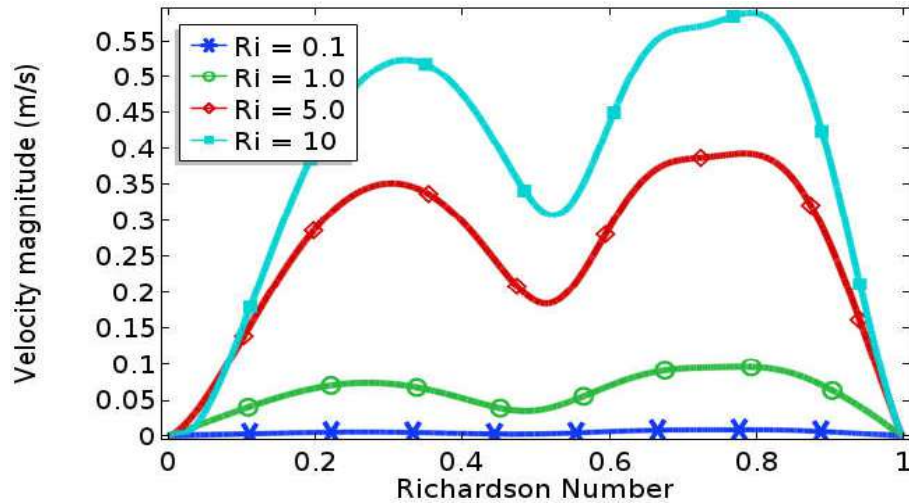


**Figure 4.16:** Variation of velocity profiles along the line  $y = 0.10$  of cavity for  $Ri = 1.0$  and  $Pr = 0.71$  varying  $Ha$

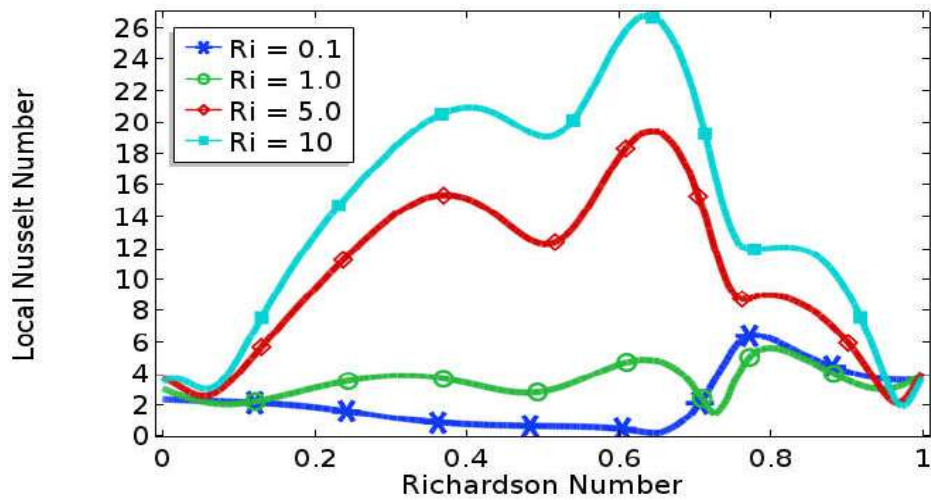


**Figure 4.17:** Variation of local Nusselt number along the line  $y = 0.10$  of cavity with Richardson number for  $Pr = 0.71$ ,  $Ha = 10$

The variation of the local Nusselt number of the enclosure for  $Pr = 0.71$  and  $Ha = 10$  varying Richardson number ( $Ri$ ) is shown in Figure 4.17. It can be seen from the figure that the local Nusselt number increases with increasing Richardson number in a major portion of the bottom heated wall. From the graph, it is seen that the impact of local Nusselt number is much more around the heat bars.

#### 4.2.3.2 Effects of Hartmann number

The influence of Hartman number on the streamlines and isotherms for different values of  $Ha (= 0, 10, 30, 50)$  with  $Ri = 1.0$ ,  $Pr = 0.71$ ,  $r = 0.1$  m has been demonstrated in figure

4.18(a)–(b) in terms of dimensionless velocity profiles and Local Nusselt Number are shown in Figure 4.19 and Figure 4.20 respectively.

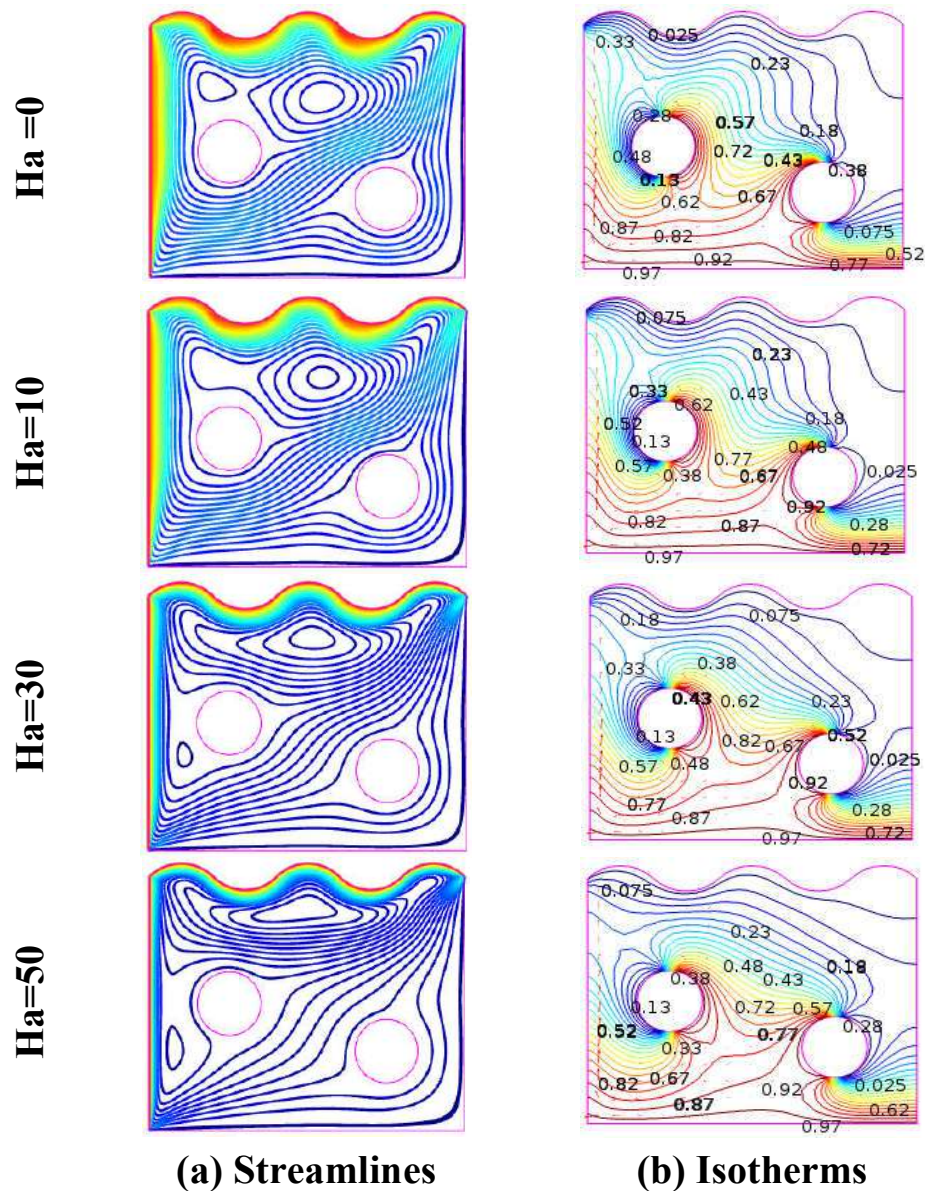


**Figure 4.18:** Effect of Hartmann number on (a) streamlines and (b) isotherms for  $Pr=0.71$ ,  $Ha = 10$  while  $CP1$  are at  $(0.10, 0.40)$  and  $CP2$  is at  $(0.60, 0.55)$  and  $r = 0.10$  m.

In this case, the cylinders positions are kept  $CP1$  at  $(0.1, 0.4)$  and  $CP2$  at  $(0.6, 0.4)$ . From Figure 4.18 (a) it can be seen that when  $Ha = 0$  and to the strength of buoyancy force inside the cavity is more significant and two vortices appear inside the cavity which one major vortex is produced by the movement of the lid wall and another one is minor vortex is produced by the right half of the cavity. Further again when  $Ha= 30$  and  $50$ , produced are also two vortices appear inside the cavity. It can be seen that one oval shape of eddy is formed near the lid wavy wall. The physical fact behind it's that the flow circulation



decreases with increasing Hartmann number (increasing the strength of the magnetic field). This is because; applied magnetic field tends to slow down the fluid motions within the cavity. This means that the flow field strongly depends on the effect of a magnetic field.

On the other hand, conduction dominant heat transfer is observed from the isotherms are almost similar and uniformly distributed due to the greater values of Hartmann number ( $Ha$ ) is shown in Figure 4.18 (b); which is consistent to the effect of the magnetic field. From figure it is shown that all those lines conjugated beside the lid walls and the heat lines are seen between the two cylinders and the heated bottom wall.

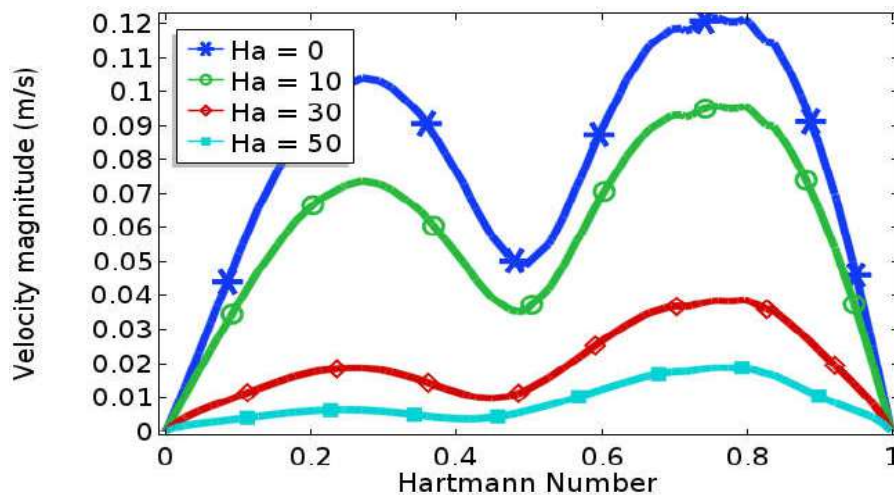


**Figure 4.19:** Variation of velocity profiles along the line  $y = 0.10$  of cavity for  $Ri = 1.0$ ,  $Pr = 0.71$  and  $r = 0.10$  m varying  $Ha$

The effect of Hartmann number ( $Ha$ ) on the vertical component of the velocity profiles along the horizontal line of the cavity at  $r = 0.1$  m,  $Pr = 0.71$  and  $Ri = 1.0$  is displayed in Figure 4.19. It can be observed that the changing rate of velocity is decreasing for increasing every Hartmann number. It can be seen from the figure that for higher values of Hartmann number, velocity profiles bring smaller change but the lower value of Hartmann number, velocity profiles cause larger change.

The variation of the local Nusselt number distribution along the line  $y = 0.1$  of the enclosure for  $Pr = 0.71$  and  $Ri = 1$  varying Hartmann number ( $Ha$ ) is shown in Figure 4.20. It can be seen from the figure that the changing rate of local Nusselt number is increasing for Hartmann number  $Ha = 0$  and  $Ha = 10$  but decreasing for  $Ha = 30$  and  $Ha = 50$ . Moreover, the local Nusselt number has one concave up and two concave down the effect of Hartmann number for  $Ha = 0$  and  $Ha = 10$ .

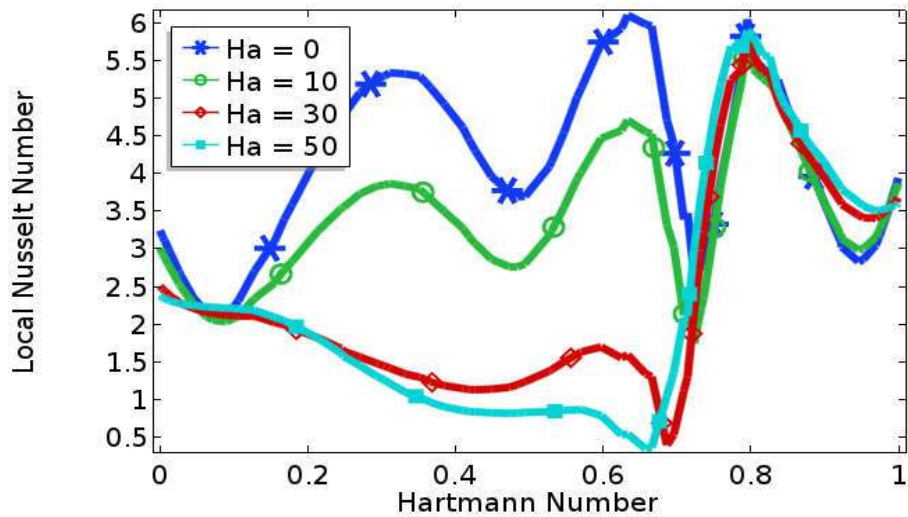


**Figure 4.20:** Variation of local Nusselt number along the line  $y = 0.10$  of cavity for  $Ri = 1$  and  $Pr = 0.71$  varying  $Ha$

#### 4.2.3.3 Heat Transfer Rates

The average Nusselt number versus Hartmann numbers and Richardson numbers heat transfer rates are shown in Figure 4.21 given below.

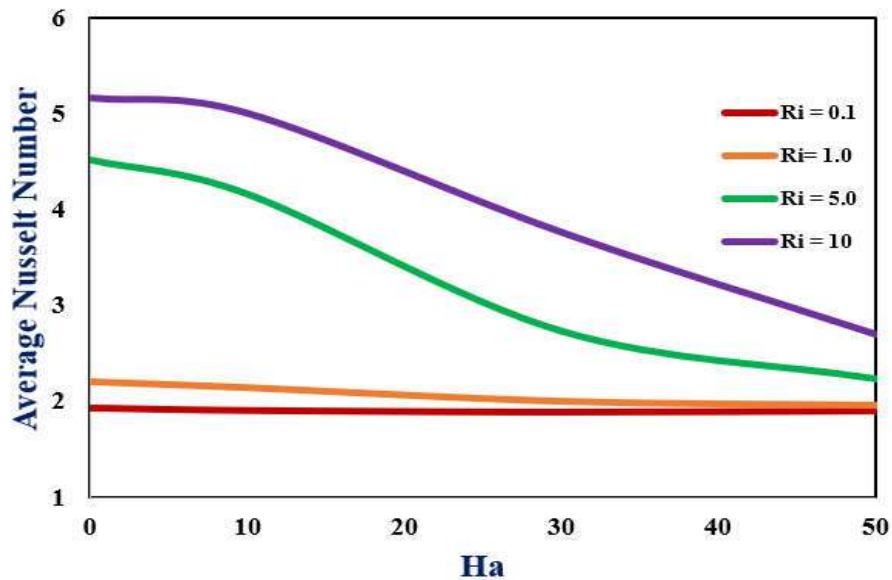


**Figure 4.21:** Variation of the average Nusselt number against  $Ha$  for selected value  $Ri$  while  $Pr = 0.71$ ,  $r = 0.10$  m

Figure 4.21 illustrate that the average Nusselt number ( $Nu_{av}$ ) versus Hartmann number along the heated bottom wall for various Richardson number ( $Ri$ ) with Radius  $r = 0.1$  m and Prandtl number  $Pr = 0.71$  while the value of the remaining parameters is kept fixed. It can be seen from this Figure, the average Nusselt number increases when the

value of the Richardson number increases. At a constant Richardson number, with a decrease in Hartmann number the buoyancy force increases and the heat transfer is enhanced.

### 4.3 Case – II (Variation of cylinders size)

In this case, the size of the semi heated cylinders has been altered from  $r = 0.10$  to  $0.20$  m and the position of the cylinders have been kept at CP1 (0.1, 0.4) & CP2 (0.60, 0.40) of the cavity. It is supposed to take only three sizes of the cylinder whose radius are  $r = 0.10$ ,  $0.15$  and  $0.20$  m, respectively. Effects of Richardson number (Ri), Hartmann number (Ha) and the heat transfer rates have been discussed in this case.

#### 4.3.1 Effect of cylinders size when $r = 0.10$ m

In this section, the results have been obtained cylinders size  $r = 0.10$  m for the Richardson number, Hartmann number and the rate of heat transfer. Since the cylinders position are kept at CP1 (0.10, 0.40) and CP2 at (0.60,0.40) and the size of radius is  $r = 0.10$  m, so the results for the effect of the Richardson numbers, Hartmann numbers and Heat Transfer rates are same as Case – I first condition 4.2.1 – Effect of cylinders position when CP1 (0.10, 0.40) & CP2 (0.60, 0.40). Hence, the Streamlines, Isotherms, Velocity profiles, Temperature profiles, Local Nusselt number and Average Nusselt numbers are also similar which are shown in Figure 4.1- 4.7 respectively.

#### 4.3.2 Effect of cylinders size when $r = 0.15$ m

The influences of  $r = 0.15$  m of the semi heated cylinders at (0.10, 0.40) & (0.60, 0.40) of the wavy top cavity have been performed in terms of different non-dimensional numbers. The results have been obtained cylinders size  $r = 0.15$  m for the Richardson number, Hartmann number and the rate of heat transfer. The results of this parametric study are shown in Figure 4.22 - 4.28 respectively.

##### 4.3.2.1 Effect of Richardson Number

The effects of Richardson number ( $Ri = 0.1, 1.0, 5.0, 10$ ) on streamlines for the present configuration for  $Ha = 10$  and  $Pr = 0.71$  is exhibited in fig. 4.22 (a). It is observed in the Fig. 4.28 (a) that the strength of the velocity magnitude increases with the increase of Richardson number (Ri) from  $Ri = 0.1$  to  $10$  for  $r = 0.15$  m of the semi heated cylinders in the cavity. The biggest vorticity of the streamlines is viewed at  $r = 0.15$  m in the cavity where  $Ri = 5$  and  $10$ ,  $Ha = 10$  and  $Pr = 0.71$ .

Fig. 4.22(b) displays the isothermal lines for different Richardson numbers with  $r = 0.15$  m of the semi heated cylinders in the cavity. A few numbers of heated isotherms are congested between the semi heated cylinders and the bottom heated wall when  $Ri = 5.0$ ,  $10.0$  when the radius,  $r = 0.15$  m.

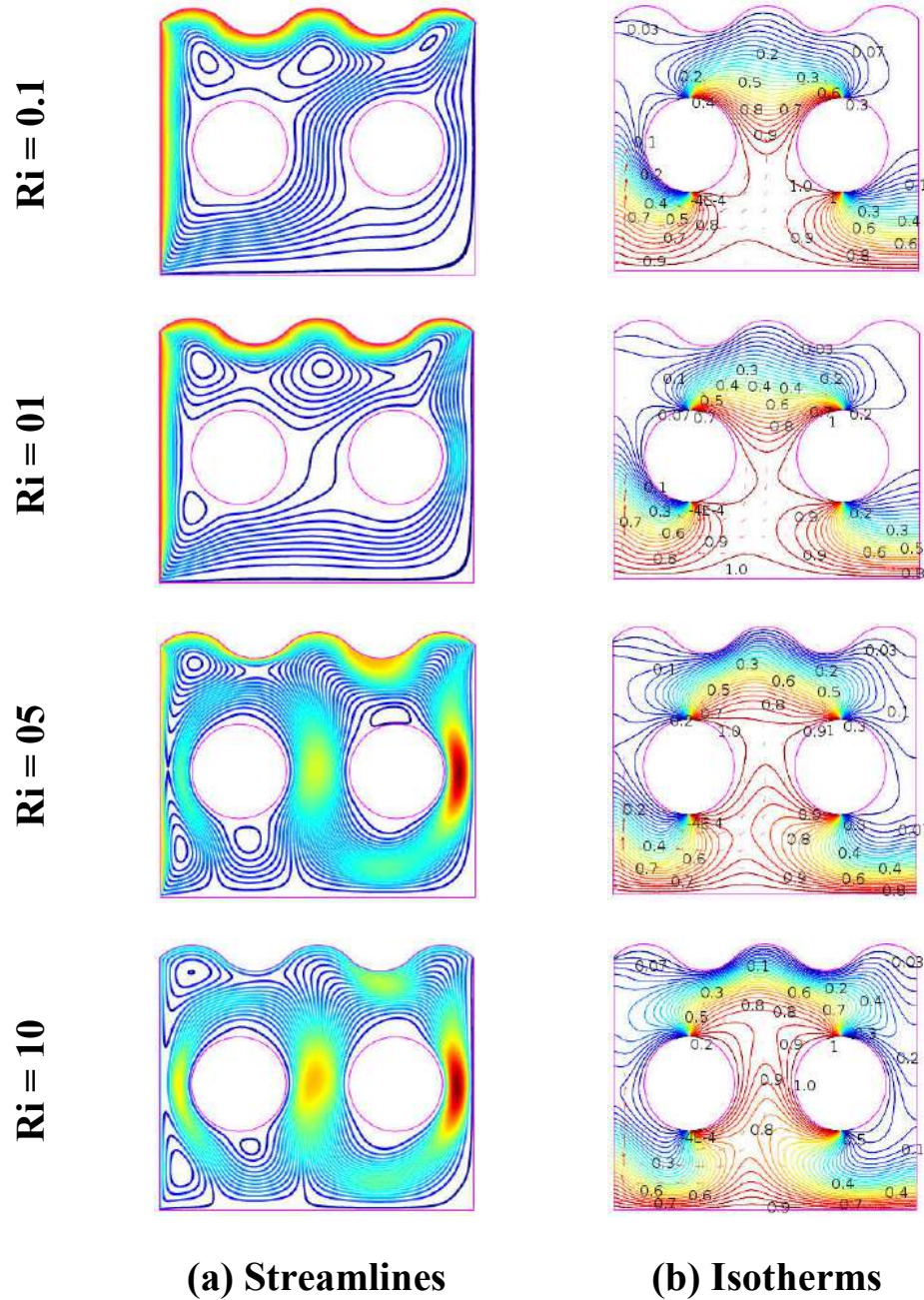


**Figure 4.22:** Effect of Richardson number on (a) streamlines and (b) isotherms for  $Pr = 0.71$ ,  $Ri = 1.0$  and  $r = 0.15$  m

The effect of Richardson number ( $Ri$ ) on the vertical component of the velocity profiles along the line  $y = 0.1$  of the cavity at  $r = 0.15$  m and  $Ha = 10$  is displayed in Figure 4.23. It can be seen from the figure that for lower values of Richardson number, velocity profiles

bring smaller change but the higher value of Richardson number, velocity profiles cause larger change.

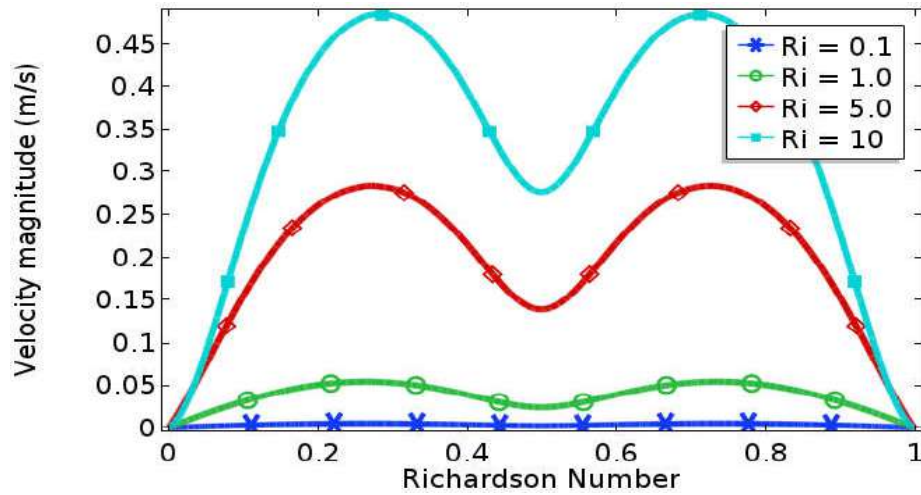


**Figure 4.23:** Variation of velocity profiles along the horizontal centre line of cavity with Richardson number for  $Pr = 0.71$ ,  $Ha = 10$

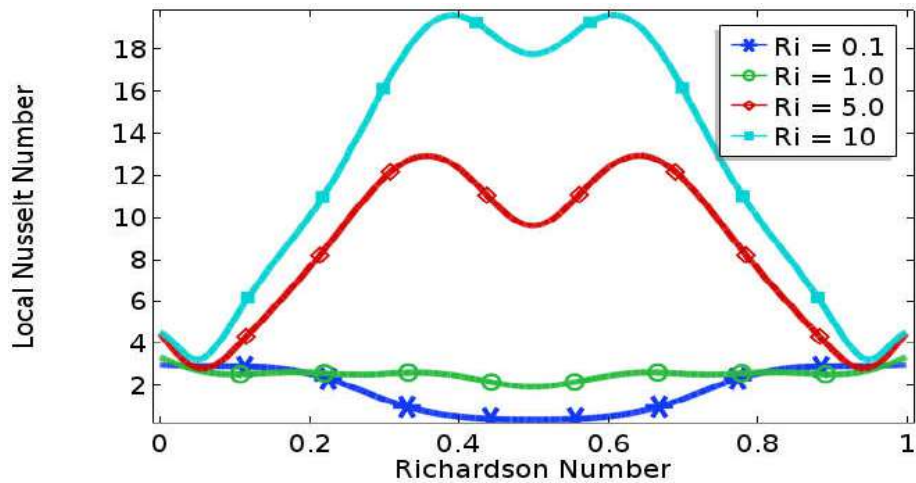


**Figure 4.24:** Variation of local Nusselt number along the line  $y = 0.10$  of cavity with Richardson number for  $Pr = 0.71$ ,  $Ha = 10$

The variation of the local Nusselt number distribution alongside the bottom heated wall of the enclosure for  $Pr = 0.71$  and  $Ha = 10$  varying Richardson number ( $Ri$ ) is shown in Figure 4.24. It can be seen from figure that local Nusselt number increases with increasing  $Ri$ .

#### 4.3.2.2 Effect of Hartmann Number

A mathematical study has been executed in this section to examine the effects of Hartmann number ( $Ha$ ) with  $r = 0.15$  m of the semi heated cylinders in the cavity.

The investigated results have been shown in terms of streamlines, isotherm lines, velocity profile, temperature profile, Local Nusselt Number and average Nusselt number. Fig 4.25

(a) explores the streamlines for different Hartmann number with the radius size  $r = 0.15$  m of the semi heated cylinders where CP1 (0.1, 0.4) & (0.60, 0.40),  $Pr = 0.71$ ,  $Ri = 0.1$ . It inquired into in Fig. 4.25 (a) that the strength of the velocity magnitude reduces for all sizes of the semi heated cylinders when the Hartmann number ( $Ha$ ) is altered from 0 to 50.

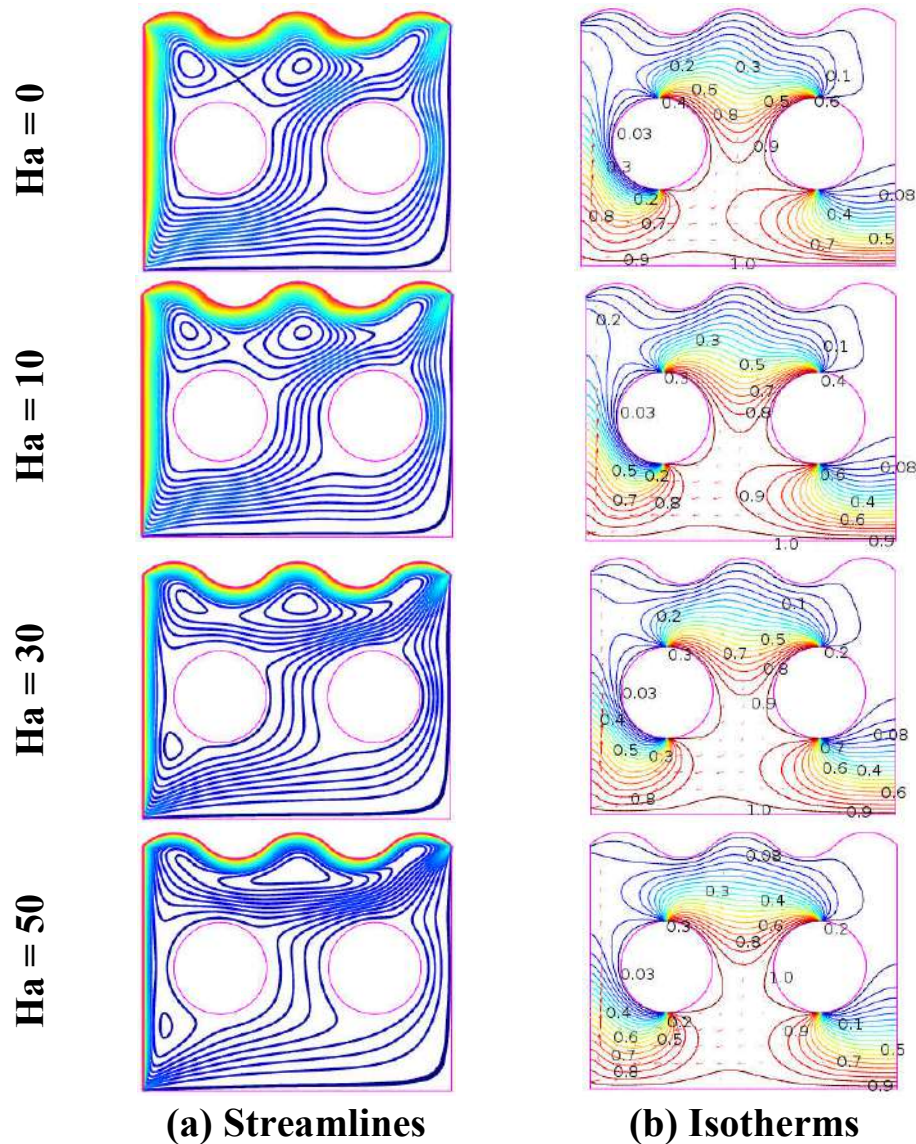


**Figure 4.25:** Effect of Hartmann number on (a) streamlines and (b) isotherms for  $Pr = 0.71$ ,  $Ri = 1.0$  and  $r = 0.15$  m

Streamlines are found less in the right half of the square cavity in Fig. 4.25(a) due to large cylindrical barrier in the cavity. From Figure 4.25 (a) it can be seen that when  $Ha = 0$  the strength of buoyancy force inside the cavity is more significant and eye shaped vortex appear inside the cavity which one is major vortex is produced by the movement of the lid wall. The physical fact behind it's that the flow circulation decreases with increasing

Hartmann number (increasing the strength of the magnetic field). This is because; applied magnetic field tends to slow down the fluid motions within the cavity.

On the other hand, conduction dominant heat transfer is observed from the isotherms are almost similar and uniformly distributed due to the greater values of Hartmann number ( $Ha$ ) is shown in Figure 4.25 (b); which is consistent to the effect of the magnetic field.

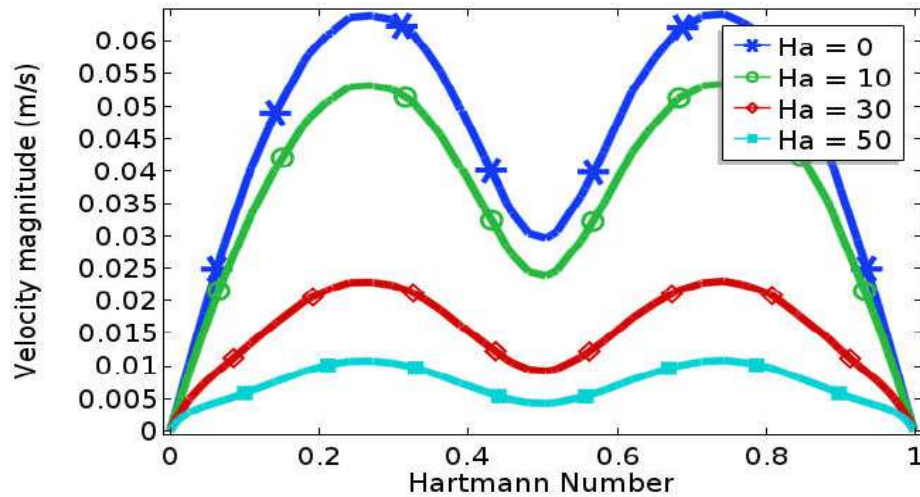


**Figure 4.26:** Variation of velocity profiles along the line  $y = 0.10$  of cavity for  $Ri = 1.0$ ,  $Pr = 0.71$  and  $r = 0.10$  m varying  $Ha$

The effect of Hartmann number ( $Ha$ ) on the vertical component of the velocity profiles along the line  $y = 0.1$  of the cavity at  $r = 0.15$  m,  $Pr = 0.71$  and  $Ri = 1.0$  is displayed in Figure 4.26. It can be observed that the changing rate of velocity is decreasing for increasing every Hartmann number. It can be seen from the figure that for higher values of Hartmann number, velocity profiles bring smaller change but the lower value of Hartmann number, velocity profiles cause larger change.

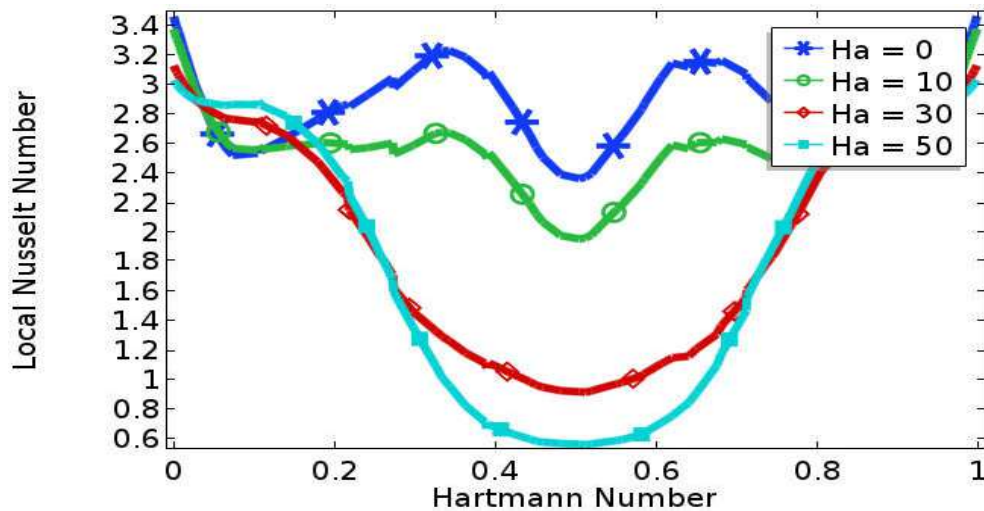


**Figure 4.27:** Variation of local Nusselt number along the line  $y = 0.10$  of cavity for  $Ri = 1$  and  $Pr = 0.71$  varying  $Ha$

The variation of the local Nusselt number distribution along the line  $y = 0.1$  of the enclosure for  $Pr = 0.71$  and  $Ri = 1$  varying Hartmann number ( $Ha$ ) is shown in Figure 4.27. It can be seen from the figure that the changing rate of local Nusselt number is increasing for increasing Hartmann number for  $Ha = 0$  and 10 and decreasing for increasing Hartmann number for  $Ha = 30$  and 50.

### 4.3.2.3 Heat Transfer Rates

In this section, the average Nusselt number versus Hartmann numbers and Richardson numbers heat transfer rates are shown in Figure 4.28 given below.

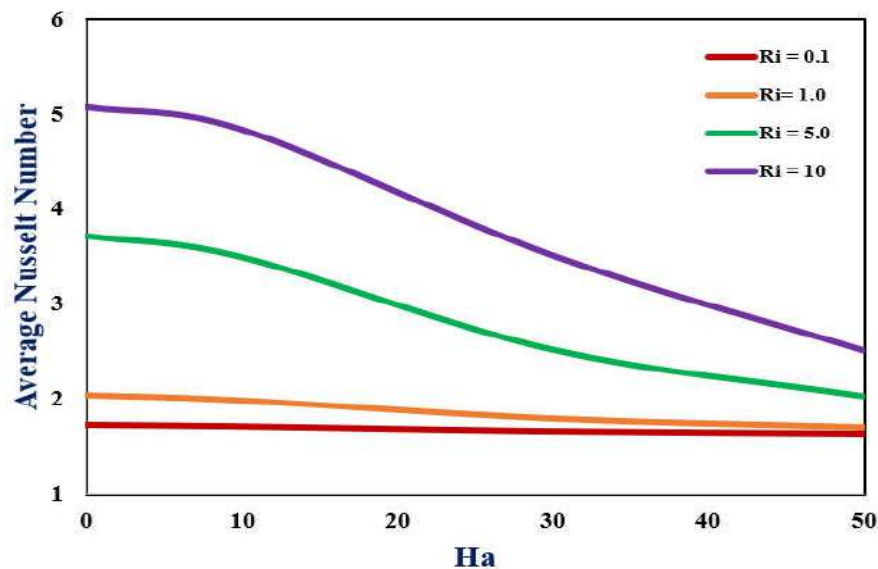


**Figure 4.28:** Variation of the average Nusselt number against  $Ha$  for selected value  $Ri$  while  $Pr = 0.71$ ,  $r = 0.10$  m

Figure 4.28 illustrate that the average Nusselt number ( $Nu_{av}$ ) versus Hartmann number along the heated bottom wall for various Richardson number ( $Ri$ ) with Radius  $r = 0.1$  m and the Prandtl number  $Pr = 0.71$  while the value of the remaining parameters is kept fixed. It can be seen from this figure that the average Nusselt number increases with increasing the value of  $Ri$  and decreases with the higher value of  $Ha$ .

### 4.3.3 Effect of cylinders size when $r = 0.20$ m

The influences of Radius  $r = 0.20$  m of the semi heated cylinders CP1 at (0.10, 0.40) and CP2 at (0.60, 0.40) of the wavy top cavity have been performed in terms of different non-dimensional numbers. The results have been obtained cylinders size  $r = 0.20$  m for the



Richardson number, Hartmann number and the rate of heat transfer. The results of this parametric study are shown in Figure 4.29 - 4.35 respectively.

### 4.3.3.1 Effect of Richardson Number

The influences of  $r = 0.20$  m of the semi heated cylinders at  $(0.1, 0.4)$  &  $(0.60, 0.40)$  of the wavy top cavity have been performed in terms of different non-dimensional numbers.

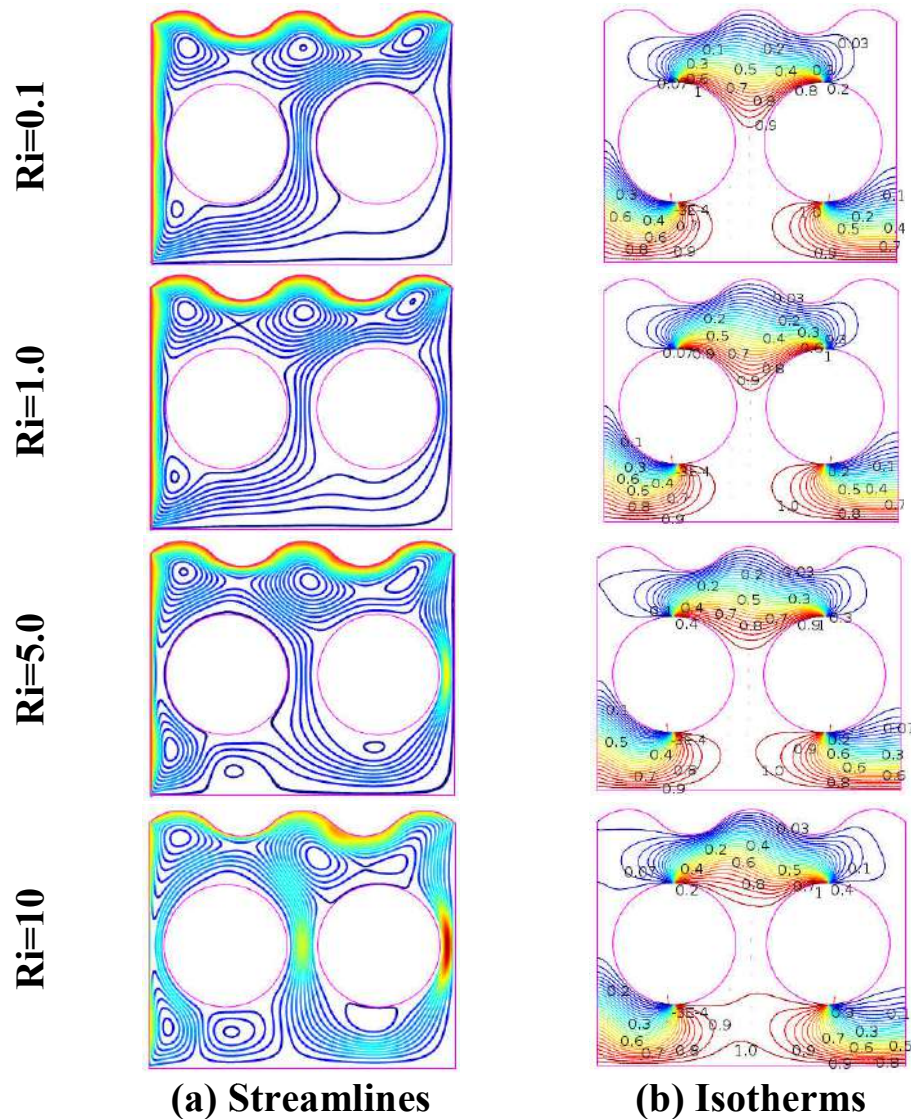
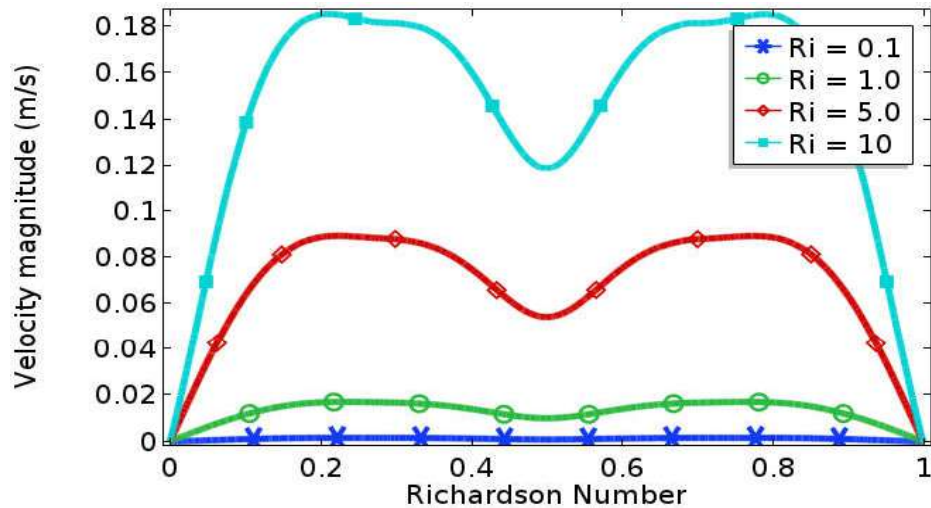


**Figure 4.29:** Effect of Richardson number on (a) streamlines and (b) isotherms for  $Pr = 0.71$ ,  $Ri = 1.0$  and  $r = 0.20$  m

The effects of Richardson number ( $Ri = 0.1, 1.0, 5.0, 10.0$ ) on streamlines for the present configuration for  $Ha = 10$  and  $Pr = 0.71$  is exhibited in fig. 4.29 (a). It is observed in the Fig. 4.29 (a) that the strength of the velocity magnitude increases with the increase of Richardson number ( $Ri$ ) from  $Ri = 0.1$  to  $10.0$  for  $r = 0.20$  m of the semi heated cylinders

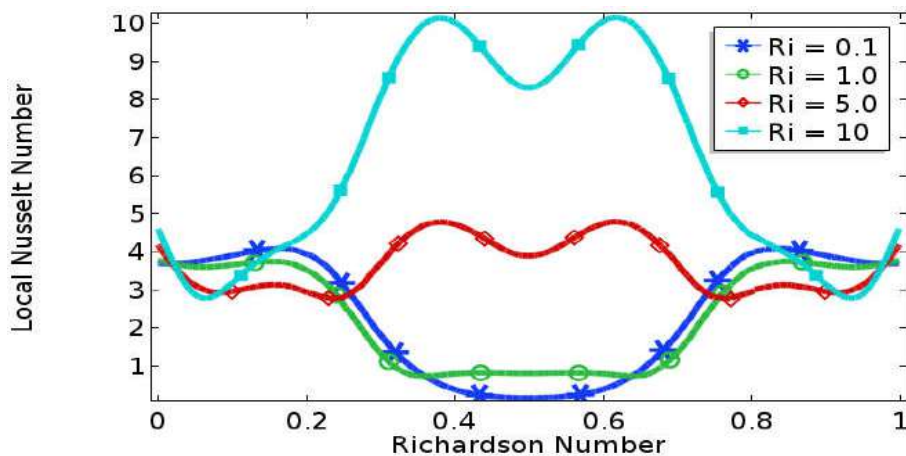
in the cavity. The biggest vorticity of the streamlines is viewed at  $r = 0.20$  m in the cavity where  $Ri = 10$ ,  $Ha = 10$  and  $Pr = 0.71$ .

Fig. 4.29 (b) displays the isothermal lines for different Richardson numbers with  $r = 0.20$  m of the semi heated cylinders in the cavity. Some heated isotherms are found between two circular cylinders and the heated bottom wall. A few numbers of heated isotherms are congested between the semi heated cylinders when  $Ri = 5.0, 10.0$  at  $r = 0.20$  m.



**Figure 4.30:** Variation of velocity profiles along the line  $y = 0.10$  of cavity for  $Ha = 10$ ,  $Pr = 0.71$  and  $r = 0.10$  m varying  $Ri$

The effect of Richardson number ( $Ri$ ) on the vertical component of the velocity profiles along the line  $y = 0.10$  of the cavity at  $r = 0.10$  m and  $Ha = 10$  is displayed in Figure 4.30. It can be seen from the figure that for lower values of Richardson number, velocity profiles bring smaller change but the higher value of Richardson number, velocity profiles cause larger change.



**Figure 4.31:** Variation of local Nusselt number along the line  $y = 0.10$  of cavity with Richardson number for  $Pr = 0.71$ ,  $Ha = 10$

The variation of the local Nusselt number distribution alongside the line  $y = 0.1$  of the enclosure for  $Pr = 0.71$  and  $Ha = 10$  varying Richardson number ( $Ri$ ) is shown in Figure 4.31. It can be seen from the figure that the local Nusselt number increases with increasing Richardson number  $Ri = 5.0$  and but decreasing for  $Ri = 0.1$  and  $Ri = 1.0$  in a major portion of the bottom heated wall.

### 4.3.3.2 Effect of Hartmann Number

A mathematical study has been executed in this section to examine the effects of Hartmann number ( $Ha$ ) with  $r = 0.15$  m of the semi heated cylinders in the cavity.

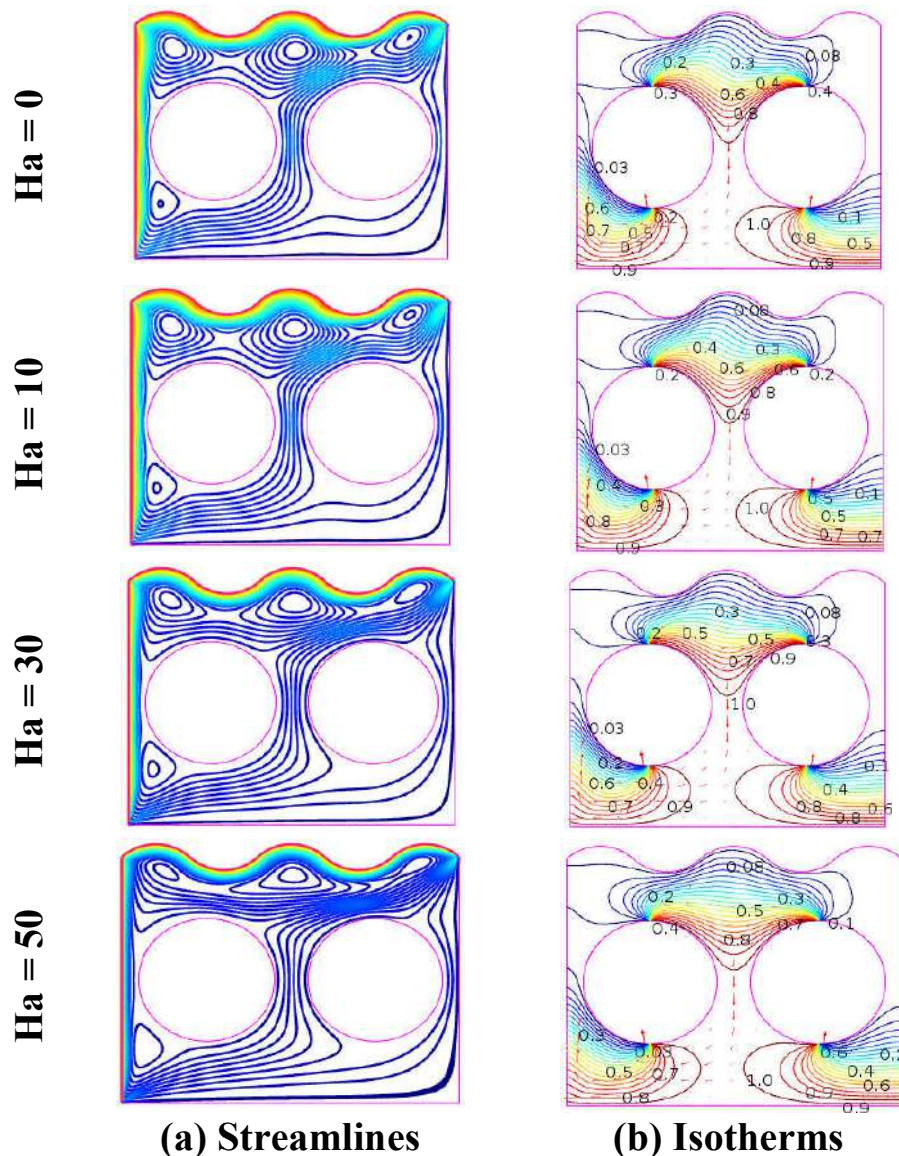


**Figure 4.32:** Effect of Hartmann number on (a) streamlines and (b) isotherms for  $Pr = 0.71$ ,  $Ri = 1.0$  and  $r = 0.10$  m

The investigated results have been shown in terms of streamlines, isotherm lines, velocity profiles, Local Nusselt number and average Nusselt number. Fig 4.32 (a) explores the

streamlines for different Hartmann number with the radius size of  $r = 0.20$  m of the semi heated cylinders where CP1 (0.1, 0.4) & (0.60, 0.40),  $Pr = 0.71$  and  $Ri=0.1$  respectively. It is also seen that the speed of the fluid is reduced at the higher value of Hartmann number. This is because of the application of transverse magnetic field which tends to slow down the movement of the buoyancy induced flow in the enclosure. It inquired into in Fig. 4.32 (a) that the strength of the velocity magnitude reduces for the semi heated cylinders when the Hartmann number ( $Ha$ ) is altered from 0 to 50.

From Figure 4.32 (a) it can be seen that when  $Ha= 0$  the strength of buoyancy force inside the cavity is more significant and three eye shaped vortex appear inside the cavity which are major vortex is produced by the movement of the lid wall. The physical fact behind it's that the flow circulation decreases with increasing Hartmann number. This is because; applied magnetic field tends to slow down the fluid motions within the cavity.

On the other hand, conduction dominant heat transfer is observed from the isotherms are almost similar and uniformly distributed due to the greater values of Hartmann number ( $Ha$ ) is shown in Figure 4.32 (b); which is consistent to the effect of the magnetic field. The isothermal lines are conjugated near the wavy wall and under the circular cylinders. The thermal lines of the isotherms are almost same without changing the point.

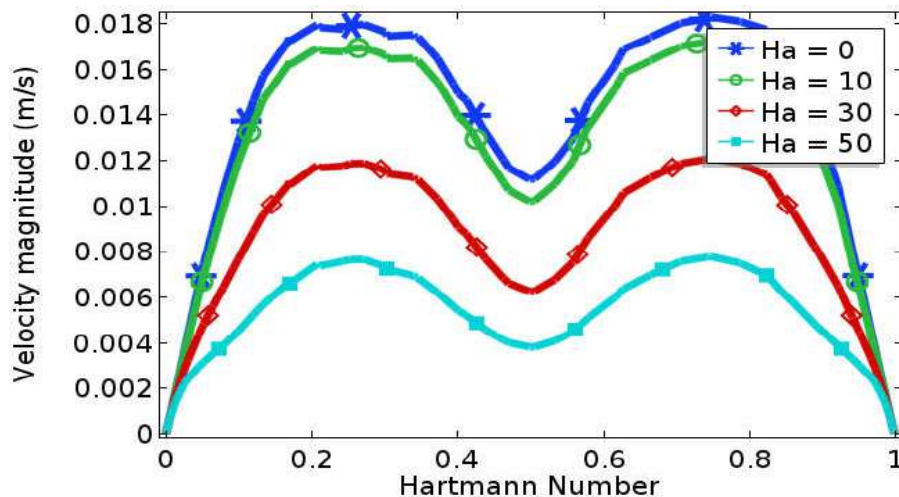


**Figure 4.33:** Variation of velocity profiles along the line  $y = 0.10$  of cavity for  $Ri = 1.0$ ,  $Pr = 0.71$  and  $r = 0.10$  m varying  $Ha$

The effect of Hartmann number ( $Ha$ ) on the vertical component of the velocity profiles along the horizontal line of the cavity at  $r = 0.20$  m,  $Pr = 0.71$  and  $Ri = 1.0$  is displayed in Figure 4.33. It can be observed that the changing rate of velocity is decreasing for increasing every Hartmann number. It can be seen from the figure that for higher values of

Hartmann number, velocity profiles bring smaller change but the lower value of Hartmann number, velocity profiles cause larger change.

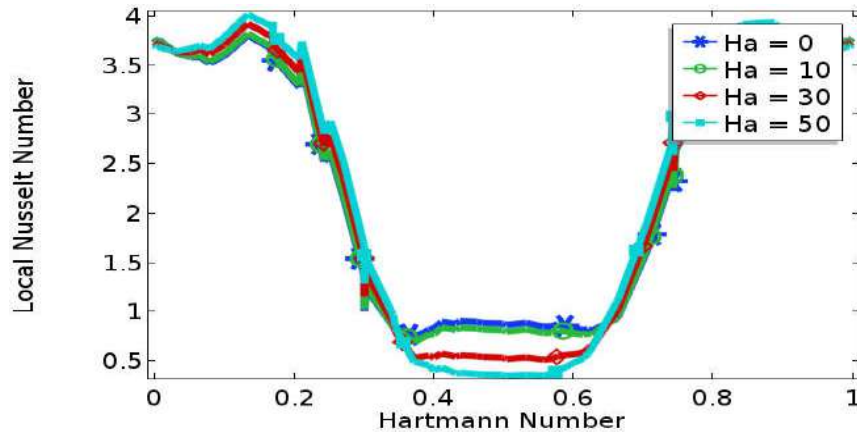


**Figure 4.34:** Variation of local Nusselt number along the line  $y = 0.10$  of cavity for  $Ri = 1$  and  $Pr = 0.71$  varying  $Ha$

The variation of the local Nusselt number distribution alongside the bottom wall of the enclosure for  $Pr = 0.71$  and  $Ri = 1$  varying Hartmann number ( $Ha$ ) is shown in Figure 4.34. It can be seen from the figure that the changing rate of local Nusselt number is decreasing for increasing Hartmann number. It can be seen from the figure that the changing lines are almost same for every Hartmann number but they showed noticeable change near the heated bottom wall of the cavity.

### 4.3.2.3 Heat Transfer Rates

The average Nusselt number versus Hartmann numbers and Richardson numbers heat transfer rates are shown in Figure 4.35 given below.

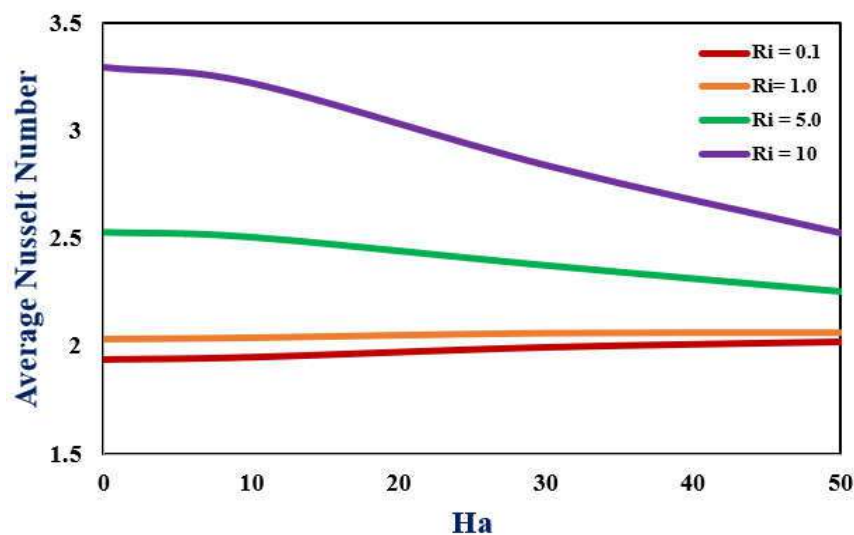


**Figure 4.35:** Variation of the average Nusselt number against  $Ha$  for selected value  $Ri$

while  $Pr = 0.71$ ,  $r = 0.10$  m

Figure 4.35 illustrate that the average Nusselt number ( $Nu_{av}$ ) versus Hartmann number along the heated bottom wall for various Richardson number ( $Ri$ ) with Radius  $r = 0.1$  m and  $Pr = 0.71$  while the value of the remaining parameters is kept fixed. It can be seen from this Figure, the average Nusselt number increases when the value of the Richardson number increases. At a constant Richardson number, with a decrease in Hartmann number the buoyancy force increases and the heat transfer is enhanced.

## 4.4 Comparative Study

### 4.4.1 Comparison of $Nu_{av}$ between with one cylinder and with two cylinders

Comparison of average Nusselt Numbers ( $Nu_{av}$ ) along the bottom heated wall of the cavity in the presence of one cylinder and in the presence of two cylinders have been investigated in table 4.1 where  $r = 0.1$  m,  $Pr = 0.71$ , CP1 at (0.1, 0.4) and CP2 (0.6, 0.4) and  $Ri = 0.1$  to 10. It is observed that the  $Nu_{av}$  increases for  $Ha = 0$  to 50 and different Richardson numbers ( $Ri = 0.1$  to 10) for both cases. The largest  $Nu_{av}$  (4.45) is obtained in the presence of two cylinders when  $Pr = 0.71$ ,  $Ri = 10$  and  $Ha = 0$ . For Richardson numbers ( $Ri = 0.1$  to 10) the  $Nu_{av}$  decreases with the increase of Hartmann Number from 0 to 50 for both cases.

Average Nusselt Number $Nu_{av}$ (along the heated bottom wall)						
Pr = 0.71	Heat Flow with one cylinder			Heat Flow with two cylinders		
	Ha = 0	30	50	Ha = 0	30	50
<b>0.1</b>	2.06329	1.43154	1.31722	1.52326	1.40958	1.39977
<b>1.0</b>	2.4765	1.48858	1.33555	2.1016	1.54656	1.4574
<b>5.0</b>	3.01895	2.02218	1.45213	3.94108	2.41526	1.78533
<b>10</b>	3.93218	2.68104	1.72821	4.45046	3.29548	2.29896

**Table 4.1:** Comparison of average Nusselt Number ( $Nu_{av}$ ) along the heated bottom wall between with one cylinder and with two cylinders of the cavity where  $r = 0.1$  m,  $Pr = 0.71$ , CP1 at (0.1, 0.4) and CP2 at (0.6, 0.4)

### 4.4.2 Comparison between present result and previous study

The comparison of the numerical results is a very imperative practice in computational dynamics. The present results are verified against the existing results available in the

literature. The numerical outcome of this study is supported by data from Chamkha [16]. To make the comparison with the examined research work, the current code has been taken the parameter variation as same as Chamkha [16]. The average Nusselt number is computed for base fluid water,  $Pr = 0.71$  as fixed and variation of Hartmann number from 0 to 50. Figure 4.36 displays a graphical representation of the average Nusselt number in terms of Hartmann number among Chamkha [16] and the current study.

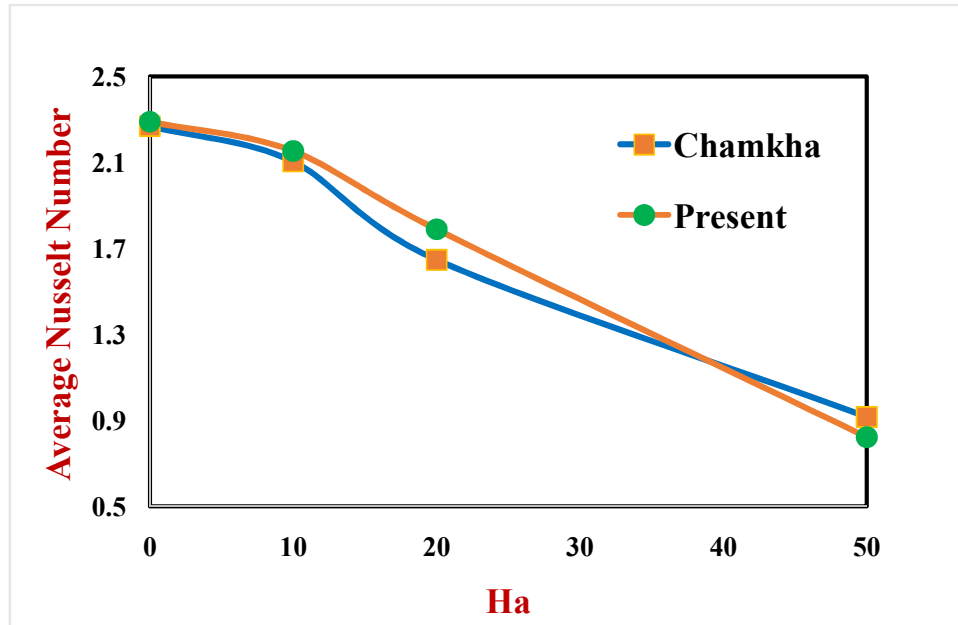


**Figure 4.36:** Comparison of average Nusselt Number with Chamkha [16], al.and Present research

Table 4.2 shows the average Nusselt number ( $Nu_{av}$ ) of the present research compared to other published researches along the left heated wall of the cavity. It has been observed from Table 4.2 that a good agreement is found among the published results with present research.

Ha	Chamkha[16]	Present result
0	2.2692	2.29023
10	2.105	2.154351
20	1.6472	1.78928
50	0.9164	0.822164

**Table 4.2:** Comparison of Average Nusselt Number ( $Nu_{av}$ ) between Chamkha [16] and Present study for different Hartmann Number (Ha)

# CHAPTER 5

## Conclusions and Future Research

The effect on the flow structure and heat transfer behaviors for mixed convection heat transfer in presence of magnetic field in a lid-driven wavy top cavity having two circular cylinders has been studied numerically. Comparisons with the published works are performed and found to be in excellent agreement. The influences of Richardson number, Hartmann number and the positions of the cylinders inside the wavy top cavity have been reported. The various ideas and results have been discussed in detail in the relevant chapters of the thesis. In the present chapter, an attempt is made to summarize the concepts presented and results obtained in the work reported already. A section on the scope of further work on associated fields of investigation is also included.

### 5.1 Summary of the Major Outcomes

Two difference cases as case – I (Variation of cylinders position) and case – II (Variation of cylinders size) have been illustrated in this research. On the basis of the analysis the following outcomes have been drawn from the present study.

#### 5.1.1 Case – I: Variation of Cylinders position

- (i) The Maximum strength of the Velocity magnitude (356.28 m/s) is obtained at CP1 (0.1, 0.4) and CP2 at (0.6, 0.25) for  $Ri = 10$  and cylinder size,  $r = 0.10$  m,  $Pr = 0.71$ ,  $Ha = 50$ .
- (ii) The greatest average velocity magnitude (1.917 m/s) is found for CP1 at (0.1, 0.4) and CP2 at (0.6, 0.25) is found for  $Ri = 10$ ,  $Pr = 0.71$ ,  $Ha = 50$  and cylinder size,  $r = 0.1$  m.
- (iii) The average Nusselt Number ( $Nu_{av}$ ) along the heated bottom wall is maximum (5.62) when CP1 at (0.1, 0.4) and CP2 at (0.6, 0.55) and is minimum (1.43) when CP1 at (0.1, 0.4) and CP2 at (0.6, 0.4) cylinders size  $r = 0.10$  m.
- (iv) The rate of heat transfer rate is increased approximately 171.8% For  $Ri$  variation and decreased as 192.37% for  $Ha$  variation when the cylinders size  $r = 0.10$  m and cylinders position are kept CP1 at (0.1, 0.4) and CP2 at (0.6, 0.25).
- (v) Finally, it can be decided that the cylinders position CP1 at (0.1, 0.4) and CP2 at (0.6, 0.25) are the ideal positions of the wavy top cavity for heat transfer.



### 5.1.2 Case – I: Variation of Cylinders size

- (i) The Maximum strength of the Velocity magnitude (357.52 m/s) is obtained CP1 at (0.1, 0.4) and CP2 at (0.6, 0.4) for  $Ri = 10$ ,  $Pr = 0.71$ ,  $Ha = 50$  and cylinder size (radius)  $r = 0.20$  m.
- (ii) The greatest average velocity magnitude (2.66 m/s) is found for CP1 at (0.1, 0.4) and CP2 at (0.6, 0.4) is found for  $Ri = 10$ ,  $Pr = 0.71$ ,  $Ha = 50$  and cylinder size,  $r = 0.20$  m.
- (iii) The average Nusselt Number ( $Nu_{av}$ ) along the heated bottom wall is maximum (5.07) when  $r = 0.20$  m and is minimum (1.43) when  $r = 0.10$  m while cylinders are kept CP1 at (0.1, 0.4) and CP2 at (0.6, 0.4).
- (iv) The rate of heat transfer rate is increased approximately 163.9% For  $Ri$  variation and decreased as 184.03% for  $Ha$  variation when the cylinders size  $r = 0.10$  m and cylinders position are kept CP1 at (0.1, 0.4) and CP2 at (0.6, 0.4).
- (v) Finally, the inner cylinders which have radius  $r = 0.10$  m, are the ideal size for heat transfer.

## 5.2 Conclusions

The study for the distribution of streamlines, isotherms, local Nusselt number and average Nusselt number have been carried out to investigate the effects of dimensionless parameters namely, Richardson number ( $Ri$ ) and Hartmann number ( $Ha$ ). The governing partial differential equations for momentum and energy are derived according to the physical model of the problem. The governing equations with boundary conditions are then made dimensionless using a set of non-dimensional variables. The resulting dimensionless nonlinear differential equations together with the corresponding boundary conditions are then solved numerically using Finite Element Method of Galerkin weighted residual approach. Finally, the numerical results have been presented graphs in terms of streamlines, isotherms, velocity, temperature and local and average Nusselt number for different values of pertinent parameters.

The following conclusions may be drawn on the basis of present analysis in this thesis:

- ✚ The variations of non-dimensional parameters in the present study are Hartman number and Richardson number has been studied. The effects of the mentioned parameters were used on the distribution of fluid motion and temperature in terms of streamlines, isotherms, velocity, local Nusselt number and temperature profiles.
- ✚ The effects of  $Ri$  and  $Ha$  on the fluid flow and heat transfer are investigated in a cavity filled with MHD fluid, containing two circular cylinders inside the cavity. Flow strength and heat transfer increases with increasing Richardson number in all

cases. As the Richardson number increases the velocity profiles, local Nusselt number and the heat transfer rate as well as the average Nusselt number changes.

- ✚ Flow velocity and rate of heat transfer decreases with increasing of Hartmann number. Thus, magnetic field plays an important role to control heat transfer and fluid flow. Velocity profiles, local Nusselt number, average Nusselt number and the average fluid temperature changes from highest to lowest as Ha changes lowest to highest.
- ✚ It is also observed that, for high Richardson numbers, by increase in the Hartmann number, mixed convection is suppressed and heat transfer occurs through conduction mainly. Moreover, the rate of heat transfer is increased for Ri variation, and decreased for Ha variation.
- ✚ The effect of Ri has also been studied in the present investigation for fixed value of Pr and Re. It is observed that the force convection dominates over natural convection as Ri increases.
- ✚ Good distributions were shown for different Hartmann numbers and Richardson numbers. The heat transfer rate is more affected for the size variation of the semi heated cylinders compare to the position variation.

### 5.3 Future Research

In consideration of the present investigation “Numerical study of magnetohydrodynamics mixed convection in a lid-driven wavy top cavity containing two circular cylinders”, the following recommendations for future works may be extended as

- ❖ The study can be extended for turbulent flow, different thermal boundary conditions such as constant heat flux or radiation.
- ❖ The study can be protracted by changing the boundary cases of the enclosures.
- ❖ Investigation can be performed by using magnetic within the porous media and changing the boundary conditions of the cavity’s walls.
- ❖ This numerical analysis can be extended for three-dimensional fluid flow and heat transfer.
- ❖ The study can be extended including Nano-fluids.
- ❖ The study can be extended by choosing different shape of enclosures.
- ❖ Natural and forced convection can also be considered to the governing equations of concentration conservation.
- ❖ Effect of conduction on MHD mixed convection heat flow in a wavy cavity with two square cylindrical blocks.

## REFERENCES

- [1] Raizah, Z., Aly, A. M., Alsedais, N., Mansour, M. A., “MHD mixed convection of hybrid nanofluid in a wavy porous cavity employing local thermal non-equilibrium condition.” *Sci Rep*, vol.11, pp. 17151 (2021). DOI:[10.1038/s41598-021-95857-z](https://doi.org/10.1038/s41598-021-95857-z)
- [2] Alsabery, A.I., Hashim, I., Hajjar, A., Ghalambaz, M., Nadeem, S., Saffari Pour, M., “Entropy Generation and Natural Convection Flow of Hybrid Nanofluids in a Partially Divided Wavy Cavity Including Solid Blocks.” *Energies*, vol. 13, pp. 2942, (2020). DOI:[10.3390/en13112942](https://doi.org/10.3390/en13112942)
- [3] Alsabery, A. I., Tayebi, T., Chamkha, A. J., and Hashim, I., "Effect of rotating solid cylinder on entropy generation and convective heat transfer in a wavy porous cavity heated from below", *International Communications in Heat Mass Transfer*, vol. 95, pp. 197-209 (2018). DOI:[10.1016/j.icheatmasstransfer.2018.05.003](https://doi.org/10.1016/j.icheatmasstransfer.2018.05.003)
- [4] Öztöp, H. F., Sakhrieh, A., Nada, E. A. and Al-Salem, K., “Mixed convection of MHD flow in nanofluid filled and partially heated wavy walled lid-driven enclosure”, *International Communications in Heat Mass Transfer*, vol. 86, pp. 42-51, (2017). DOI:[10.1016/j.icheatmasstransfer.2017.05.011](https://doi.org/10.1016/j.icheatmasstransfer.2017.05.011)
- [5] Cheong, H. T., Sivasankaran, S., and Bhuvaneswari M., “Natural convection in a wavy porous cavity with sinusoidal heating and internal heat generation”, *International Journal of Numerical Methods for Heat and Fluid Flow*, vol. 27, pp. 287–309, (2017). DOI:[10.1108/HFF-07-2015-0272](https://doi.org/10.1108/HFF-07-2015-0272)
- [6] Sheremet, M. A., Cimpean, D., Pop, I., “Free convection in a partially heated wavy porous cavity filled with a nanofluid under the effects of Brownian diffusion and thermophoresis”, *Applied Thermal Engineering*, vol. 113, pp. 413–418 (2017). DOI:[10.1016/j.applthermaleng.2016.11.033](https://doi.org/10.1016/j.applthermaleng.2016.11.033)
- [7] Sheremet, M. A., and Pop, I., “Natural convection in a wavy porous cavity with sinusoidal temperature distributions on both side walls filled with a nanofluid: Buongiorno's mathematical model”, *Transport in Porous Media.*, vol. 105, pp. 072601-8 (2015). DOI:[10.1007/s11242-014-0375-7](https://doi.org/10.1007/s11242-014-0375-7)
- [8] Abu-Nada, E., and Chamkha, A. J., “Mixed convection flow of a nanofluid in a lid-driven cavity with a wavy wall”, *Int. Commun. Heat Mass Transf.*, vol. 57, pp. 36–47 (2014). DOI: [org/10.1016/j.icheatmasstransfer.2014.07.013](https://doi.org/10.1016/j.icheatmasstransfer.2014.07.013)
- [9] Mansour, M., El-Aziz, M. A., Mohamed, R., and Ahmed, S. E., “Numerical simulation of natural convection in wavy porous cavities under the influence of thermal radiation using a thermal non-equilibrium model”, *Transp. Porous Media*, vol. 86, pp. 585–600 (2011). DOI [10.1007/s11242-010-9641-5](https://doi.org/10.1007/s11242-010-9641-5)

- [10] Nasrin R., and Parvin S., “Hydro-magnetic effect on mixed convection in a lid-driven cavity with sinusoidal corrugated bottom surface,” *Inter. Commun. in Heat and Mass Transf.*, vol.38, pp. 781-789 (2011). DOI:[10.1016/j.icheatmasstransfer.2011.03.002](https://doi.org/10.1016/j.icheatmasstransfer.2011.03.002)
- [11] Rostami, J., “Unsteady natural convection in an enclosure with vertical wavy walls”, *Heat Mass Transf.*, vol. 44, pp. 1079–1087 (2008).DOI:[10.1007/s00231-007-0349-1](https://doi.org/10.1007/s00231-007-0349-1)
- [12] Al-Amiri, A. K. Khanafer, J. Bull and I. Pop, “Effect of sinusoidal wavy bottom surface on mixed convection heat transfer in a lid-driven cavity”, *International Journal of Heat and Mass Transfer*, vol. 50, pp. 1771–1780 (2007).
- [13] Misirlioglu, A.C. Baytas and I. Pop, “Natural convection inside an inclined wavy enclosure filled with a porous medium”, *Transport in Porous Media*, vol. 64, pp. 229–246 (2006). DOI:[10.1007/s11242-005-2857-0](https://doi.org/10.1007/s11242-005-2857-0)
- [14] Das, P. K., and Mahmud, S., “Numerical investigation of natural convection inside a wavy enclosure”, *International Journal of Thermal Sciences*, vol. 42, pp. 397–406 (2003).DOI: [org/10.1016/S1290-0729\(02\)00040-6](https://doi.org/10.1016/S1290-0729(02)00040-6)
- [15] Mahmud, S., Das, P. K., Hyder, N., and Islam, A. K. M. S., “Free convection in an enclosure with vertical wavy walls”, *International Journal of Thermal Sciences*, vol. 41, pp. 440–446 (2002).DOI:[10.1016/S1290-0729\(02\)01336-4](https://doi.org/10.1016/S1290-0729(02)01336-4)
- [16] Chamkha, A. J., “Hydromagnetic combined convection flow in a vertical lid -driven cavity with internal heat generation or absorption”, *Heat transfer Part A*, vol. 41, pp. 529 – 546, (2002).
- [17] Selimefendigil, F., Oztop, H. F., “Combined effects of double rotating cones and magnetic field on the mixed convection of nanofluid in a porous 3D U-bend.” *International Communications of Heat and Mass Transfer*, vol.116, pp. 104703, (2020). DOI:[10.1016/j.icheatmasstransfer.2020.104703](https://doi.org/10.1016/j.icheatmasstransfer.2020.104703)
- [18] Munshi, J. H., Mostafa, G., Manik Munshi, A. B. S., Waliullah, Md., "Hydrodynamic Mixed Convection in a Lid-Driven Hexagonal Cavity with Corner Heater." *American Journal of Computational Mathematics*, Scientific Research Publishing, vol 8, pp. 245-258, (2018) DOI: [10.4236/ajcm.2018.83020](https://doi.org/10.4236/ajcm.2018.83020)
- [19] Munshi, M.J.H., Alim, M.A., Bhuiyan, A.H. and Ali, M., “Hydrodynamic Mixed Convection in a Lid-Driven Square Cavity Including Elliptic Shape Heated Block with Corner Heater.” *Procedia Engineering*, vol. 194, pp. 442-449, (2017). DOI:[10.1016/j.proeng.2017.08.169](https://doi.org/10.1016/j.proeng.2017.08.169)
- [20] Ali, M. M., Alim, M. A., Ahmed, S. S., "Magnetohydrodynamic Mixed Convection Flow in a Hexagonal Enclosure." *Procedia Engineering*, 10th International Conference on Marine Technology, vol 194, pp. 479-486, (2017).
- [21] Udhayakumar, S., Rejeesh, A. D. A., Sekhar, T. V. S., Sivakumar, R. "Numerical investigation of magnetohydrodynamic mixed convection over an isothermal

- circular cylinder in presence of an aligned magnetic field." *International Journal of Heat and Mass Transfer*, Elsevier Ltd, vol 95, pp. 379-392, (2016).
- [22] Rashidi, M. M., Nasiri, M., Khezerloo, M., Laraqi, M. "Numerical investigation of magnetic field effect on mixed convection heat transfer of nanofluid in a channel with sinusoidal walls." *Journal of Magnetism and Magnetic Materials*, Science Direct, vol 401, pp. 159-168, (2016). DOI: [10.1016/j.jmmm.2015.10.034](https://doi.org/10.1016/j.jmmm.2015.10.034)
- [23] Aghaei, A., Khorasanizadeh, H., Sheikhzadeh, G., Abbaszadeh, M. "Numerical study of magnetic field on mixed convection and entropy generation of nanofluid in a trapezoidal enclosure." *Journal of Magnetism and Magnetic Materials*, Science Direct, vol 403, pp. 133-145, (2016). DOI: [10.1016/j.jmmm.2015.11.067](https://doi.org/10.1016/j.jmmm.2015.11.067)
- [24] Malleswaran<sup>1</sup>, A., and Sivasankaran, S., "A Numerical simulation on MHD mixed convection in a lid-driven cavity with corner heaters," *Journal of Applied Fluid Mechanics*, vol.9, pp. 311-319 (2016). DOI: [10.18869/acadpub.jafm.68.224.22903](https://doi.org/10.18869/acadpub.jafm.68.224.22903)
- [25] Saha, L. K., Uddin, K. M. S., Taher, M. A. "Effect of Internal Heat Generation or Absorption on MHD Mixed Convection Flow in a Lid Driven Cavity." *American Journal of Applied Mathematics*, vol 3, pp. 20-29, (2015).
- [26] Khudheyer, A. F., "MHD mixed convection in double lid-driven differentially heated trapezoidal cavity", *International Journal of Application*, vol. 4, pp. 100-107, (2015). DOI: [ijaiem.org/pabstract.php?vol=Volume4Issue2&pid=IJAIEM-2015-02-17-29](http://ijaiem.org/pabstract.php?vol=Volume4Issue2&pid=IJAIEM-2015-02-17-29)
- [27] Selimefendigil, F., Oztop, H. F., "Numerical study of MHD mixed convection in a nanofluid filled lid driven square enclosure with a rotating cylinder." *Int J Heat Mass Transf.*, vol. 78, pp. 741-754, (2014). DOI: [10.1016/j.ijheatmasstransfer.2014.07.031](https://doi.org/10.1016/j.ijheatmasstransfer.2014.07.031)
- [28] Malleswaran, A., Sivasankaran, S., Bhuvaneshwari, M. "Effect of heating location and size on MHD mixed convection in a lid-driven cavity." *International Journal of Numerical Methods for Heat & Fluid Flow*, Emerald Group Publishing Limited, vol 23(5), pp. 867-884, (2013). DOI: [10.1108/HFF-04-2011-0082](https://doi.org/10.1108/HFF-04-2011-0082)
- [29] Farid, S. K., Billah, M. M., Rahman, M. M., Sharif, M. U., "Numerical study of fluid flow on magneto-hydrodynamic mixed convection in a lid-driven cavity having a heated circular hollow cylinder," *Procedia Engineering*, vol. 56, pp. 474-479, (2013). DOI: [10.1016/j.proeng.2013.03.149](https://doi.org/10.1016/j.proeng.2013.03.149)
- [30] Rahman, M. M., Alim, M. A., Sarker, M. A., "Numerical study on the conjugate effect of joule heating and magneto-hydrodynamics mixed convection in an obstructed lid-driven square cavity," *International Communications in Heat Mass Transfer*, vol. 37, no. 5, pp. 524-534, (2010). DOI: [10.1016/j.icheatmasstransfer.2009.12.012](https://doi.org/10.1016/j.icheatmasstransfer.2009.12.012)

- [31] Rabani, M., “Numerical analysis of mixed convection heat transfer in a triangular cavity with moving walls.” *Heat Transfer Research*, vol. 50(5), pp. 463–485, (2019). DOI: [10.1615/HeatTransRes.2018025276](https://doi.org/10.1615/HeatTransRes.2018025276)
- [32] Ekici, O., “Lattice boltzmann simulation of mixed convection heat transfer in a lid-driven square cavity filled with nanofluid: a revisit.” *J Heat Transf.*, vol. 140(7), pp. 072501, (2018). DOI: [10.1115/1.4039490](https://doi.org/10.1115/1.4039490)
- [33] Omari, R. "Numerical Investigation of a Mixed Convection Flow in a Lid-Driven Cavity." *American Journal of Computational Mathematics, Scientific Research*, vol 6, pp. 251-258, Jordan, (2016). DOI: [10.4236/ajcm.2016.63026](https://doi.org/10.4236/ajcm.2016.63026)
- [34] Parvin, S., Alim, M. A., Hossain, N. F. "Heat and Mass Transfer Due to Double Diffusive Mixed Convection in a Parallel Plate Reactor in Presence of Chemical Reaction and Heat Generation." *International Journal of Chemical and Process Engineering Research, Conscientia Beam*, vol 2(2), pp. 17-29, (2015). DOI: [10.18488/journal.65/2015.2.2/65.2.17.29](https://doi.org/10.18488/journal.65/2015.2.2/65.2.17.29)
- [35] Sivasankaran S., Sivakumar V., Hussein A.K., and Prakash P., “Mixed convection in a lid-driven two-dimensional square cavity with corner heating and internal heat generation,” *Numerical Heat Transfer*, vol.65, pp. 269-286 (2014). [doi.org/10.1080/10407782.2013.826017](https://doi.org/10.1080/10407782.2013.826017)
- [36] Billah, M.M., Rahman, M.M., Sharif, U.M., Rahim, N.A., Saidur, R. and Hasanuzzaman, M., “Numerical Analysis of Fluid Flow Due to Mixed Convection in a Lid-Driven Cavity Having a Heated Circular Hollow Cylinder”, *International Communications in Heat and Mass Transfer.*” vol. 38, pp. 1093-1103, (2011). [doi.org/10.1016/j.icheatmasstransfer.2011.05.018](https://doi.org/10.1016/j.icheatmasstransfer.2011.05.018)
- [37] Darzi, A. A. R., Farhadi, M., Sedighi, K., “Numerical study of the fin effect on mixed convection heat transfer in a lid-driven cavity”, *J. Mechanical Eng. Sci.*, vol. 225, pp. 397–406, (2011). [doi.org/10.1243/09544062JMES2307](https://doi.org/10.1243/09544062JMES2307)
- [38] Rahman, M. M., Alim, M. A., Saha S., Chowdhury, M. K., “Numerical study of mixed convection in a square cavity with a heat conducting square cylinder at different locations.” *Journal of Mechanical Engineering*, vol-02 (2008).
- [39] Manca O., Nardini S., and Vafai K., “Experimental investigation of opposing mixed convection in a channel with an open cavity below,” *Experimental Heat Transfer*, vol.21, pp. 99–114 (2008). [doi.org/10.1080/08916150701815820](https://doi.org/10.1080/08916150701815820)
- [40] Manca O., Nardini S., and Vafai K., “Experimental investigation of mixed convection in a channel with an open cavity,” *Experimental Heat Transfer*, vol.19, pp.53–68 (2006). [doi.org/10.1080/08916150500318380](https://doi.org/10.1080/08916150500318380)
- [41] Öztop H.F., and Dagtekin I., “Mixed convection in two-sided lid-driven differentially heated square cavity,” *International Journal of Heat Mass Transfer*, vol.47, pp.1761–1769 (2004). [doi.org/10.1016/j.ijheatmasstransfer.2003.10.016](https://doi.org/10.1016/j.ijheatmasstransfer.2003.10.016)

- [42] Hossain S.A., Alim M. A., and Saha S. K., “A finite element analysis on MHD free convection flow in open square cavity containing heated circular cylinder,” *American Journal of Computational Mathematics*, vol.5, pp.41-54 (2015).